Mair, R. J. (2008). *Géotechnique* **58**, No. 9, 695–736 [**doi:** 10.1680/geot.2008.58.9.695]

Tunnelling and geotechnics: new horizons

R. J. MAIR*

New developments in both the theory and the practice of tunnelling are covered in the lecture. The important relationship between tunnelling and geotechnics is highlighted, and recent advances in research and practice are described, drawing on model studies, theoretical developments and field measurements from case histories from around the world. Simplified plasticity models are presented that can be used by designers to assess ground movements and tunnel lining loads in complex ground conditions. The important role of pilot tunnels and in situ measurements to validate such models, drawing on a case history from Bolu, Turkey, and on other tunnelling projects, is described. Recent technical advances in earth pressure balance tunnelling are considered, illustrated by measurements from the Channel Tunnel Rail Link project, with emphasis on key factors influencing volume loss, such as face pressure, soil conditioning and effective screw conveyor operation. A recent case history in Bologna is described, in which the innovative use of directional drilling to install curved grout tubes was employed for a compensation grouting project in granular soils. Time-dependent ground movements and tunnel lining distortions occurring after tunnelling are discussed, their magnitude depending on the relative permeability of the tunnel lining and soil, the degree of anisotropy of the soil permeability, and the initial pore pressure prior to tunnelling. The effects of tunnelling-induced settlements on pipelines are considered, drawing on centrifuge tests and analytical solutions, and a new design approach is presented, taking into account the reduction of soil stiffness with increasing shear strain as a result of tunnel volume loss. The lecture concludes with a description of a distributed strain sensing technique using fibre optic technology, based on Brillouin optical time domain reflectometry (BOTDR), and its innovative application to field monitoring of a masonry tunnel subjected to new tunnel construction beneath it.

KEYWORDS: case histories; centrifuge modelling; design; field instrumentation; ground movement; grouting; monitoring; numerical modelling and analysis; pipelines; theoretical analysis; tunnels

La communication porte sur des développements nouveaux dans la théorie et la pratique du percement de tunnels, et met en valeur les rapports existants entre le percement de tunnels et la géotechnique. On y décrit des progrès réalisés récemment, découlant d'études de modèles, de développements théoriques et de mesures sur place issus d'histoires de cas dans le monde entier. Des modèles à plasticité simplifiée, pouvant être utilisés par des concepteurs pour évaluer les mouvements du sol et les charges des revêtements du tunnel dans des conditions complexes du sol, sont décrits. On y décrit également le rôle important que jouent des tunnels pilote et des mesures in-situ dans la validation de ces modèles, sur la base d'une histoire de cas à Bolu, en Turquie, et de projets de percement de tunnels divers. On examine des progrès techniques réalisés récemment dans le percement de tunnels avec équilibre de la pression terrestre (EPB), illustrés par des mesures effectuées dans le cadre de la liaison ferroviaire du Tunnel sous la Manche, en mettant l'accent sur des facteurs clé influant sur des pertes de volume, par exemple la pression sur la face, le conditionnement du sol et le fonctionnement efficace du transporteur à vis sans fin. On décrit une étude de cas effectuée récemment à Bologne, dans laquelle on a employé de façon innovante le percement directionnel pour l'installation de tubes de scellement courbes, dans le cadre d'un projet de scellement de compensation dans des sols granulaires. On y discute de mouvements du sol et de déformations du revêtement des tunnels avec le temps, dont la magnitude est fonction de la perméabilité relative du revêtement des tunnels et du sol, du degré d'anisotropie dans la perméabilité du sol, et de la pression interstitielle initiale, préalablement au percement des tunnels. On examine en outre les effets, sur les canalisations, du tassement dus au percement de tunnels, sur la base de tests centrifuges et de solutions analytiques ; on présente une nouvelle méthode conceptuelle en tenant compte de la réduction de la rigidité du sol avec l'augmentation de la déformation de cisaillement découlant de la perte du volume du tunnel. La communication se termine par la description d'une technique de détection distribuée des déformations, faisant usage de la technologie des fibres optiques, basée sur la réflectométrie optique à domaine temporel de Brillouin (BOTDR), et son application innovante dans les contrôles in situ sur un tunnel de maçonnerie, sous lequel on construit un nouveau tunnel.

INTRODUCTION

This lecture focuses on a number of new developments in both the theory and practice of tunnelling—and on the fundamental role of geotechnics in all of these. The lecture draws on new research—involving analysis, centrifuge model tests and field measurements—together with a selected number of recent case histories of tunnel construction where there has been significant innovation.

Discussion on this paper closes on 1 May 2009, for further details see p. ii.

* University of Cambridge.

The following five topics are covered:

(*a*) the role of simplified models and their application to deep tunnels in clays
(*b*) ground movement control
  (i) advances in earth pressure balance (EPB) tunnelling machine technology
  (ii) recent developments in compensation grouting
(*c*) long-term ground movements
(*d*) effects of tunnelling on buried pipes
(*e*) advances in fibre optic technology for field monitoring.

These particular topics have been selected because they all

have important new implications for the design and construction of tunnels. Also, they all illustrate the fundamental role of geotechnics in enhancing innovation in tunnelling practice.

First, the lecture discusses the role of simplified models and their usefulness in application to the design of deep tunnels in clays: this will be illustrated by a recent case history in complex and challenging ground conditions. Second, the lecture focuses on ground movement control: this is undoubtedly a crucial issue for all tunnelling projects in soft ground in urban areas. This topic is divided into two parts: recent advances in earth pressure balance tunnelling machine technology for ground movement control are discussed, and then some important new developments in the practice of compensation grouting are presented. Both of these are illustrated by case histories. The third topic also covers ground movements, but focuses on long-term ground movements and their influence on tunnel lining behaviour: this is becoming increasingly important, as it is recognised that in some cases ground movement caused by tunnelling can be very significant, and can continue for many years.

Ground movements due to tunnelling, and their effects on structures, are increasingly important as more underground construction is undertaken in urban areas, but their effects on services are all too often neglected. The fourth part of the lecture presents some new insights into the effects of tunnelling on buried pipes. Field monitoring is vital for all tunnelling projects, and the final part of the lecture addresses some recent advances in fibre optic technology for field monitoring, illustrated by some case histories.

SIMPLIFIED MODEL FOR DEEP TUNNEL CONSTRUCTION IN CLAYS

Cavity contraction

The behaviour of an advancing tunnel in clay is illustrated in Fig. 1. As a simplification, axisymmetric conditions are assumed: that is, all ground movements around the tunnel are radial, and equal at any radius, so that vertical movements equal horizontal movements. The movements are radial in a spherically symmetric sense at the tunnel heading, and in an axisymmetric sense further back from the heading. This assumption is therefore strictly applicable only to deep tunnels (typically with cover-to-diameter ratios in excess of 5). The tunnel is of outside diameter D, and the lining is installed at a distance P behind the face. It is assumed that the rate of advance of the tunnel is sufficiently fast that the clay behaviour around the heading is undrained. There is a build-up of pressure σ_L on the lining, from zero (when the lining is installed) to a maximum value σ_L at some distance back from the face (typically about 2D). As shown in Fig. 1, radial ground movement (δ) at the position of the tunnel extrados begins some distance ahead of the tunnel face, and increases to a value δ_1 at the point when the lining is installed. Pressure then builds up on the lining as the tunnel face moves away from it, and further radial movement of the soil and lining, δ_2, takes place.

In the case of open-face tunnelling, particularly where the lining is being installed reasonably close to the face (i.e. for small P/D), the ground response ahead of the tunnel can be idealised in terms of spherical cavity unloading (Mair *et al.*, 1992a; Mair & Taylor, 1993); the inner radius of the sphere is equal to that of the tunnel. This is illustrated in Fig. 2(a). Assuming that the radius of the boundary of the clay is large in comparison with the radius of the tunnel, the soil movement δ ahead of the tunnel face (at a radius r) is given by classical spherical cavity contraction theory as

$$\delta = a\frac{s_u}{E_u}\left(\frac{a}{r}\right)^2 \exp\left(0{\cdot}75N^* - 1\right) \tag{1}$$

where a is the tunnel radius, s_u is the undrained shear strength of the clay, E_u is the undrained Young's modulus of the clay, and $N^* = \sigma_0/s_u$ (σ_0 being the total overburden pressure at the tunnel axis). The ground movement at the face, δ_1, is given by substituting $r = a$ in equation (1) to give

$$\delta_1 = a\frac{s_u}{E_u} \exp\left(0{\cdot}75N^* - 1\right) \tag{1a}$$

A further idealisation is that, as tunnel construction progresses and the tunnel face moves away from the lining that

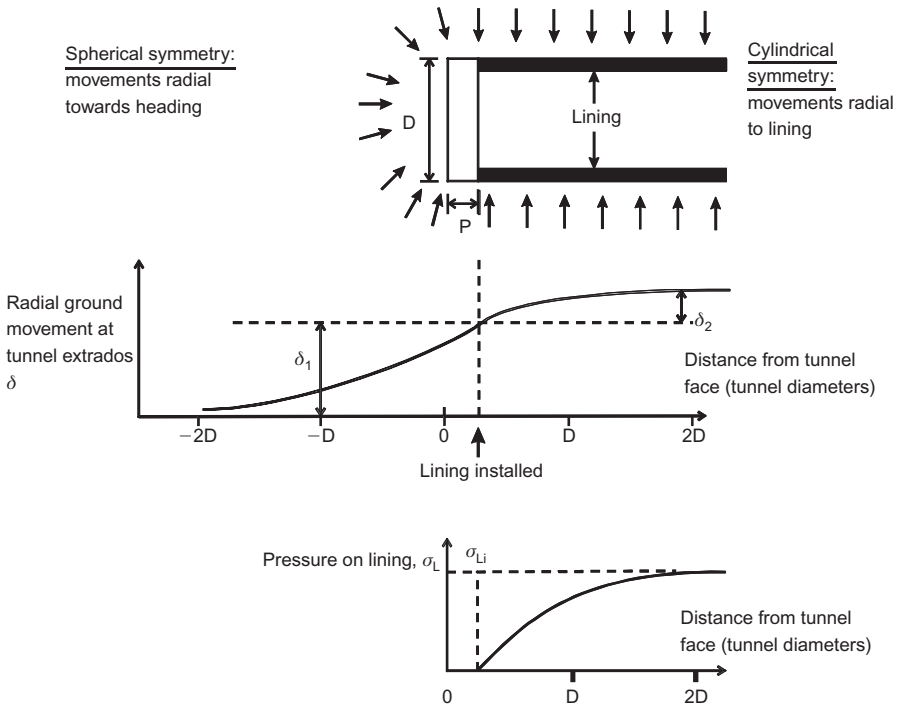

Fig. 1. Simplified model for an advancing tunnel in clay

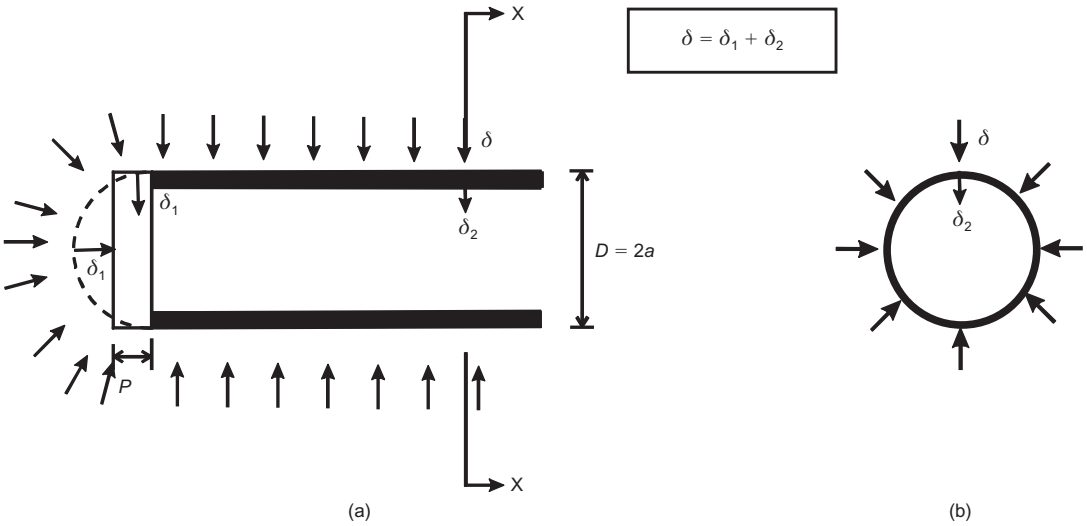

Fig. 2. Simplified assumptions for a tunnel heading: (a) spherical cavity unloading at tunnel face; (b) section X–X, cylindrical cavity unloading away from tunnel face

has been installed, the conditions become more like those corresponding to cylindrical cavity unloading, as illustrated in Fig. 2(b). The radial ground movement δ_r (at a radius r) is given by classical cylindrical cavity contraction theory (Mair & Taylor, 1993) as

$$\delta_r = 3a\frac{s_u}{2E_u}\left(\frac{a}{r}\right)\exp(N-1) \tag{2}$$

where N is the stability ratio $= (\sigma_0 - \sigma_{L)}/s_{u.}$

The immediate lining pressure σ_{Li} can be derived by considering the elastic-plastic ground response to unloading of a cylindrical cavity, taking into account the stiffness of the lining, as shown in Fig. 3. Line ABD is the calculated response of the ground to cavity unloading, and line XC is the lining response. This classical calculation, linking ground response to support reaction, is well known in the context of underground support for tunnels in rocks (e.g. Ward, 1978; Hoek & Brown, 1980; Panet & Guenot, 1982). As the total radial stress (acting at the external radius of the tunnel lining) σ_r is released from its initial value σ_0 at point A, radial soil deformation δ takes place. Idealising the clay as linear elastic-perfectly plastic, the behaviour is initially elastic until point B, when a plastic zone begins to develop around the tunnel boundary. For $N \leqslant 1$ the cylindrical cavity is elastic. By substituting $N = 1$ (and, associated with this, $s_u = \sigma_0 - \sigma_L$) into equation (2) it can be easily shown that the straight line AB in Fig. 3, for $r = a$ and $\sigma_L = \sigma_r$, is given by

$$\sigma_r = \sigma_0 - \frac{2E_u\delta}{3a} \tag{3}$$

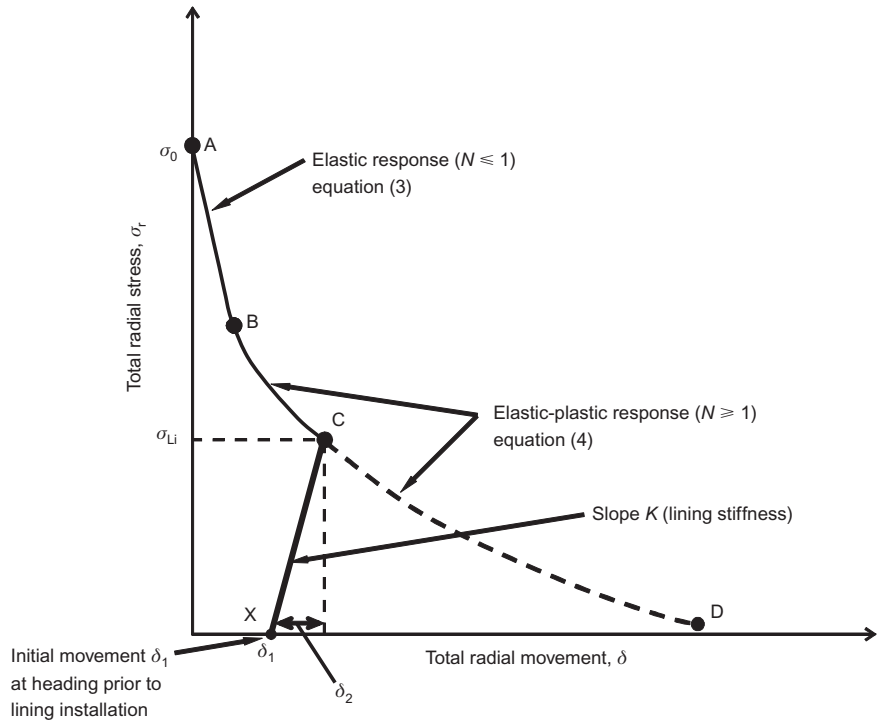

Fig. 3. Ground reaction curve (cylindrical cavity unloading): elastic response (equation (3)); elasto-plastic response (equation (4))

The elastic-plastic ground response, for $N \geqslant 1$, corresponding to the curve BD, can be obtained by rearranging equation (2), putting $r = a$ to give

$$\sigma_r = \sigma_0 - s_u \ln\left(\frac{2E_u\delta}{3as_u}\right) - s_u \quad (4)$$

The ground response ABD in Fig. 3 is often referred to by tunnel lining designers as the *ground reaction curve*. The tunnel lining is installed at point X, after the radial movement δ_1 has already occurred, as shown in Fig. 1. Pressure then builds up on the tunnel lining, and the subsequent soil and lining displacement δ_2 is determined by the stiffness of the lining. Equilibrium is reached at C, and the maximum value of lining pressure (in the short term, under undrained conditions) is σ_{Li}.

The initial ground movement δ_1 prior to lining installation is of key importance. The effect of a larger value of δ_1 would be a smaller lining stress σ_{Li} being obtained. This important effect has been understood for a long time in the tunnelling industry; it is also one of the underlying principles of the New Austrian Tunnelling Method (NATM), in which delay of installation of tunnel support leads to reduced pressures and loads being induced on the support. Hence, if δ_1 can be predicted, reasonable estimates of the lining pressure can be made.

Influence of lining stiffness

The influence of lining stiffness on the predicted lining pressure can be seen from Fig. 4. A more flexible lining results in a lower pressure, as can be seen from the line XC_1 compared with XC. The radial stress on the lining is given by

$$\sigma_{Li} = K\delta_2 \quad (5)$$

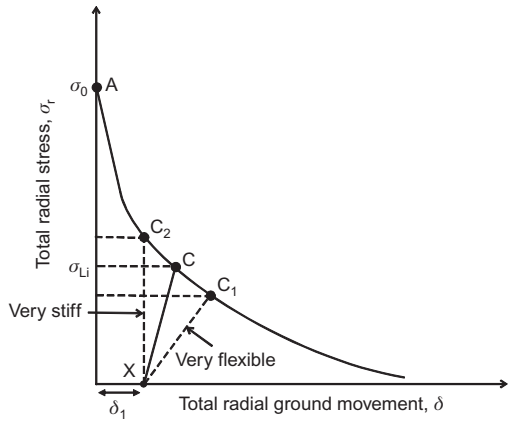

Fig. 4. Influence of lining stiffness on predicted lining pressure: very stiff lining gives upper bound to lining pressure σ_{Li} ($\delta = \delta_1$)

where K is an equivalent spring stiffness relating the inward movement of the lining, δ_2, to the radial stress acting on it. For a solid tunnel lining of thickness t and outer diameter D, and assuming that t/D is small, it can be shown (Ward, 1978) that

$$K \approx \frac{4E_l t}{D(D-t)} \quad (6)$$

where E_l is the Young's modulus of the lining.

A generalised form of the simplified model for tunnel construction in clay soils is shown in non-dimensional form in Fig. 5. Different ground response curves, derived from equations (3) and (4), are shown for a range of stability ratios (Mair *et al.*, 1992a). The initial ground movement δ_1 at the tunnel face is assumed to be that calculated from the spherical cavity contraction idealisation (equation (1a)). The

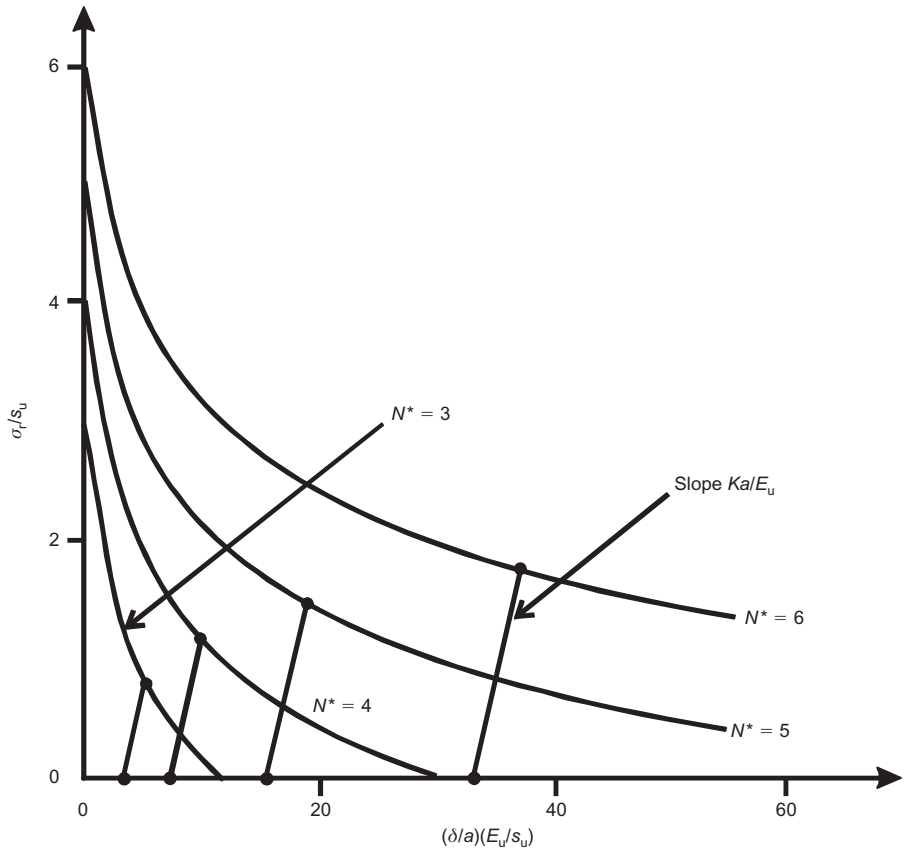

Fig. 5. Normalised ground reaction curves for design: $N^* = \sigma_0/s_u$; K = lining stiffness (Mair *et al.*, 1992a)

lines representing the lining response, with slope Ka/E_u, are shown with a slope of 20, which is typical for many tunnel linings in stiff clays. The intersection of the ground response curves with the lines representing the lining response enables designers to rapidly assess the immediate lining pressure (expressed in terms of the total radial stress σ_r normalised by the undrained shear strength s_u).

Upper bound to lining pressure: a very stiff lining

A very stiff lining is represented by the vertical line XC_2 in Fig. 4 and results in an upper bound to the lining pressure. In this case, the radial soil movement δ_r at $r = a$ (given by equation (2)) is equal to the soil movement at the face, δ_1 (given by equation (1a)). Setting δ (for $r = a$) equal to δ_1 and combining equations (1a) and (2) leads to an expression for the tunnel lining pressure as a proportion of the total overburden pressure:

$$\frac{\sigma_{Li}}{\sigma_0} = 0{\cdot}25 + \left(\frac{1}{N^*}\right)\ln\left(\frac{3}{2}\right) \tag{7}$$

Equation (7) is applicable only where both the ground adjacent to the spherical cavity (ahead of the tunnel) and the ground adjacent to the cylindrical cavity (the lined tunnel) are in a plastic state. The ground surrounding the cylindrical cavity will be in an elastic state for $N \leqslant 1$; substituting $N = 1$ in equation (2), setting $\delta_r = \delta_1$ (both for $r = a$) and combining equations (1a) and (2), it is found that $N^* = 1{\cdot}87$. Hence equation (7) is applicable only for $N^* \geqslant 1{\cdot}87$. The ground adjacent to the spherical cavity will be in an elastic state for $N^* \leqslant 4/3$, and therefore for $4/3 \leqslant N^* \leqslant 1{\cdot}87$ the spherical cavity will be in a plastic state with the cylindrical cavity remaining in an elastic state. Hence for $4/3 \leqslant N^* \leqslant 1{\cdot}87$ the tunnel lining pressure as a proportion of the total overburden pressure can be derived for a very stiff lining by combining equations (1a) and (3), leading to

$$\frac{\sigma_{Li}}{\sigma_0} = 1 - \left(\frac{2}{3N^*}\right)\exp\left(0{\cdot}75N^* - 1\right) \tag{8}$$

For $N^* \leqslant 4/3$, ground around both the spherical and cylindrical cavities will be elastic. Substituting $N^* = \sigma_0/s_u = 4/3$ in equation (1a), the deformation of the elastic spherical contracting cavity is given by

$$\delta_1 = \frac{3\sigma_0 a}{4E_u} \tag{9}$$

Hence for fully elastic conditions the tunnel lining pressure as a proportion of total overburden pressure can be derived for a very stiff lining by combining equations (3) and (9) and putting $\sigma_r = \sigma_{Li}$, leading to the simple relation

$$\frac{\sigma_{Li}}{\sigma_0} = 0{\cdot}5 \text{ (for } N^* \leqslant \tfrac{4}{3}) \tag{10}$$

Equations (7), (8) and (10) are shown plotted in Fig. 6, from which it can be seen that the tunnel lining pressure varies between 30% and 50% of the total overburden pressure for the wide range of stability ratio N^* of 0–6, the proportion reducing with increasing N^*. It is interesting to note that the tunnel lining pressure for a very stiff lining, given by equations (7), (8) and (10), is independent of the ground stiffness, and is simply a function of stability ratio N^* (for $N > 4/3$). This is because the term E_u/s_u cancels out in the algebra leading to equations (7), (8) and (10). It is also of interest to note that for weaker ground (i.e. for high values of N^*) the ratio σ_{Li}/σ_0 predicted by equations (7) and (8) reduces (albeit slowly, as shown in Fig. 6). This is because the weaker ground leads to higher deformations occurring ahead of the face prior to installation of the lining; the consequence of more ground deformation before installation is a smaller pressure induced on the lining (see Fig. 3).

Summary

The simplified model for characterising ground movements around a tunnel and the development of the immediate short-term load on the tunnel lining can be summarised as follows. First, using the spherical cavity contraction idealisation, estimate the maximum soil movement δ_1 at the tunnel face prior to installing the tunnel lining. Second, combine this with the cylindrical contraction idealisation and the appropriate lining stiffness to calculate the immediate lining pressure. By assuming that the lining circumferential stiffness is high, simple upper bounds to the lining pressure are derived, giving $\sigma_{Li}/\sigma_0 = 0{\cdot}3$–$0{\cdot}5$ for a wide range of stability ratios.

COMPARISON OF SIMPLIFIED MODEL WITH FIELD DATA

Ground movements

The idealised spherical contraction model for the ground movements ahead of the tunnel face (equation (1)) implies a linear relationship between the non-dimensional quantities δ/a and $(a/r)^2$; similarly the idealised cylindrical contraction model (equation (2)) implies a linear relationship between

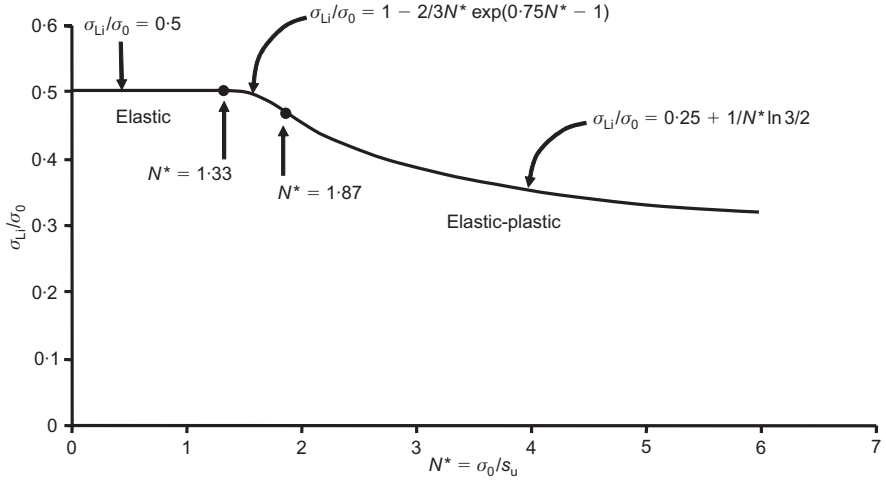

Fig. 6. Short-term lining pressure predicted for very stiff lining

δ_r/a and a/r. These are shown in Figs 7(a) and 7(b) respectively (Mair & Taylor, 1993).

Field measurements by Ward (1969) of axial ground movements ahead of an advancing tunnel in London Clay are shown in Fig. 8(a): these are shown plotted in non-dimensional terms (see Fig. 7(a)) in Fig. 8(b), assuming that the centre of the contracting sphere is one tunnel radius from the tunnel face (Mair & Taylor, 1993). The tunnel was 4·1 m in diameter at a depth of 24 m, and the measurements were made by means of rod extensometers installed from another tunnel (see Fig. 8(a)). The linear nature of the dimensionless plot in Fig. 8(b) confirms that the idealisation of the spherical contraction model is reasonable. Adopting a linear elastic-perfectly plastic model for the soil behaviour, and assuming that N^* is generally around 2·5 for London Clay, the slope of the line in Fig. 8(b) gives a ratio E_u/s_u of 300: this is also consistent with analysis of radial soil movements around tunnels in London Clay (Mair & Taylor, 1993).

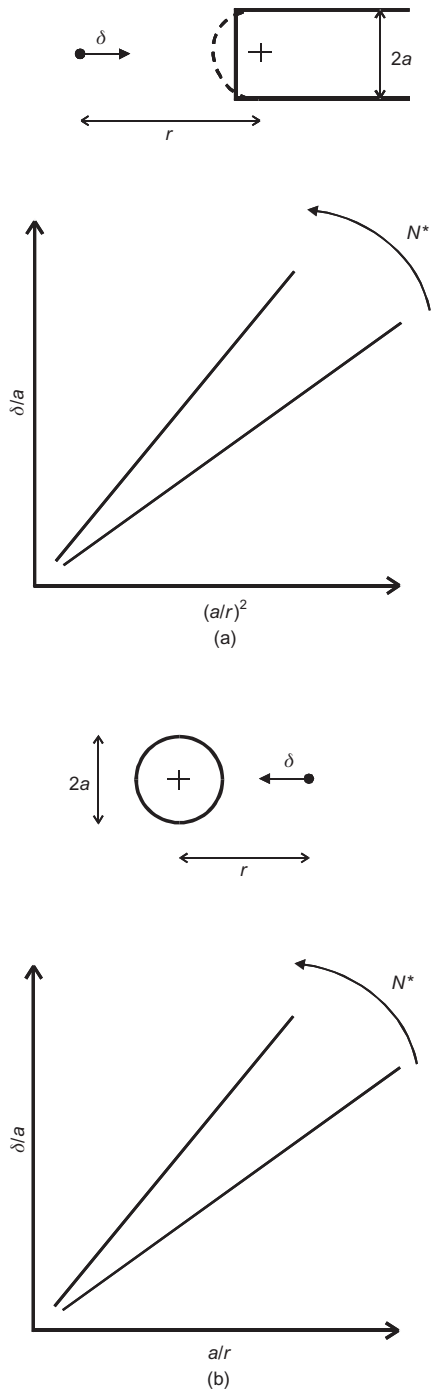

Fig. 7. Radial deformation associated with cavity unloading: (a) spherical (tunnel heading); (b) cylindrical (away from tunnel heading)

Field measurements of axial ground movements were also reported by Wong *et al.* (1999), in this case for the Tartaguille tunnel for a TGV project in France. A 14·8 m diameter tunnel in a mudstone of undrained shear strength 1·2 MPa was constructed with an open face, and lined with sprayed concrete, at a depth of 110 m: the range of axial ground movement measurements is shown in Fig. 9. These measurements were obtained by means of horizontal multiple-point extensometers installed in the centre of the tunnel face at two separate locations. Fibreglass face bolts were employed, but Wong *et al.* concluded that their stiffness relative to the ground was relatively low, and therefore their contribution in reducing the axial ground movements was small. The measurements in Fig. 9 are plotted in non-dimensional terms in Fig. 10; as for the London Clay data considered earlier, it has been assumed that the centre of the contracting sphere is one tunnel radius from the tunnel face. The general linearity of the plot in Fig. 10 again confirms that the idealisation of the spherical contraction model is reasonable. The solid line shown in Fig. 10 represents a reasonable fit through the data: taking the total overburden pressure of 2·3 MPa assumed by Wong *et al.* (corresponding to the tunnel depth of 110 m and a bulk unit weight of 21 kN/m^3), and an undrained shear strength of 1·2 MPa, the ratio E_u/s_u derived from the slope of the line is 390, giving $E_u = 469$ MPa.

Dilatometer tests, self-boring pressuremeter tests and plate load tests were undertaken for the Tartaguille project, from which Wong *et al.* report that design parameters of $s_u = 1{\cdot}2$ MPa and $E_u = 400$ MPa were selected. Taking these parameters, together with the total overburden pressure of 2·3 MPa assumed by Wong *et al.* (corresponding to the tunnel depth of 110 m and a bulk unit weight of 21 kN/m^3), the predicted axial ground movement from the spherical contraction model (equation (1)) is shown plotted in Fig. 10. Reasonably good agreement is obtained between the prediction using the assumed design parameters and the field measurements, confirming the value of the simplified model in validating the selected design parameters.

Lining pressures

Measurements of lining performance were made for a 4·7 m OD tunnel constructed at a depth of 223 m in hard Boom Clay at Mol, Belgium (Neerdael & de Bruyn, 1989). Full details of the measurements and their interpretation are given by Mair *et al.* (1992a) and Mair (1993). Fig. 11 shows data from load cells incorporated in the lining, converted to equivalent radial pressure acting on the lining. Construction progress was slow: the time to construct a length of tunnel equal to an excavated diameter was about 20 days. The measurements show a build-up of lining pressure to an approximately constant value after about 60 days, which is equivalent to a tunnel length of about three diameters. The lining pressure predicted by the simplified model is shown in Fig. 11: this assumed a linear elastic-perfectly plastic total stress model ($s_u = 1{\cdot}0$ MPa, $E_u = 400$ MPa derived from laboratory and in situ testing), and took into account the actual stiffness of the lining, allowing for wood packing between the lining blocks (Mair *et al.*, 1992a). A lining pressure similar to that predicted by the simplified model was predicted by axisymmetric finite element analyses, assuming various soil models, reported by Mair *et al.* (1992a) and by Gaerber (2003).

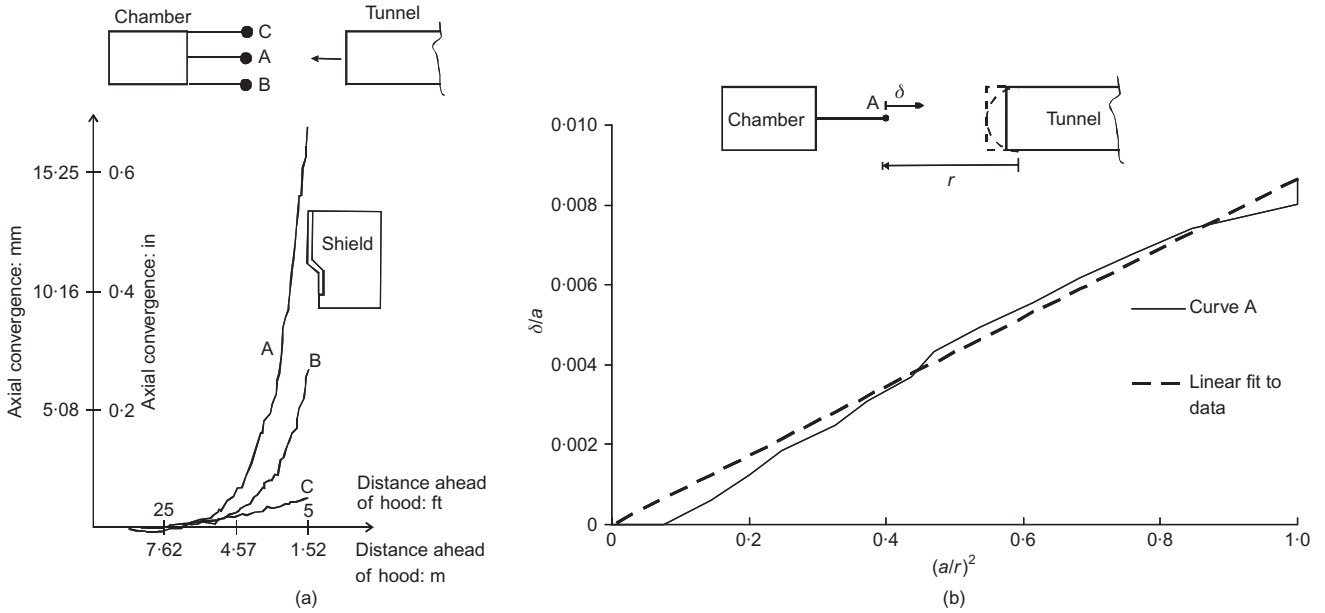

Fig. 8. Deformations in front of an advancing tunnel heading in London Clay: (a) after Ward (1969); (b) from Mair & Taylor (1993)

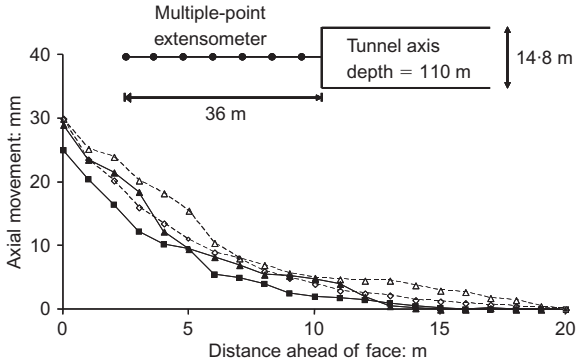

Fig. 9. Field data from Tartaguille tunnel: axial ground movements (Wong *et al.*, 1999)

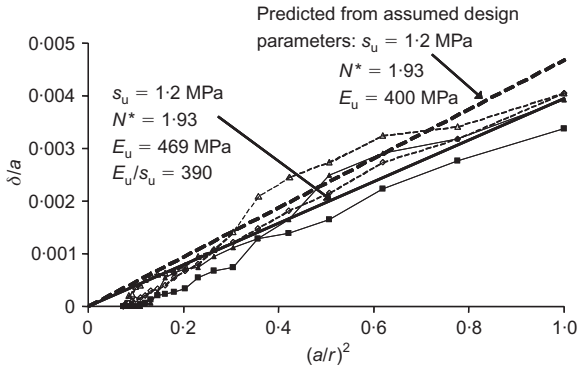

Fig. 10. Non-dimensional plot of Tartaguille tunnel axial movements (see Fig. 9)

Despite the significant scatter in the measurements, Fig. 11 shows that there is reasonable agreement between the field data and the lining pressure predicted by the simplified model.

Summary

The essence of the simplified model is the idealisation of open-face tunnelling as spherical cavity contraction (at the tunnel heading) and cylindrical cavity contraction. Axial ground movement patterns and short-term lining pressures

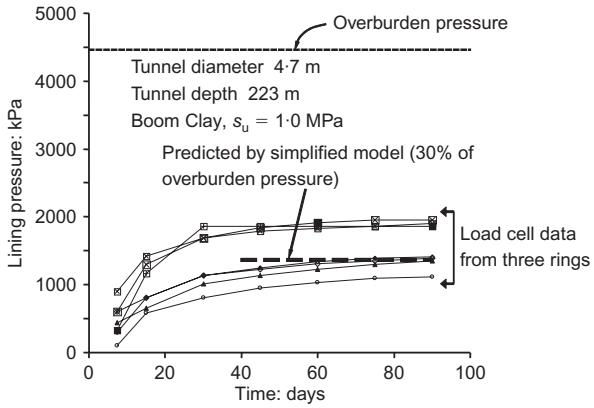

Fig. 11. Tunnel lining pressures at Mol (Mair *et al.*, 1992a)

predicted by the model are in good agreement with field measurements. The model predicts short-term lining pressure 30–50% of overburden for very stiff linings—and this depends only on N^* ($= \sigma_0 / s_u$).

The attraction of the model is its simplicity. In this age of increasing availability of sophisticated software for numerical analysis it is all too easy to lose the basic understanding of the essence of the problem, particularly if the ground conditions are complex. Engineers need pragmatic solutions for design that capture the key aspects of ground behaviour, without necessarily reproducing every detail: this was also emphasised by Poulos *et al.* (2005). The simplified model presented here provides such a pragmatic solution for tunnel construction in clay soils.

APPLICATION OF SIMPLIFIED MODEL TO TUNNELLING IN COMPLEX GROUND CONDITIONS: A CASE HISTORY IN BOLU, TURKEY

The simplified model described above was successfully applied to evaluate the ground behaviour during recent construction of tunnels in Bolu, Turkey, in complex ground conditions. Problems were encountered during construction of the twin highway tunnels, of about 16 m excavated diameter, in a faulted and highly tectonised sequence of rocks, using sprayed concrete and cast in situ concrete linings. Full details are given by Menkiti *et al.* (2001a). The

Bolu tunnels, which are 3·3 km long, are located in rugged, heavily forested and mountainous terrain. They are also located in a first-degree seismic environment, close to the North Anatolian Fault Zone, and were significantly affected by the 1999 Turkish earthquakes; the relevant seismic aspects are considered elsewhere (e.g. Menkiti *et al.*, 2001b; O'Rourke *et al.*, 2001). Here the focus is on design, construction and tunnel performance under static loading. The tunnel depth reached a maximum of 250 m, with the majority of the tunnels at a depth of 100–150 m; Fig. 12 shows 2 km of the southern section of the tunnels. The geology consists of highly tectonised and intermixed series of mudstones, siltstones and limestones, with very stiff to hard, heavily slickensided, highly plastic, fault gouge clay. Generally the ground comprises sub-angular blocks of hard material within a clayey matrix. The proportion of the clayey matrix varies substantially, and the poorest ground comprises zones of uniform fault gouge clay; the locations of some of the more extensive zones are shown in Fig. 12. Groundwater levels were also high, being 45–85% of the overburden cover above the tunnels, as indicated in Fig. 12.

The combination of poor ground conditions, high overburden pressures and high water levels resulted in extremely difficult tunnelling conditions. The original design was based on the New Austrian Tunnelling Method (NATM), with a sprayed concrete primary lining augmented with rock bolts and light steel ribs. In line with NATM philosophy the primary lining had been intended to support the immediate ground loads, with the aim of providing a relatively stable environment within which the inner lining could be cast to achieve the required long-term safety. The original design cross-section is shown in Fig. 13: the thickness of the shotcrete lining was 450 mm, and the shotcrete design cube strength was 20 MPa. In the more clayey ground, large deformations in excess of 1 m were recorded, as shown in Fig. 14; these were accompanied by serious shotcrete damage and deterioration, in the form of compression crushing and 'onion peeling'. At one location, where the tunnel was being excavated through very poor fault gouge clay, partial collapse of the top heading occurred during bench and invert excavation, as shown in Fig. 15: a bearing capacity failure resulted in excessive settlement of the top heading and failure of the temporary top heading invert.

A full design review was undertaken. Information on the geotechnical properties of the ground was very sparse, mainly because of the difficulties of undertaking sampling from boreholes in excess of 150 m deep in mountainous terrain. An exploratory pilot tunnel was therefore constructed over a length of 829 m (in the worst ground conditions), with the principal aims being

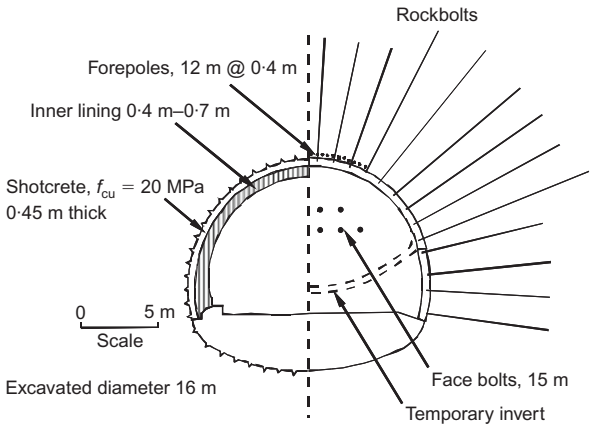

Fig. 13. Typical cross-section of Bolu tunnels: original design (Menkiti *et al.*, 2001a)

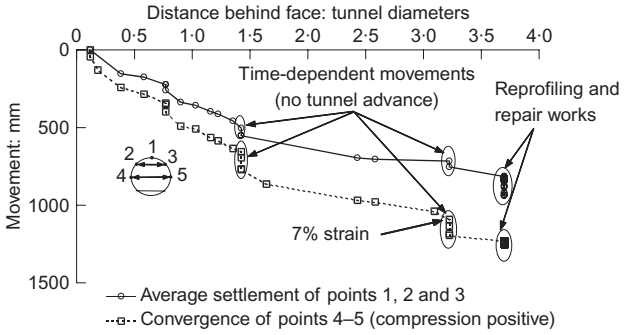

Fig. 14. Bolu tunnels: typical deformations, original design, high-plasticity Flyschoid Clay (Menkiti *et al.*, 2001a)

(*a*) to define the geology in advance of the main tunnel drives
(*b*) to take high-quality block samples for laboratory testing (classification, index and strength tests)
(*c*) to measure axial ground movements ahead of the tunnel face, and to undertake in situ tests (pressuremeter tests and pore pressure measurements).

The pilot tunnel was circular, and of excavated diameter 5·6 m. The simplified model described earlier was applied to select a suitable thickness of lining for the pilot tunnel. At the stage of designing the pilot tunnel the geotechnical properties of the clayey ground were not well established (particularly its strength), but, as shown in Fig. 5, the stress on the lining predicted by the simplified model is not

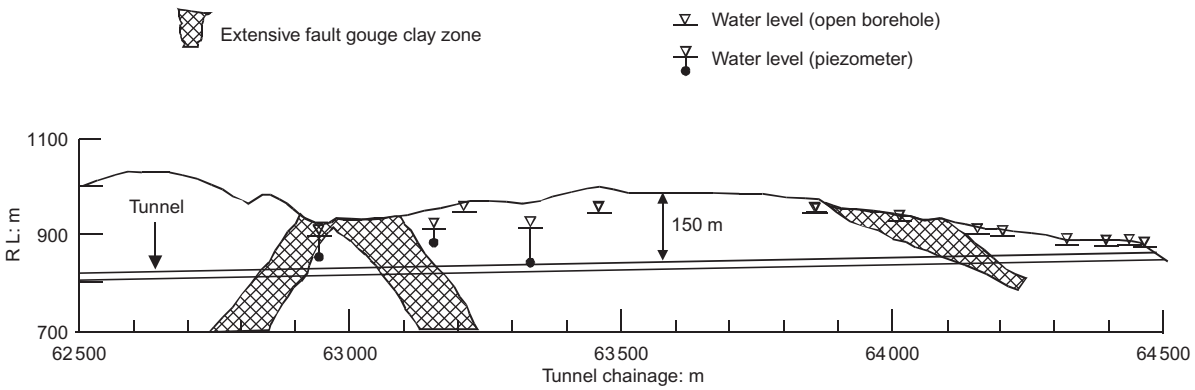

Fig. 12. Longitudinal section through southern section of Bolu tunnels (Menkiti *et al.*, 2001a). Ground conditions comprise highly tectonised, intermixed mudstones, siltstones and limestones. The materials exist as blocks of hard material within a very stiff to hard, slickensided, high-plasticity clay matrix ('Flyschoid Clay'). Fault gouge clay zones comprise very stiff to hard, heavily slickensided, high-plasticity fault gouge clay

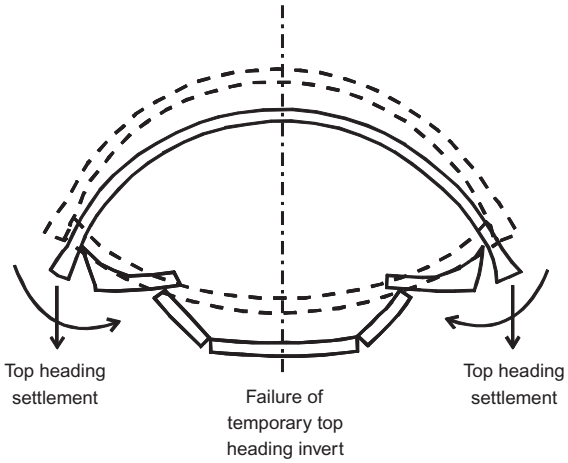

Fig. 15. Bolu tunnels: top heading collapse mechanism in fault gouge clay (Schubert *et al.*, 1997)

particularly sensitive to the value of N^*. The extreme range of N^* was estimated to be 3–6, for which equation (7) predicts the ratio σ_{Li}/σ_0 to be in the range 32–38·5%. On the basis of this simplified model, the lining stress was estimated to be 35% of the total overburden stress, and consequently a lining thickness of 400–500 mm was selected for the pilot tunnel, depending on the ground conditions (the design cube strength for the sprayed concrete was 20 MPa, which is somewhat lower than usual). The pilot tunnel was excavated full face in lengths of 1–1·5 m at an average progress rate of 1·9–2·3 m/day.

Radial stress cells were incorporated in the shotcrete lining of the pilot tunnel, but these are notoriously difficult to interpret (e.g. Clayton *et al.*, 2002), and therefore reliable measurements of the ground loading on the lining were not obtained. However, at two locations there was a failure of the pilot tunnel invert, one of which is illustrated in Fig. 16.

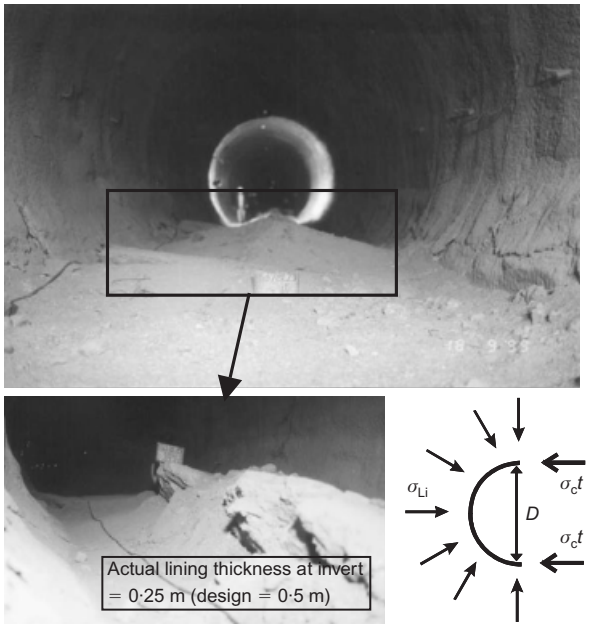

Fig. 16. Bolu pilot tunnels: failure of pilot tunnel in fault gouge clay due to reduced thickness of lining in the invert. Assuming axisymmetric conditions, $\sigma_{Li} = (2\sigma_c t)/D$, where σ_{Li} = total radial stress, σ_c = compressive stress in lining, t = thickness of lining. (Using this, back-analysis of failure gives σ_{Li} = 40% of the overburden pressure. For comparison, the simplified model gives σ_{Li} = 35% of the overburden pressure.)

This provided an opportunity to back-calculate the ground loading acting on the pilot tunnel using the classical equilibrium condition for a smooth circular ring illustrated in Fig. 16, assuming axisymmetric conditions and ignoring any bending. The radial ground loading σ_{Li} is given by

$$\sigma_{Li} = \frac{2\sigma_c t}{D} \tag{11}$$

where σ_c is the average compressive stress in the lining, and t and D are the thickness and diameter of the lining respectively.

Investigation showed that the invert thickness in the region of both failures was only 250 mm, compared with the 500 mm that had been designed. At the time of the invert failure the shotcrete lining was only 14 days old, and in situ cores gave a cube strength of 22 MPa. By applying the commonly assumed factor of 0·67 to the cube strength to obtain the equivalent cylindrical compressive strength and putting this equal to σ_c in equation (11), and by assuming t = 0·25 m and D = 5·6 m, a radial ground loading acting on the lining of 40% of the overburden pressure is obtained (the pilot tunnel axis was at a depth of 150 m and the bulk unit weight was assumed to be 21·5 kN/m^3). This compares reasonably well with the value of 35% estimated from the simplified model.

Table 1 summarises the geotechnical description and index properties of the various units encountered in the pilot tunnel, and Table 2 lists their measured stiffness and strength parameters. Full details of the laboratory testing are given by Menkiti *et al.* (2001a).

The strength parameters were obtained from shear box tests and triaxial tests on block samples taken from the face of the pilot tunnel. The three geotechnical units of particular significance were the High PI Flyschoid Clay, the Blocky Flyschoid Clay, and the Area 3 Fault Gouge Clay. Typical results from shear box tests on the High PI Flyschoid are shown in Fig. 17. The shear box tests on the more tectonised samples, which are more representative of the mass strength of the ground, show τ/σ'_n values in the range 0·16–0·21, corresponding to residual angles of friction of 9–12°. By assuming a realistic range for the groundwater levels (from the piezometer readings) and applying the effective stress parameters derived from the laboratory tests, estimates of the undrained shear strength of the Flyschoid Clays are in the range 600–750 kPa. This is consistent with results of undrained triaxial tests performed on tectonised specimens cut from the block samples and with pressuremeter tests performed in situ in the pilot tunnel. The tectonised Flyschoid Clays illustrated ductile behaviour, as can be seen from Fig. 17.

Axial ground movements ahead of the face of the pilot tunnel were measured with the system shown in Fig. 18. A hollow closed-end tube with two sets of sliding joints was grouted into a horizontal borehole, using a high-quality grout at the end of the tube and a weak grout along its length. A measuring rod was inserted to the end of the tube to measure its position relative to a reference plumb line fixed to the tunnel lining. As the pilot tunnel face was advanced, the tube was progressively cut off. Measurements using this system were undertaken at three locations approximately equally spaced over a distance of 170 m in the pilot tunnel. Test 1 was undertaken in mixed face conditions, comprising the High PI Flyschoid Clay and the Blocky Flyschoid Clay; Tests 2 and 3 were principally in the High PI Flyschoid Clay. The measured axial ground movements are shown in Fig. 19, and are plotted in dimensionless form (as in Fig. 7(a)) in Fig. 20. In most cases it was not possible to obtain the measurements of the axial ground movement close to the tunnel face, because of interference by the

Table 1. Geotechnical description and index properties of ground conditions encountered at Bolu (Menkiti *et al.*, 2001a)

Unit	Consistency	PI: %	CP and mineralogy
High PI Flyschoid Clay	Stiff, highly plastic, heavily slickensided, clay matrix with occasional rock fragments	55	35–50%; smectite, with traces of kaolin
Blocky Flyschoid Clay	Medium plastic, silty clay matrix with gravel, cobbles and boulder-sized inclusions	25	30–50%; smectite, with traces of kaolin
Area 3 fault gouge clay (Ch 64140–64200)	Highly plastic, heavily slickensided, stiff clay gouge	55	30–60%
AS/EL fault gouge clays (Ch 62840–62905)	Very heavily slickensided, highly plastic, stiff to hard clay fault gouge	40–60	20–50%; smectite
Metasediments	Gravel, cobble- and boulder-sized shear bodies in soil matrix. Soil matrix is 20–60% by volume	10–15	5–25%; illite (58%) and smectite (23%) predominant
Crushed MCB	Crushed, weathered, highly sheared, clayey, very weak rock with slickensided, sandy silty clay fault gouge matrix	15	0–20%
Sound MCB	Fractured but competent rock UCS 6–12 MPa	NA	NA

PI, plasticity index; CP, clay percentage by weight (i.e. finer than 0·002 mm); MCB, metacrystalline basement rock; UCS, unconfined compression strength; NA, not applicable.

Table 2. Measured stiffness and strength parameters at Bolu (Menkiti *et al.*, 2001a)

Unit	Peak strength		Residual strength		G_0/σ'_v
	ϕ': degrees	c': kPa	ϕ': degrees	c': kPa	
High PI Flyschoid Clay	15–17	100	9–12	50	500*
Blocky Flyschoid Clay	20–25	100	13–17	50	650*
Area 3 fault gouge clay (Ch 64140–64200)	13–16	100	9–12	50	700*
AS/EL fault gouge clays (Ch 62840–62905)	18–24	100	6–12	50	NA
Metasediments	25–30	50	20–25	25	825*
Crushed MCB[2]	20–25	50	15–20	25	950*
Sound MCB[2]	55	1500	NA	NA	High

* From high-quality pressuremeter tests.
MCB, metacrystalline basement rock; NA, not available; PI, plasticity index; ϕ', effective stress friction angle; c', effective cohesion; G_0, maximum shear modulus; σ'_v, initial vertical effective stress

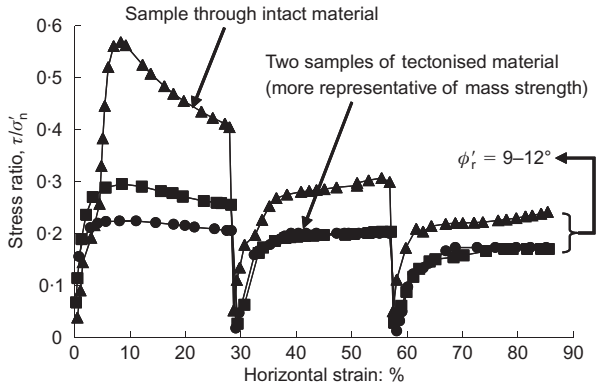

Fig. 17. Bolu tunnels: drained shear box tests on tectonised Flyschoid Clay

tunnel construction operations. Nevertheless, there is reasonable agreement for the three different tests, especially considering the complexity of the ground conditions. The general linearity of the data plotted in Fig. 20 confirms the validity of the spherical cavity contraction model, which is the framework for the simplified model. Taking the slope of the plot in Fig. 20 and applying the simplified model, the corresponding E_u/s_u ratios for the range of s_u values of 600–750 kPa are in the range 80–170.

The final design of the main tunnels proceeded using these geotechnical parameters derived from the pilot tunnel. Various tunnel cross-sections were designed, depending on the ground conditions established by the pilot tunnel: full details are given by Menkiti *et al.* (2001a). In the worst ground conditions, where there were zones of thick Fault Gouge Clay, it was concluded that top heading stability could not be achieved even with a temporary invert. This was because the depth and size of the tunnel, combined with the low undrained shear strength of the ground (600–750 kPa), meant that a bearing capacity failure was likely beneath the footing of the temporary invert (see Fig. 15). To overcome this problem, as shown in Fig. 21, the contractor chose to drive two pilot tunnels in the bench area, which were then backfilled with concrete, thus providing foundations with adequate bearing capacity to support the top heading. Primary support consisted of 300 mm of sprayed concrete, augmented by an 800 mm thick precast lining installed and grouted in place a short distance behind the face (8–16 m). The bench and deep monolithic invert were installed 22–35 m behind the face to achieve ring closure. No rock bolts were incorporated, these being judged to be ineffective in the fault gouge clay. A 600 mm thick inner reinforced concrete lining was finally installed, which had been designed taking into account seismic effects (O'Rourke *et al.*, 2001).

In summary, construction of the pilot tunnel for the Bolu

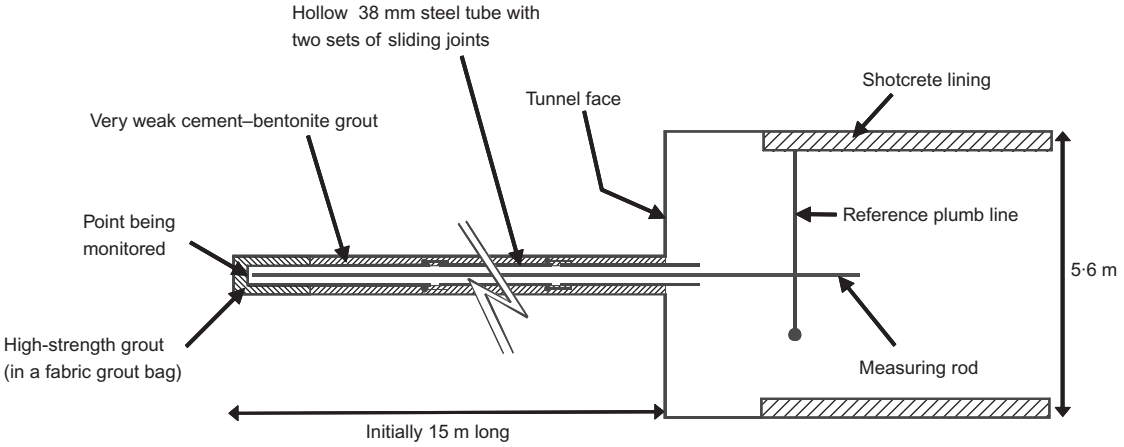

Fig. 18. Bolu pilot tunnel: system for measuring axial ground movements ahead of face

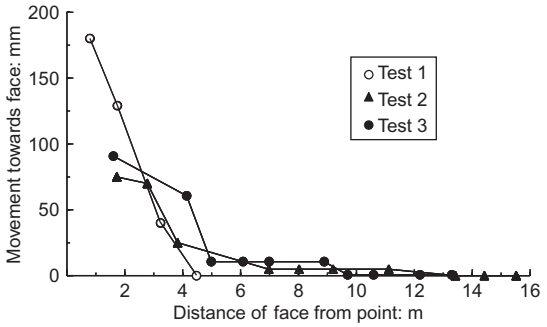

Fig. 19. Bolu pilot tunnel: measured axial ground movements ahead of face. Data from three tests over 170 m of tunnel (high-PI Flyschoid Clay)

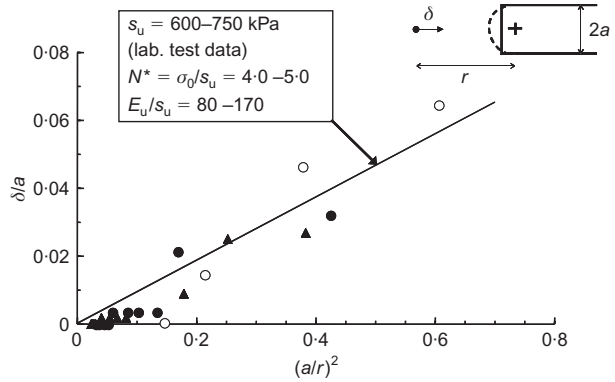

Fig. 20. Bolu pilot tunnel: non-dimensional axial ground movements (key as Fig. 19)

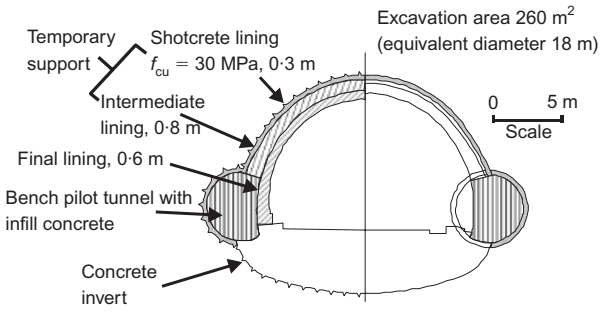

Fig. 21. Bolu tunnels: final design for thick fault gouge clay zone (Menkiti *et al.*, 2001a)

tunnel project provided an invaluable opportunity to investigate the ground behaviour, take samples, undertake in situ testing, and make measurements of axial ground movements ahead of the tunnel face. The simplified model provided a sound basis for estimating the immediate (short-term) radial stress acting on the pilot tunnel lining. It was then applied to interpret the measured axial ground movements ahead of the pilot tunnel face and establish a consistent set of geotechnical parameters for use in design.

It is clear from the pilot tunnel and subsequent investigations that the original design cross-section for the 16 m diameter tunnel, shown in Fig. 13, was failing in compression; the 450 mm thick lining was unable to sustain the lining pressure of around 40% of the overburden pressure indicated by the simplified model (and confirmed by the local failures of the invert of the pilot tunnel). The final design of the full-size tunnels proceeded successfully using the geotechnical parameters derived from observations made during construction of the pilot tunnel.

GROUND MOVEMENT CONTROL: ADVANCES IN EARTH PRESSURE BALANCE (EPB) TUNNELLING MACHINE TECHNOLOGY

Ground movements and volume loss

A key parameter of major importance in soft ground tunnelling is volume loss. Fig. 22 shows the development of surface settlement as a tunnel progresses (Attewell *et al.*, 1986), and Fig. 23 shows a transverse section through the resulting settlement trough. Extensive field measurements

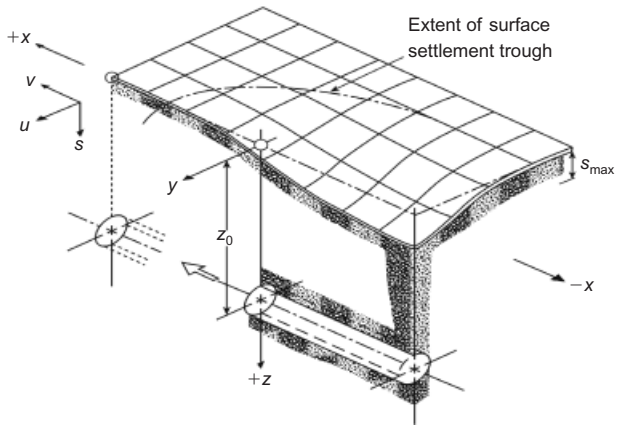

Fig. 22. Surface settlement trough above an advancing tunnel (Attewell *et al.*, 1986)

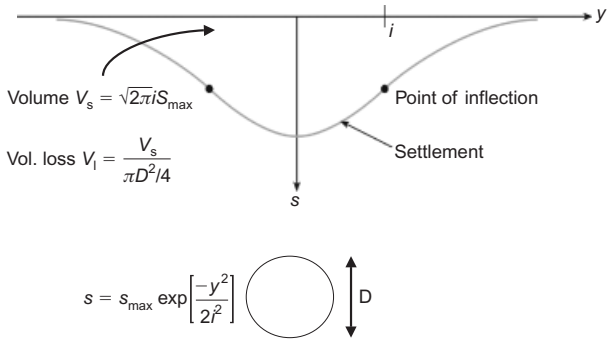

Fig. 23. Transverse settlement trough: Gaussian curve

have shown that the settlement trough can be well characterised by the Gaussian distribution (Peck, 1969; Schmidt, 1969; Rankin, 1988; Mair & Taylor, 1997), with the settlement given by the equation

$$S = S_{\max} \exp\left(-\frac{y^2}{2i^2}\right) \tag{12}$$

The volume of the settlement trough (per metre length of tunnel), V_S, can be evaluated by integrating equation (12) to give

$$V_S = \sqrt{2\pi}iS_{\max} \tag{13}$$

and this volume, expressed as a proportion of the theoretically excavated tunnel volume (usually expressed as a percentage) is the volume loss:

$$V_L = \frac{4V_S}{\pi D^2} \tag{14}$$

Typical volume losses for open-face tunnelling in soft ground are generally in the range 1–3% (Mair, 1996; Mair & Taylor, 1997). Closed-face tunnelling, with significant face support, tends to result in lower values than open-face tunnelling. Open-face tunnelling in London Clay can in some circumstances give rise to higher values: for example, in St James's Park in London volume losses as high as 3% were recorded, but this is exceptional, and can be attributed to particular features of the geology and the operational methods of tunnelling (Dimmock & Mair, 2006a, 2006b; Standing & Burland, 2006).

EPB tunnelling: key aspects

There have been considerable developments in earth pressure balance (EPB) tunnelling machine technologies in recent years: excellent ground movement control in a wide variety of ground conditions is now achievable, especially in ground that would be unstable in the absence of face support. The essence of an EPB machine is provision of substantial support to the excavated face at all times, thereby controlling ground movements. Fig. 24 shows the principal features of a modern EPB tunnel boring machine (TBM). The primary function of the cutterhead (1) is to excavate the soil; it is powered by the drive motor (2), all of which is within the circular steel skin (or 'shield') (3) of the TBM. The excavated soil passes into the pressurised head chamber immediately behind the cutterhead. Access into the chamber, if necessary, can be facilitated by means of compressed air being applied and access being via an air lock (4). A key feature of the EPB machine is the extraction of the excavated soil from the pressurised head chamber by means of a screw conveyor (5), which is an Archimedian screw within a cylindrical steel casing.

The screw conveyor plays an important role in the excavation process. The soil is extruded along the screw conveyor to the discharge outlet (7), where the soil is discharged at atmospheric pressure onto a conveyor belt (9). The rotational speed of the screw, its geometry, the restriction of the discharge outlet, and the soil properties all influence the soil flow rate and pressure gradient along the conveyor. The head chamber pressure supporting the tunnel face is regulated by controlling the rate of soil discharge in relation to the advance rate of the machine (and this leads to the pressure dissipation along the screw conveyor). Laboratory tests using an instrumented model screw conveyor with a range of soft clay samples and operating conditions, and their theoretical interpretation, are reported by Merritt (2004) and Merritt & Mair (2006, 2008). The factors influencing the chamber pressure during the excavation period are complex, but the details of the screw conveyor operation are of particular relevance. It is important that the extraction of the soil is well controlled, synchronised with the speed of excavation, and that the soil mixture is converted to a low-shear-strength paste (typically in the range 20–30 kPa) by suitable soil conditioning (Milligan, 2000; Merritt, 2004). Control of soil flow through the screw conveyor is necessary to control the volume of soil discharged, as well as the dissipation of pressure between the head chamber (in which it is high) and the conveyor outlet (which is at atmospheric pressure). If the soil is too 'fluid', control of the flow rate and pressure

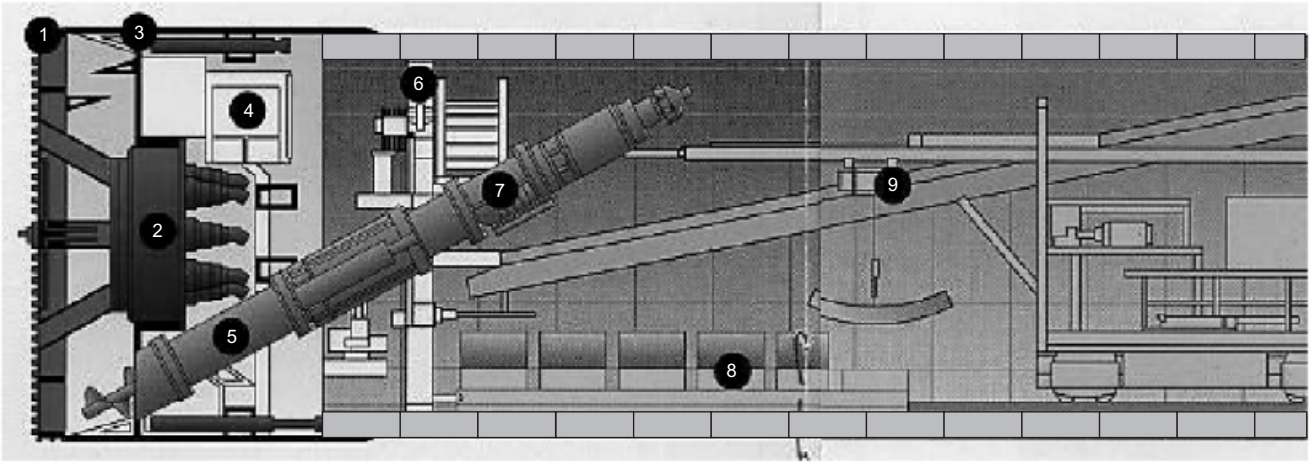

Fig. 24. Earth pressure balance tunnelling machine: 1, cutter head; 2, drive motor; 3, TBM skin; 4, airlock; 5, screw conveyor; 6, lining erector arm; 7, soil discharge; 8, lining segments; 9, belt conveyor

gradient can be problematic, because proper face control requires that the chamber is always filled with soil, whereas if the soil is too stiff the conveyor can require excessive power to operate or it can become jammed. Natural soils do not usually have ideal properties when excavated, and soil conditioning is often used to modify the properties to improve the operation of EPB machines.

Soil conditioning

Soil conditioning is achieved by injecting conditioning agents, most commonly foams or polymers, from the cutterhead and into the head chamber to mix with the soil during the excavation process. The effects of soil conditioning on soil properties are varied and complex: many of them are summarised by Maidl (1995), Leinala *et al.* (2000), Milligan (2001), Merritt *et al.* (2003), Merritt (2004), Boone *et al.* (2005), O'Carroll (2005) and Borghi (2006). The properties of the soil–chemical mixtures depend strongly on the type and quantity of the conditioning agent, or combination of agents, mixed with the ground. Operation of the tunnelling machine and control of the face pressure may be significantly affected by these different properties. The parameters that have to be selected for the soil conditioning comprise the type of agent (water, bentonite, polymer, foam or any combination of these) and their quantities. Further details of soil conditioning, definitions of injection parameters and typical quantities used for different ground conditions are given in Appendix 1.

Conditioning agents are sometimes also injected into the screw conveyor in order to modify further the properties of the spoil as it passes through the conveyor. This can also have the effect of reducing the screw torque. However, the sensitivity of the screw conveyor operation to the shear strength of the spoil suggests that the excavated soil should best be conditioned as early as possible (i.e. at the cutterhead and in the head chamber before it enters the screw conveyor) in order to maximise the mixing time and hence improve the homogeneity of the spoil in the excavation chamber (Borghi, 2006).

Tail void grouting

Following an excavation cycle, when the jacks are retracted, tunnel lining segments, (8) in Fig. 24, are erected within the TBM tail skin by means of an erector arm (6). As the tail skin leaves the tunnel lining, grout is injected under pressure to fill the annular void between the extrados of the segmental lining and the excavated ground. Tail skin seals prevent the grout from entering the TBM. This process of tail void grouting, together with high-quality face pressure control, is a vital part of ground movement control.

Provision of face pressure

In an EPB machine the support pressure to the excavation face is provided partly by the thrust from the cutterhead and partly by the chamber pressure, the relative proportion depending on the opening ratio η, defined as the ratio of the total openings surface area A_0 to the total face area A. Values of η vary for different machines; for larger values of η control of face pressure will depend more on the chamber pressure.

The pressure in the excavation chamber is controlled by the mass flow rate of soil and conditioning agents entering the chamber, and by that of the spoil discharged at the outlet of the screw conveyor. If the machine advances steadily, a reduction in the screw conveyor extraction rate will cause an increase in pressure in the excavation chamber: correspondingly, an increase in extraction rate will result in a reduction in chamber pressure. The control of the extraction rate is strongly affected by the mechanical properties of the spoil. The bulk modulus of the spoil (i.e. the mixture of soil and conditioning agents) also has a strong influence on the chamber pressure fluctuations. Compressible mixtures with low modulus (e.g. sand and foam) give less fluctuations. However, if the excavation chamber is full of spoil and the mixture is almost incompressible (for example if it is principally clayey soils and liquid conditioning agents), differences in the rates of excavation and spoil discharge may result in significant pressure fluctuations (Borghi, 2006).

EPB tunnelling on CTRL Contract 220

A simplified view of the geology for Contract 220 of the Channel Tunnel Rail Link (CTRL) in London is shown in Fig. 25. The tunnelling works on Contract 220 comprised 7·5 km of twin tunnels of outside diameter 8·1 m excavated with EPB machines westwards from the Stratford Box to the portal near St Pancras station in London. Full details of the project are given by Woods *et al.* (2007). A very wide range of ground conditions was encountered, as can be seen from Fig. 25: details are summarised by Borghi (2006). Upon launching from Stratford Box the tunnelling machines first encountered about 80 m of mixed face conditions of the

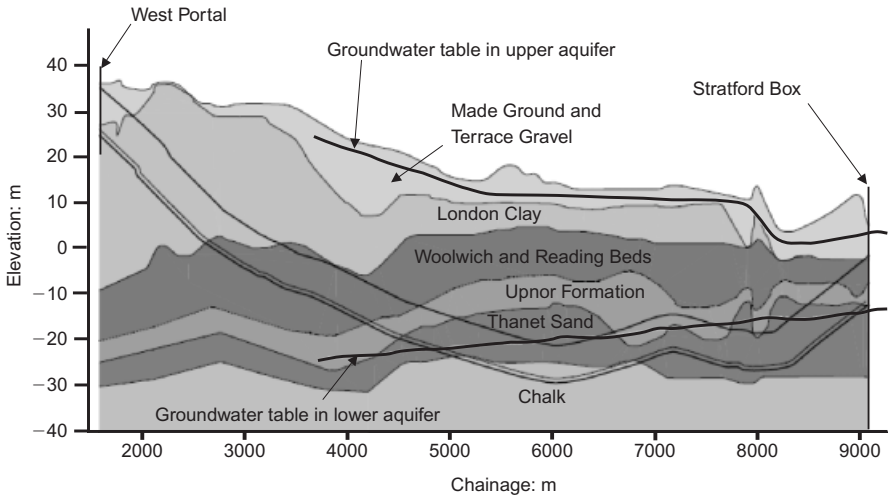

Fig. 25. Geology of CTRL Contract 220

Lambeth Group (Upnor Formation (UF), comprising sands, silts, clay, gravels and pebbles, and the Woolwich and Reading Beds, comprising very stiff clays). The proportion of the Lambeth Group soils then gradually reduced for the next 140 m, while the very dense silty Thanet Sand appeared in the invert; full-face Thanet Sand was encountered after 560 m of tunnel drive. Subsequently chalk was encountered in the invert, before the tunnels started rising in elevation crossing the full sequence of tertiary soils, including the gravels of the Harwich Formation (HF) at the base of the London Clay, with full-face London Clay in the final 1000 m of the drive. The tunnels were thus driven in a very wide variety of ground conditions, varying from dense sands and gravels to stiff clays and chalk, often in mixed face conditions.

Research has been undertaken at Cambridge University (Wongsaroj, 2005; Borghi, 2006) in collaboration with the contractor, Nishimatsu Construction, and the client, Rail Link Engineering. Surface settlement measurements from 48 instrumentation arrays were analysed (Wongsaroj *et al.*, 2005), and the results in terms of volume loss measured at the ground surface are shown in Fig. 26. It can be seen that, with only two exceptions, the measured volume loss was always less than 0·8% and often as low as 0·2%.

The high degree of ground movement control illustrated in Fig. 26 can be attributed to a number of important advances in EPB technology (British Tunnelling Society, 2005; O'Carroll, 2005). There have been significant developments in the technique of tail void grouting; good control of pressure and volume of grout injection is essential for effective control of ground movements. Also, filling the annulus around the EPB shield with a bentonite paste, as was undertaken on CTRL Contract 220, can significantly reduce ground movements.

Another key aspect of ground movement control is the control of chamber pressure. Fig. 27 shows an example of difficult chamber pressure control during three cycles of excavation and ring build during tunnelling in the Lambeth Group (Borghi & Mair, 2006): this example has been deliberately selected as a case of poor pressure control. The average chamber pressure (recorded by five pressure sensors) is plotted against time for the three construction cycles, each comprising two phases: the excavation phase, when the EPB machine is advancing; and the ring-build phase, when the machine is stationary during erection of the tunnel lining.

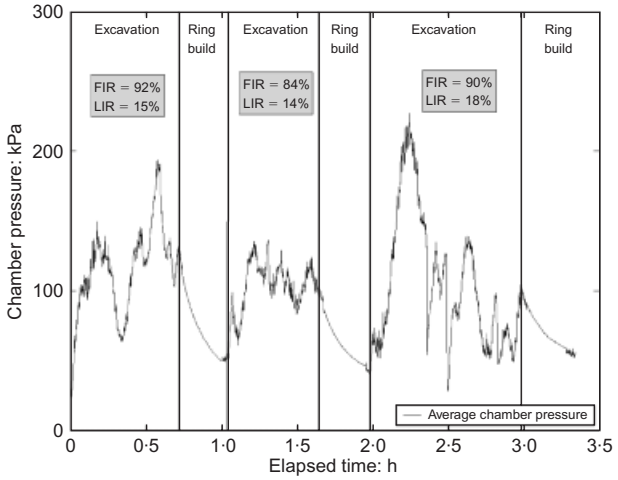

Fig. 27. Example of difficult face pressure control in the Lambeth Group formation (Borghi & Mair, 2006): FIR, foam injection ratio; LIR, liquid injection ratio (see Appendix 1 for definitions)

The foam and liquid injection ratios (see Appendix 1 for the definitions) recorded for these cycles were in the ranges 84–92% and 14–18% respectively. The duration of the excavation phase was typically 0·7–1 h—the time taken for the EPB machine to advance 1·5 m, which is the length of one ring of the tunnel segments. During this excavation period it can be seen that the chamber pressure fluctuates significantly, sometimes rising substantially: there is no clear explanation for this, but it may be a consequence of a reduction in screw conveyor extraction rate, as discussed earlier, as well as injection of significant quantities of pressurised foam into the excavation chamber.

Figure 27 shows that there was always a substantial drop in chamber pressure during the ring-build phase, when the machine was stationary for 0·3–0·5 h. This may be because the chamber was not completely full of spoil, but it is also believed to be partly due to the foam breaking down during stoppage of the machine owing to sorption of the foaming liquid into the clay (Borghi, 2006). This process of sorption was also observed in the laboratory (Mair *et al.*, 2003; Merritt *et al.*, 2003). The injection of significant quantities of foam may act counter-productively when tunnelling in

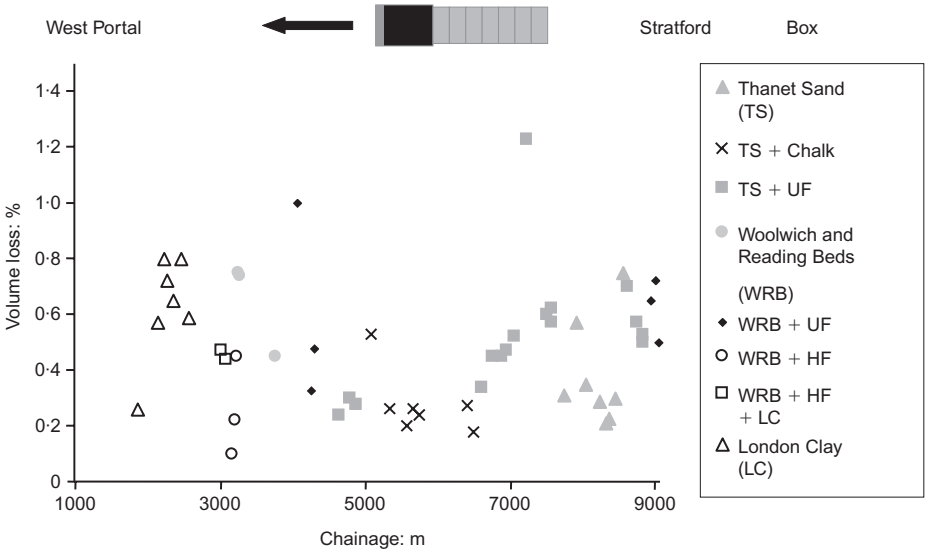

Fig. 26. Observed volume loss for Up-Line tunnel CTRL Contract 220 (Wongsaroj *et al.*, 2005): UF, Upnor Formation; HF, Harwich Formation

clays by exacerbating the drop of pressure in the head chamber during the ring-build phase; this is particularly the case if this phase takes longer for any reason, as the foam breaks down and the spoil mixture effectively compresses.

In contrast, Fig. 28 shows an example of good control of chamber pressure (Borghi, 2006). A number of cycles of excavation and ring build in a full-face of London Clay are shown; the tunnel axis was at a depth of 31 m. In the upper part of the figure, the average measured chamber pressure is plotted against time; in the lower part the total shield thrust (measured from the total load of the jacks reacting off the most recently completed segments) is plotted against time. During the excavation cycles the shield thrust is reasonably constant at around 20 MN. During the ring build, between the excavation cycles, the thrust is considerably reduced as jacks are retracted to allow erection of the lining segments. Fig. 28 shows that there is sometimes a drop in chamber pressure during the ring-build phase (this may be partly a consequence of the corresponding reduction in shield thrust). Two ring-build cycles are highlighted, one showing a larger chamber pressure drop and the other a smaller drop. Nevertheless, the average chamber pressure throughout the period of 8·5 h shown in Fig. 28 remains reasonably constant at around 220 kPa, with fluctuations generally not exceeding ±30 kPa.

The average chamber pressure p of 220 kPa in Fig. 28, expressed as a ratio of the total overburden pressure σ_{v0} at tunnel axis level, is $p/\sigma_{v0} = 0{\cdot}35$. It is reasonable to expect this average chamber pressure ratio to be linked to the volume loss, and at first sight this is indicated by the data in Fig. 29, which show different face pressure ratios plotted against measured volume loss for seven tunnel sections in full-face London Clay (after Wongsaroj *et al.*, 2005). However, it should be noted that six of the seven cases are for tunnels with axis depths of 25–30 m, and for these cases there appears to be no significant reduction of volume loss with increasing average chamber pressure ratio. This can possibly be attributed to the small stability ratio and load factor prevailing in the stiff London Clay at these depths (Mair *et al.*, 1981; Macklin, 1999). It should be noted, however, that the chamber pressure was varied only over a small range for these six cases at tunnel axis depths of 25–30 m. Also, the small volume losses measured corresponded to only a few millimetres' settlement at the ground surface, and therefore the assessed volume losses are prone to error. It should also be recalled that the chamber pressure is only one component of the total face pressure, albeit the major one for many tunnelling machines for

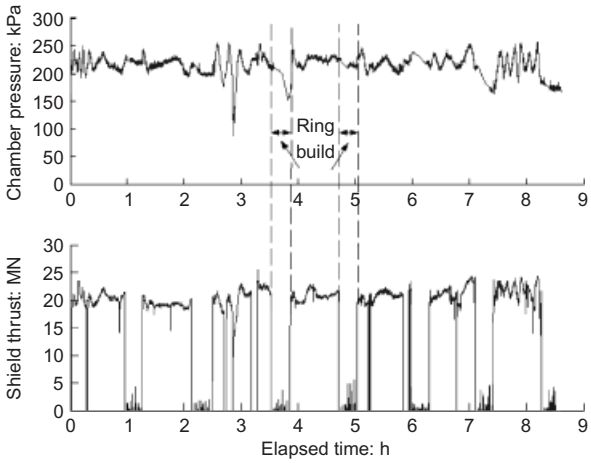

Fig. 28. EPB chamber pressure and shield thrust for full face in London Clay (Borghi, 2006)

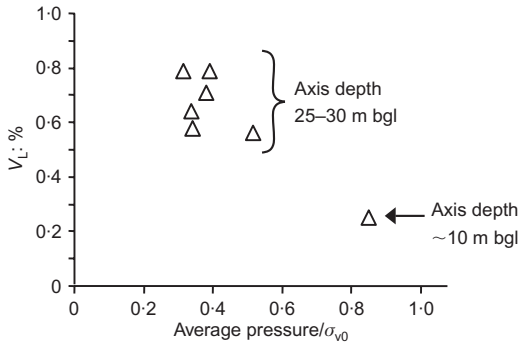

Fig. 29 Influence of EPB chamber pressure on volume loss for full face in London Clay (Wongsaroj, 2005; Borghi, 2006)

which the opening ratio η is large (as for the case of the machines on CTRL Contract 220, where η was 57%). Nevertheless, Fig. 29 shows that a significantly lower volume loss was measured when a higher average chamber pressure ratio was operating for the much shallower tunnel in London Clay, for which the axis depth was only 10 m below ground level.

The immediate volume loss can be split into different components (Dimmock, 2003; Dimmock & Mair, 2006a). In the case of EPB closed-face tunnelling these were defined by Wongsaroj *et al.* (2005) as follows:

(*a*) ahead of the face, termed *face volume loss*
(*b*) around the shield, termed *shield volume loss*
(*c*) around the tailskin and tunnel lining, termed *tailskin volume loss*.

Shirlaw *et al.* (2003) advocated that, for soft clays, occasional low face pressures (by which they meant chamber pressures) may have a significant effect on face volume loss, because small face pressures cause stress relief (and associated ground movements) that cannot easily be reversed by increasing the face pressure. However, Wongsaroj *et al.* (2005) and Borghi (2006) found that, in the case of the full-face tunnels in London Clay, there was little or no correlation between component 1 and $p_{10\%}$, where $p_{10\%}$ is defined as the 10th percentile of the distribution of the chamber pressure p, that is, the value of the chamber pressure below which 10% of the measured values fell. This is probably because such fluctuations in chamber pressure for tunnels at great depth in stiff London Clay have only very small effects on the stability ratio and load factor (as discussed earlier for the average chamber pressure ratios shown in Fig. 29). Fluctuations in chamber pressure appear to be of considerably more significance in the case of shallow tunnels. This is discussed in the following section.

Shallow tunnels and piled foundations

As part of his PhD studies at Cambridge University, Selemetas (2005) reported measurements of the field response to tunnel construction of instrumented piles and a number of piled structures on Contract 250 of the CTRL project. Fig. 30 shows a cross-section through the two tunnels at shallow depth beneath part of a 250 m long piled reinforced concrete rectangular culvert. Because of the presence of 5 m of very soft and compressible silts and peat, the culvert was supported by 6 m long piles at 4 m spacing driven into the underlying dense sand and gravel. The 8 m diameter CTRL tunnels were constructed, using EPB Lovat tunnelling machines, with their crowns 4 m below the base of the piles and with only 3 m of cover of London Clay.

The up-line tunnel was constructed first, and caused 3 mm

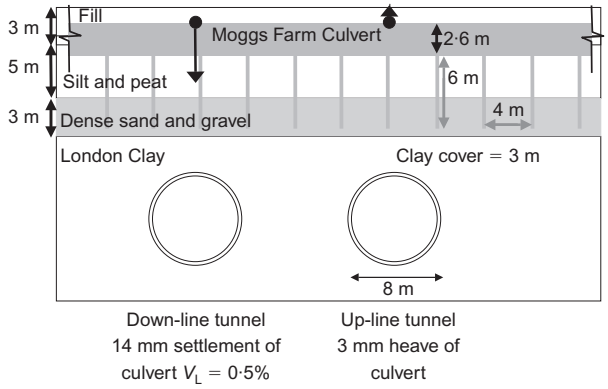

Fig. 30. Effect of EPB tunnelling on piled culvert at Moggs Farm (Selemetas, 2005)

of heave of the culvert above the tunnel centreline. Shortly afterwards the down-line tunnel was constructed, but this time 14 mm of settlement was experienced by the culvert above the tunnel centreline owing to construction of the down-line tunnel alone. An insight into the difference in response can be gained from the chamber pressure records for the two tunnels, shown in Fig. 31. The average chamber pressures were similar: 1·5 bar and 1·3 bar respectively for the up-line and down-line tunnels (1 bar = 100 kN/m^2); but it is evident that there was considerably more fluctuation in chamber pressure for the down-line tunnel. Significantly, the $p_{10\%}$ value for the down-line tunnel was 0·9 bar, which was considerably less than the corresponding value of 1·3 bar for the up-line tunnel. The control of chamber pressure was much better for the up-line tunnel, with much less fluctuation.

Summary

Good control of face pressure, through effective control of chamber pressure, is now possible with EPB tunnelling machines in a wide variety of ground conditions. Low volume losses, well below 1%, are now readily achievable. The principal features of successful EPB machine operation are the pressurised excavation chamber, the conditioning of the excavated spoil, the screw conveyor, and both annulus and tail void grouting. There have been considerable advances in soil conditioning technologies, and through a combination of laboratory and field measurements there is now an improved understanding of the interaction of soil-conditioning agents with excavated soils. Model tests have also provided insight into the interaction between conditioned soil mixtures and the operating conditions of screw conveyors.

Good control of face pressure, through proper control of the excavation chamber pressure, depends on appropriate soil conditioning and screw conveyor operation. During the excavation phase, the pressure in the chamber is controlled by the mass flow rate of soil and conditioning agents entering the chamber and that of the spoil discharged at the outlet of the screw conveyor. During the ring-build phase, when the tunnelling machine is stationary, there is a tendency for the chamber pressure to drop, especially if the chamber is not completely full of spoil, and this may be exacerbated by longer stoppage times and excessive use of foam for conditioning of clay soils.

For EPB tunnelling in stiff London Clay, in cases where the axis depths were 25–30 m, there appeared to be no significant reduction of volume loss with increasing average chamber pressure ratio (at least for the range of pressures measured). At shallow tunnel depth, however, the average chamber pressure ratio was more significant in reducing volume loss. Chamber pressure fluctuations are also of more significance in relation to ground and structure movements in cases of shallow tunnels.

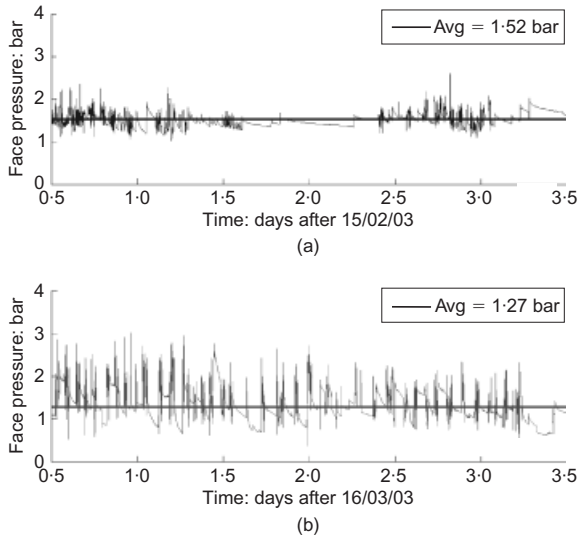

Fig. 31. EPB chamber pressures at Moggs Farm (Selemetas, 2005): (a) up-line tunnel (slight heave); (b) down-line tunnel (significant settlement)

RECENT DEVELOPMENTS IN COMPENSATION GROUTING: A CASE HISTORY IN BOLOGNA

Principles of compensation grouting

Compensation grouting is a very promising technique being used increasingly to control ground and building movements during tunnelling in soft ground. The principles of the method were presented by Mair & Hight (1994), and the basic concept is illustrated in Fig. 32. Grout is injected between the tunnel and the building foundations to compensate for ground loss and stress relief caused by the tunnel excavation. Sleeved grout tubes (tubes à manchette, TAMs) are installed in the ground prior to tunnelling, often from a vertical shaft. Before tunnelling commences, conditioning grouting is undertaken to tighten the ground and reverse any settlement or loosening of the ground caused by drilling for TAM installation. Grout injection is then undertaken simultaneously with tunnelling in response to detailed observations, the aim being to limit building settlements and distortions to specified, acceptable amounts. Experience of compensation grouting is reported by, among others, Mair *et al.* (1994), Harris *et al.* (1994), Harris *et al.* (1996), Mair & Taylor (1997) and Harris (2001). The technique was successfully used on the Jubilee Line Extension Project in London for the protection of many historic buildings, including the

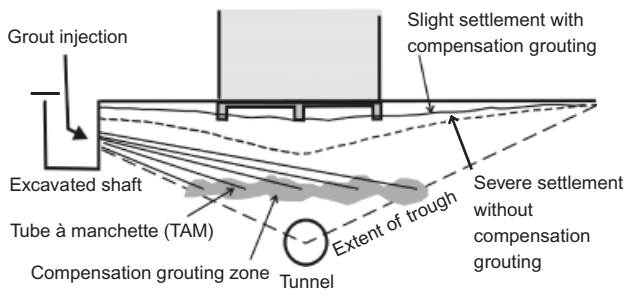

Fig. 32. Principle of compensation grouting

Big Ben Clock Tower at the Palace of Westminster (Harris *et al.*, 1999; Harris, 2001).

The majority of experience of compensation grouting has been in stiff clays, and in most cases the grout tubes have been installed from vertical shafts. The recent case history in Bologna, described in the following section, illustrates the success of the technique in granular soils and also introduces the innovative use of directional drilling for installation of the grout tubes.

The Bologna project

The project was part of a new high-speed rail link under construction between Milan, Rome and Naples. A section in Bologna passes beneath a number of railway bridges and follows the alignment of the existing railway. The most important of these bridges is a nine-arch masonry viaduct, which is 112 m long. Fig. 33 shows a longitudinal section through the viaduct and the new high-speed rail twin tunnels of diameter 9·1 m that were constructed parallel to the viaduct and directly beneath its alignment. The viaduct comprises nine masonry arches, each of 8 m clear span, with one longer 16 m clear span. It is 112 m long and 11 m wide, with 8–10 m high embankments at each end. The piers of the viaduct are supported on shallow foundations. The ground generally comprises made ground up to 8 m thick over a substantial depth of alluvial deposits, which are predominantly dense gravelly sands or very sandy gravels, with fines content (particles $<$ 0·063 mm diameter) generally less than 15% by weight. Coring through the masonry piers indicated that at least two of the pier foundations extend to the top of the sands and gravels. The crown of the tunnels would be 10·6 m below the deepest pier foundations, that is, a distance of just over one tunnel diameter. The groundwater table was below tunnel invert.

Construction of the twin 9·1 m tunnels, using EPB tunnelling machines, was expected to generate large settlements, typically around 20 mm but potentially up to 50 mm for volume losses of 1%. Such settlements would have induced excessive distortions of the viaduct, which was a cause of concern, particularly as suspension of train services was not permitted. There were also major concerns about potential cracking of the masonry arches, some of which were already cracked. Compensation grouting was therefore implemented during tunnelling, with the grout injected in the nominally 4 m thick zone shown in Fig. 33. Also shown in Fig. 33 are the three lines of automatic water level settlement gauges, which provided real-time monitoring data (further details are given by Kummerer *et al.*, 2007); precise levelling was also undertaken.

Directional drilling

Figure 34 shows a cross-section through the viaduct and the underlying tunnels. The viaduct crossed busy streets, and suitable shaft locations were not available; the contractor therefore proposed that curved TAMs be installed by directional drilling from shallow pits, typically about 2 m deep. Site trials were conducted to prove the feasibility of this. For a 60 m long tube the typical vertical control was up to 1 m, and the horizontal control up to 0·5 m; the minimum radius of curvature was 90 m. Two layers of TAMs were installed, with very tight control on the directional drilling operations, such that the nominally 4 m thick treatment zone was no closer than 1·5 m below the pier foundations and 3 m above the crown of tunnel 2. The directional drilling in progress is shown in Fig. 35. Fig. 36 shows a plan diagrammatic view of the full coverage of TAMs beneath the foundations of the

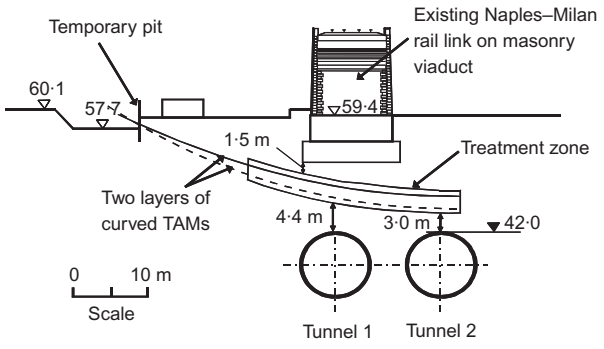

Fig. 34. Bologna tunnels: typical cross-section showing compensation grouting tubes and treatment zone

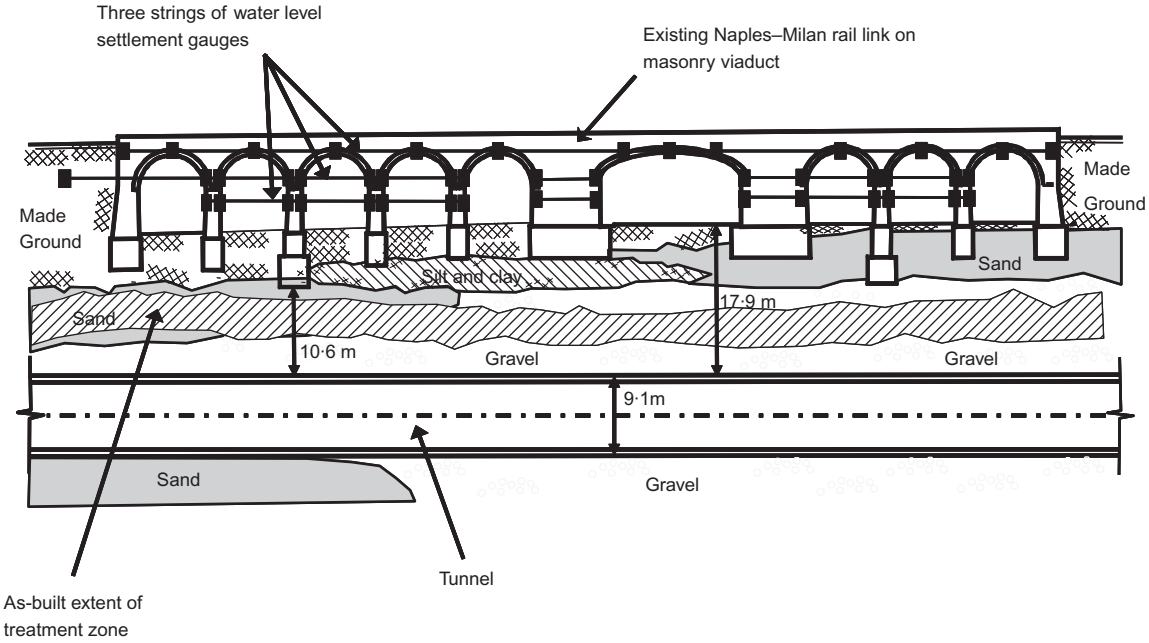

Fig. 33. Bologna tunnels: viaduct and geotechnical section

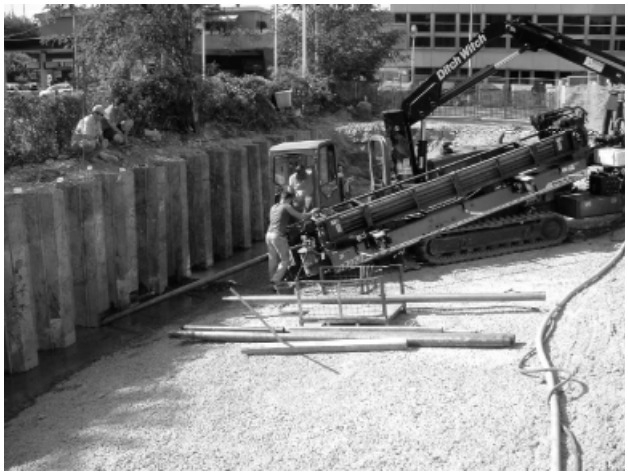

Fig. 35. Bologna tunnels: directional drilling in progress to install grouting tubes

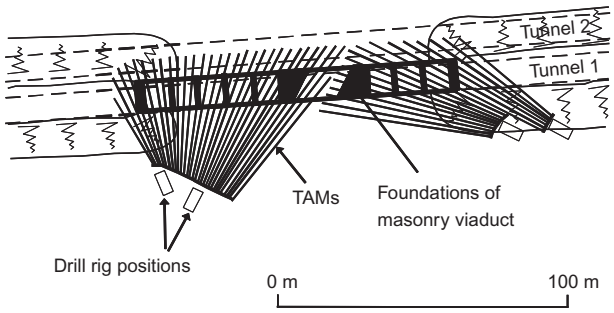

Fig. 36. Bologna tunnels: plan view and layout of grouting tubes

viaduct. A TAM installation progress rate of 65 m/day/rig was achieved.

Compensation grouting

A field trial was carried out adjacent to the viaduct, in advance of the main works. The trial was used to refine the grout mix and grouting processes for the ground conditions, and to demonstrate the ability to generate controlled heave. The trial also allowed evaluation of the proposed monitoring system. Some temperature sensitivity was observed under the diurnal temperature variations of up to 30°C, measured on the viaduct. Two grouting stages were undertaken prior to commencement of tunnelling and compensation grouting: (a) pre-treatment grouting to permeate and fill the larger voids in the ground; and (b) conditioning grouting to tighten the ground and reverse any settlement or loosening of the ground caused by drilling for TAM installation.

A relatively fluid grout mix was adopted by the contractor. The water : cement ratio was 0·78; bentonite was added (weight of bentonite powder to weight of water = 11%), resulting in a ratio of volume of solids to total volume = 23%. However, after injection into the granular soils the process of pressure filtration would rapidly squeeze out the water from the mix, leaving a more viscous mix that would tend to remain relatively local to the injection point.

The viaduct was monitored against predetermined, tolerable settlement and differential settlement limits. Compensation grouting activities were implemented as necessary to keep the movements of the structure within these limits. The masonry of the viaduct was already cracked in a number of locations, which were a cause of concern. Following detailed structural analysis of the viaduct, project contract specifications limited differential settlement for each span of the structure to 1 : 1000, and this was adopted as the maximum tolerable value or the 'alarm' value for the viaduct. A 'trigger' level of differential settlement of 1 : 3000 was accordingly established, and the contractor was obliged to carry out compensation grouting if this trigger level was reached.

Figure 37 shows the cumulative volume of grout injected during tunnelling, together with the EPB machine progress for the first tunnel, both plotted against time. The average progress rate for the tunnelling was 23 m/day. The measured volume loss immediately prior to the tunnel reaching the viaduct was 0·2%. Earlier it had been significantly larger—up to 1%—but a high standard of face pressure control and tail void grouting was exerted as the tunnelling machine approached the viaduct. Also plotted in Fig. 37 is the ratio of volume of injected grout to volume of ground excavated, expressed as a percentage. During the period when the tunnelling machine was beneath the viaduct (and within 4 m beyond each end), this ratio was in the range 0·4–0·6%. Grouting continued when the tunnelling machine passed beyond the viaduct, and the ratio correspondingly increased.

Performance of the viaduct

Figure 38 shows the performance of the viaduct at a particular stage of the construction of tunnel 1 (when the face of the TBM was at chainage 3410). Also shown is the estimated transient longitudinal settlement profile without any grouting, assuming a volume loss of 0·2%, and a trough width value $K = 0{\cdot}4$ (Mair *et al.*, 1996), based on 'greenfield' measurements. The actual settlements of the viaduct achieved at this stage are shown in Fig. 38 (for both the west and east sides of the viaduct); at one location, at chainage 3330, a slight heave was measured. The grout intensity in litres/m^2 is also shown, assuming the area of coverage of each grout injection in plan was 3 m × 3m, based on observations during the field trial; the influence of the assumed area of coverage on derived grout intensity is discussed by Viggiani (2001). Slopes corresponding to the 'trigger' and 'alarm' differential settlement levels of 1 : 3000 and 1 : 1000 respectively are shown in Fig. 38, and it can be seen that grouting was necessary because the 'trigger' level was exceeded. Excellent control of the viaduct movements was achieved. It should be recalled that the tunnelling volume loss was only 0·2% while the EPB machine was beneath the viaduct. If the volume loss had been as high as 1%, which had been measured earlier, the likely settlement of the viaduct due to tunnel 1 in the absence of grouting would have been 50 mm rather than 10 mm: significantly more grouting would then have been necessary to maintain

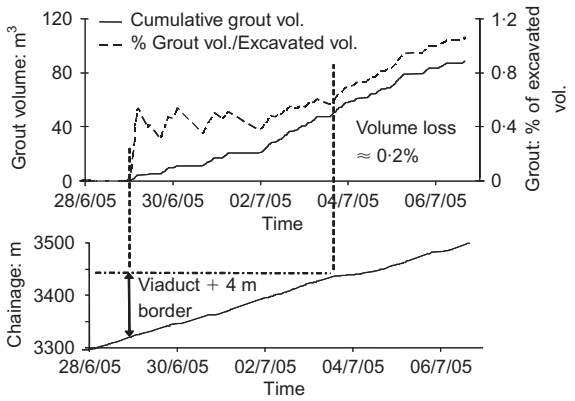

Fig. 37. Bologna tunnels: injected grout volume and progress of TBM 1

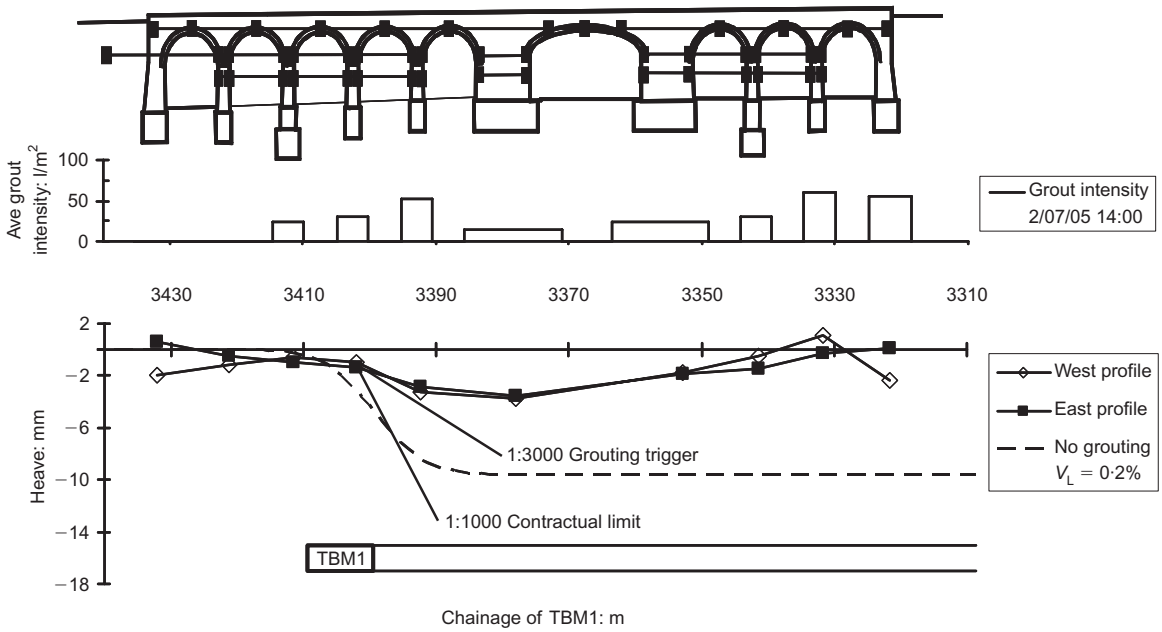

Fig. 38. Bologna tunnels: performance during TBM passage. The maximum permitted differential settlement between adjacent piers allowed by the contract was 1 : 1000. The design required compensation grouting injections to be implemented if differential settlement between adjacent piers exceeded 1 : 3000

the differential settlement within the contractual limit of 1 : 1000.

Summary

The compensation grouting at Bologna has demonstrated the innovative use of directional drilling to install curved grout tubes. This is of practical importance for projects in congested urban areas where it might not be possible to construct shafts. The project has also demonstrated the successful application of compensation grouting to granular soils, for which there has been generally less experience in comparison with clay soils. The importance of field trials cannot be overemphasised: these were vital to prove the feasibility of both the directional drilling and the proposed grout mixes prior to tunnelling. The sensitive masonry viaduct experienced only small and acceptable levels of distortion, and the existing rail services continued without interruption. The compensation grouting provided a high degree of control.

LONG-TERM GROUND MOVEMENTS

Influence of drainage into tunnels

Our understanding of tunnelling-induced ground movements and settlements is centred principally around the immediate, short-term movements associated with tunnel construction. However, tunnelling in low-permeability soils often results in ground surface settlement that continuously increases over a long period of time. If the tunnel acts as a drain, it introduces a new drainage boundary condition that leads to long-term reductions in pore pressure and associated consolidation settlements, as depicted in Fig. 39. This is because, on the inside face of the tunnel lining, the pressure is usually atmospheric. If the tunnel is not totally impermeable, a flow of pore water into the tunnel occurs, and a new steady-state flow condition is eventually reached. The final pore pressures will generally be lower than those prior to tunnel construction: settlement will therefore occur as pore pressures reduce to their long-term steady-state values, increasing effective stresses and thereby inducing consolidation

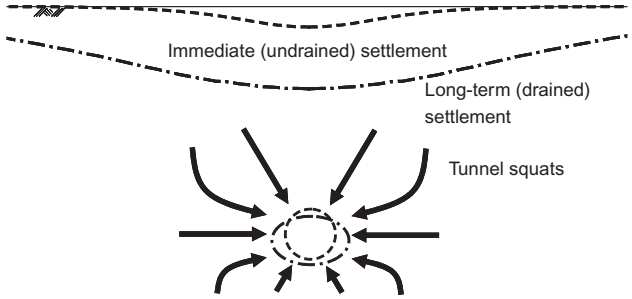

Fig. 39. Tunnel in clay acting as long-term drain

in the clay. As indicated in Fig. 39, the resulting settlement profile at the ground surface will tend to be considerably wider than the profile associated with construction (Mair & Taylor, 1997). There will also be an accompanying tendency for the tunnel to squat with time as consolidation occurs, that is, reduce in vertical diameter and increase in horizontal diameter, as shown in Fig. 39: this has been noted for tunnels in London Clay and in other clays (Ward & Pender, 1981).

The evidence that tunnels in low-permeability soil act as new drainage boundaries has been demonstrated from field measurements of pore pressure around tunnels (Ward & Thomas, 1965; Palmer & Belshaw, 1980). Ward & Pender (1981) concluded that in most cases segmentally lined tunnels in London Clay act as drains, despite the linings having been grouted. This is generally confirmed by recent measurements of pore pressures around five very old London Underground tunnels in London Clay, shown in Fig. 40. The measurements were all made at tunnel axis level at various distances from the tunnel extrados. Each of these tunnels, which are at least 80 years old, had been constructed with bolted cast iron linings, which were grouted. Details of the year of construction and the depth of each tunnel are given in Table 3.

In cases A–D, as can be seen from Fig. 40, there is a clear trend of decreasing pore pressure close to the tunnel, and the pattern is reasonably consistent with the pore

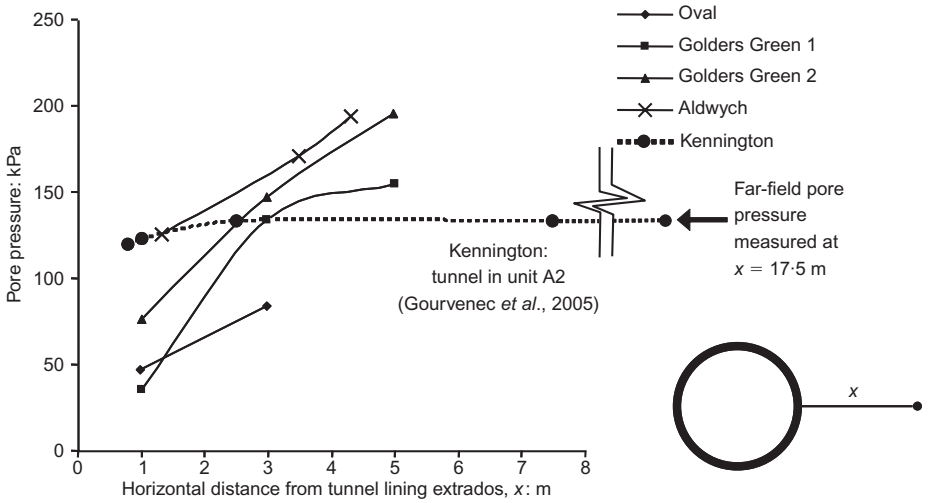

Fig. 40. Pore pressures near old tunnels in London Clay (bolted cast iron linings) (measurements made by Tube Lines Ltd)

Table 3. Year of construction and tunnel depth for tunnels in Fig. 40

Tunnel	Year of construction	Depth of tunnel below ground level: m
A. Oval	1890	15
B. Golders Green 1	1907	39
C. Golders Green 2	1907	65
D. Aldwych	1906	28
E. Kennington	1924	21

pressure distribution that would be expected for a tunnel acting as a drain in a uniform deposit of clay. However, case E (at Kennington) shows a markedly different trend. In this case, the pore pressures in the clay even within a few metres from the tunnel are the same as the 'far-field' value measured 17·5 m from the tunnel, and very close to the tunnel (0·7 m from the extrados) only a small reduction of pore pressure is seen (Gourvenec *et al.*, 2005). The probable reason for this difference is that in the case of the Kennington tunnel the London Clay at tunnel level is more permeable, resulting in the tunnel lining system being effectively impermeable.

The permeability of London Clay can be highly variable, as shown in Fig. 41 (Hight *et al.*, 2007). The data are all from in situ measurements of horizontal permeability, inferred from falling- or rising-head tests in piezometers, from self-boring permeameter tests, or from self-boring pressuremeter tests (Ratnam *et al.*, 2005). It can be seen that at any given depth the variation of permeability can be as much as two orders of magnitude, varying from around 5×10^{-11} m/s to 5×10^{-9} m/s. This wide variation can in part be explained by the different units of London Clay identified by King (1981). The unit A2, at the bottom of the London Clay stratum, has a higher permeability than the overlying unit A3, as shown by the lines in Fig. 41; moreover, the London

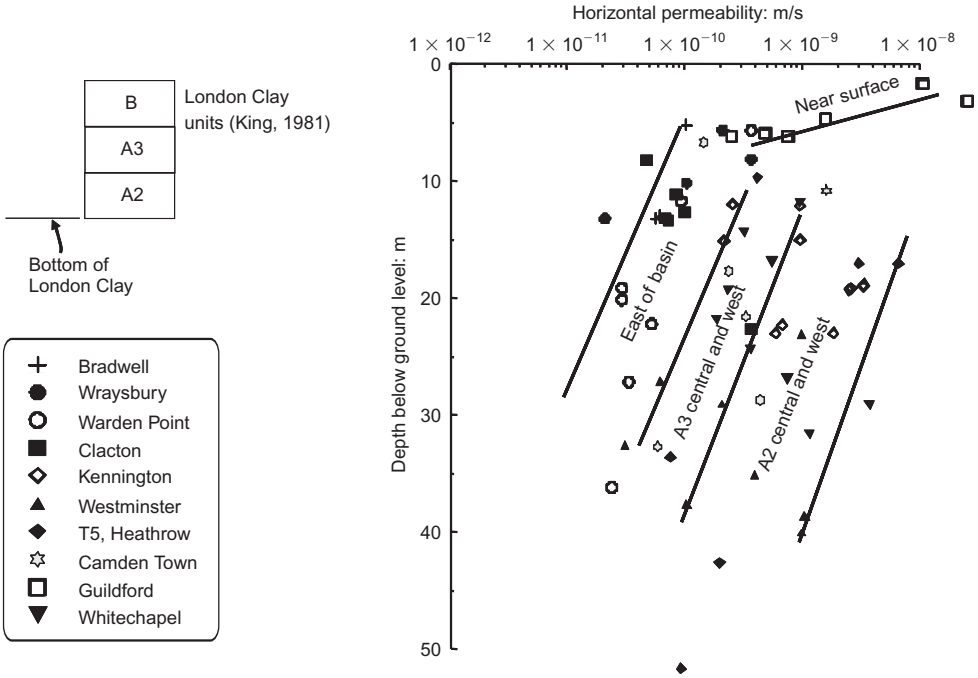

Fig. 41. London Clay permeability: in situ tests (Hight *et al.*, 2007)

Clay units to the east of the London basin all exhibit lower permeabilities than in the central and western parts of the basin (Hight *et al.*, 2007).

The considerable variation of permeability within the London Clay is the probable explanation of case E (Kennington) showing a markedly different trend in observed long-term pore pressures: see Fig. 40. Only a small reduction of pore pressure was observed very close to the tunnel (0·7 m from the extrados). This is because the tunnel was in the A2 unit, for which the horizontal permeability inferred from self-boring permeameter tests was 2×10^{-9} m/s; consequently the tunnel lining was relatively impermeable in relation to the surrounding soil (Gourvenec *et al.*, 2005).

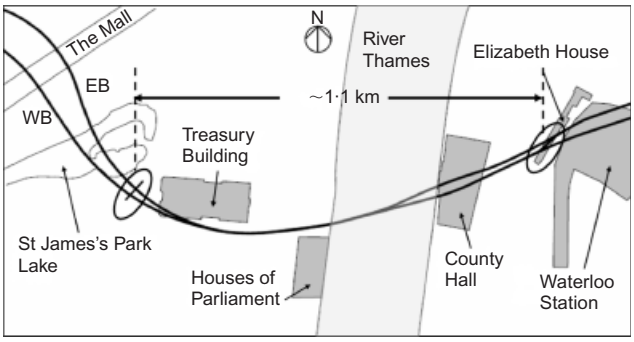

Fig. 42. Jubilee Line Extension: locations of long-term settlement monitoring

Field measurements of long-term settlements

Field measurements of long-term settlements above tunnels in clays are comparatively rare, not least because on most projects monitoring tends to cease soon after completion of the tunnel. Evidence that the ground surface continues to settle after tunnel excavation in clays has been illustrated by Peck (1969), O'Reilly *et al.* (1991), Lake *et al.* (1992), Shirlaw (1995), Bowers *et al.* (1996), Nyren (1998) and Harris (2002b). Post-construction settlements were reviewed by Mair & Taylor (1997), who concluded that the major factors influencing their development are

(*a*) the magnitude and distribution of excess pore pressure generated by the construction of the tunnel
(*b*) the compressibility and permeability of the soil
(*c*) the pore pressure boundary conditions, particularly the permeability of the tunnel lining relative to the permeability of the soil
(*d*) the initial pore pressure distribution in the ground prior to tunnel construction.

O'Reilly *et al.* (1991) reported monitoring of longer-term settlements over a period of 11 years for a 3 m diameter tunnel constructed in normally consolidated silty clay in Grimsby; they also measured pore pressures in the ground surrounding the tunnel and found no evidence of reduced pore pressures, even within a few metres of the tunnel. However, in a back-analysis using the finite element method the closest match to the observed consolidation settlements was obtained by assuming the permeability of the combined primary segmental lining and secondary in situ concrete lining to be 5×10^{-11} m/s, compared with the permeability of the clay (deduced from in situ constant head tests) of about 10^{-10} m/s (Mair *et al.*, 1992b). It was concluded that the tunnel at Grimsby was acting as a drain, albeit partially, such that the pore pressures in the ground were reduced only very close to the tunnel (probably within a metre or so).

It is often observed that tunnels are visibly wet, despite precautions taken in an attempt to make them watertight. In the case of the Jubilee Line Extension tunnels in London, substantial consolidation settlements were observed over tunnels in most locations for periods of up to 5 years following construction: these observations were irrespective of the lining type, whether bolted spheroidal graphite iron or concrete (both of which were grouted), or expanded concrete, or in situ concrete (Harris, 2002b). Measurable consolidation settlements were found at distances up to 100 m from the tunnels.

Longer-term settlement monitoring has been undertaken for almost 11 years at two sites in London since completion of the Jubilee Line Extension. The two sites are at St James's Park and Elizabeth House, separated by about 1·1 km; their locations are shown on the plan in Fig. 42. At St James's Park, as shown in Fig. 43, the westbound (WB) and eastbound (EB) tunnel axes are located at approximately 31 m and 20·5 m below the ground surface respectively. The 4·85 m OD tunnels are lined with 200 mm thick expanded precast concrete segments: these were not grouted. Detailed descriptions of the St James's Park 'greenfield' instrumented site and the tunnel excavations beneath are given by Nyren (1998). Further details of the ground conditions, the tunnelling methodology and the observed ground movements during tunnel construction are given by Standing & Burland (2006) and Dimmock & Mair (2006a, 2006b). As shown in Fig. 43, piezometer measurements at the site indicate initial pore pressures (prior to tunnelling) close to hydrostatic conditions in the London Clay above and around the positions of the tunnels to be constructed: these are consistent with measurements at the nearby Westminster site (Higgins *et al.*, 1996). (Underdrainage below about 35 m and in the underlying Lambeth Group is probable, as observed at Westminster, although piezometers were not installed at depths at St James's Park to verify this.)

Figure 43 shows post-construction settlement measurements at St James's Park (Standing, personal communication, 2006), taken at a depth of 5 m below ground level (to eliminate seasonal effects observed closer to the ground surface). Two sets of data are shown, each directly above each one of the tunnels. The westbound tunnel was constructed first, followed by the eastbound tunnel about 8 months later. Consolidation settlements only are shown in Fig. 43: that is, settlements occurring during construction of the two tunnels are not shown. The time axis is measured from the completion of the westbound tunnel; the change in gradient of the settlements shown in Fig. 43 can be seen after 8 months, reflecting the change occurring after completion of the eastbound tunnel. It is evident that considerable consolidation settlement has occurred since tunnel construction, approaching 80 mm after 11 years, with the rate of settlement remaining almost constant (with some indication of this beginning to reduce after about 10 years). It is also evident that the magnitudes of the consolidation settlements above each tunnel are almost identical.

Elizabeth House is a reinforced-concrete-framed ten-storey building, which was closely monitored during construction of the Jubilee Line Extension tunnels beneath it (Standing, 2001). The building is shown in Fig. 44. Prior to tunnelling, Class A predictions (as defined by Lambe, 1973) of the settlements caused by tunnel construction were made: full details of the building construction, the tunnels and the method of prediction are given by Mair & Taylor (2001). The building has two levels of basement, and is founded on a 1·2 m reinforced concrete raft; the base of the raft is in Thames Gravel, a short distance above the interface with the underlying London Clay, as shown in Fig. 45. Mair & Taylor (2001) concluded that the building would respond to tunnel

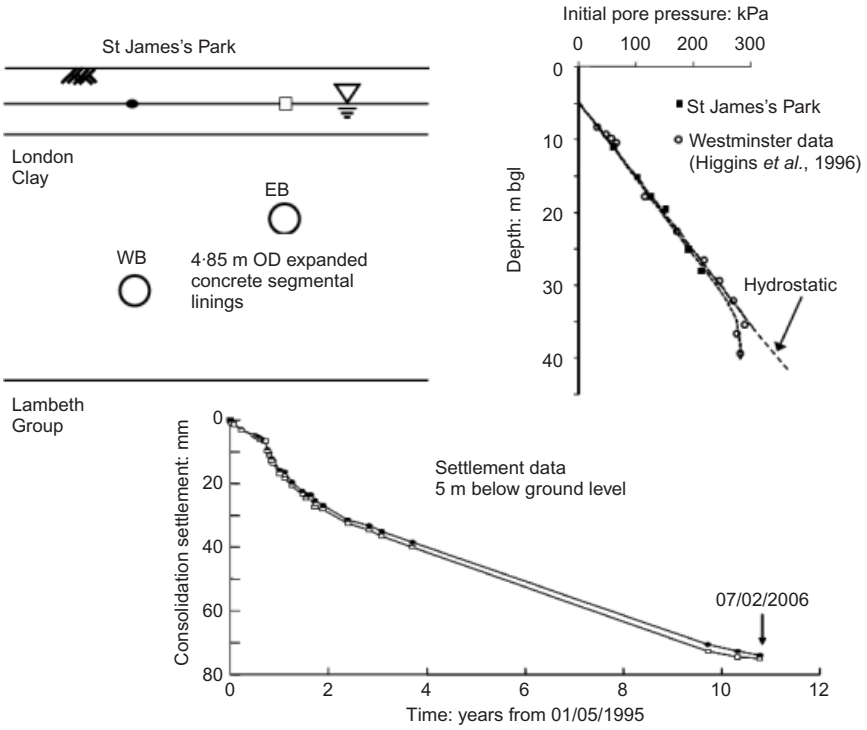

Fig. 43. St James's Park tunnels: cross-section, initial pore pressure prior to tunnelling, and settlement measurements since completion (image courtesy J. Standing)

Fig. 44. Elizabeth House: detailed settlement monitoring during and after construction of Jubilee Line Extension

construction almost perfectly flexibly, and the subsequent measurements confirmed this to be the case.

As shown in Fig. 45, in contrast with the St James's Park site, piezometer measurements close to Elizabeth House indicate initial pore pressures (prior to tunnelling) in the London Clay to be significantly less than hydrostatic, consistent with underdrainage due to deep-level pumping (Hight *et al.*, 1993); the reduced pore pressures may also be partly a result of the presence of existing tunnels in the Waterloo area. The new tunnels to be constructed, for which the axis level was 22 m below the raft foundation, also differed from those at St James's Park: the two 5 m eastbound (EB) and westbound (WB) tunnels were lined with sprayed concrete and an in situ reinforced concrete secondary lining; a crossover tunnel was constructed between the eastbound and westbound tunnels, this being lined with sprayed concrete only (further details are given by Standing, 2001).

Figure 45 shows post-construction settlement measurements taken in the lower basement level of Elizabeth House (Standing, personal communication, 2006). Three sets of data are shown, one above each of the eastbound and westbound tunnels and one above the crossover tunnel between them: the three sets are very similar. Fig. 46 shows a comparison of the consolidation settlements from St James's Park and Elizabeth House plotted against time, from which it can be seen that the magnitude of the Elizabeth House settlements is only about 20% of those observed at St James's Park. Also shown in Fig. 46 are the variations of the consolidation settlements after 11 years with distance transverse to the tunnels for the two sites: in each case the settlement profile is very wide and exhibits very little curvature.

In summary, the field evidence from St James's Park and Elizabeth House indicates the following.

(*a*) Substantial long-term consolidation settlements can occur above tunnels constructed in London Clay.
(*b*) The magnitude and rate of settlement are very different for the two sites.

The reasons for the difference between the two sites may be attributable to one or more of the four factors identified earlier. Of these, the most obvious differences are

(*a*) the permeability of the tunnel lining relative to the permeability of the soil
(*b*) the initial pore pressure distribution in the ground prior to tunnel construction.

The linings at St James's Park were expanded precast concrete segments, which were not grouted; at Elizabeth House, in contrast, the linings were sprayed concrete, which mostly had a secondary in situ reinforced concrete lining. The linings at St James's Park were therefore likely to be of significantly higher permeability than at Elizabeth House, and this could be one of the reasons for the substantially larger consolidation settlements. Comparison of Figs 43 and 45 shows that the initial pore pressure distribution (prior to

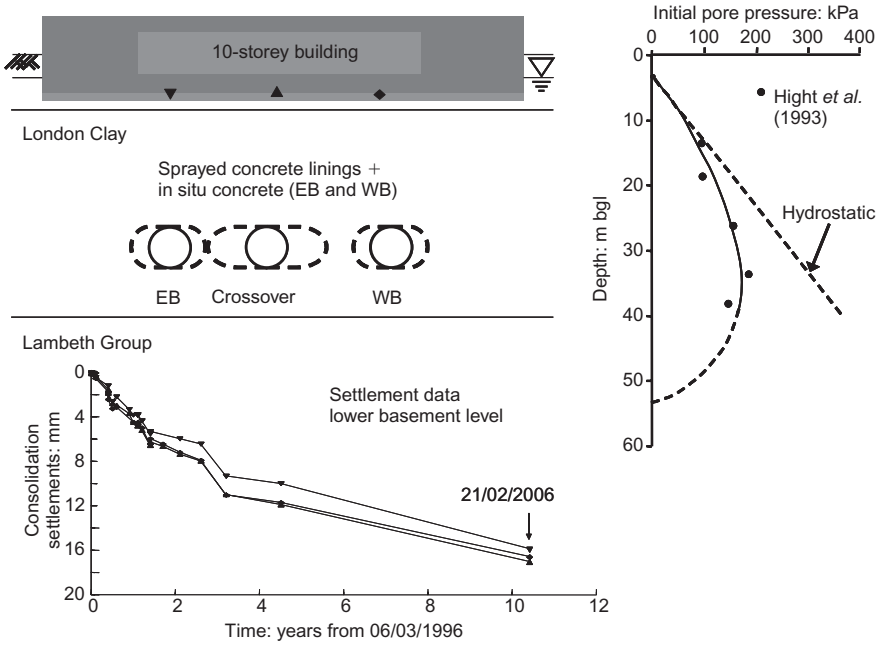

Fig. 45. Elizabeth House: cross-section through tunnels, initial pore pressure prior to tunnelling, and settlement measurements since completion (image courtesy J. Standing)

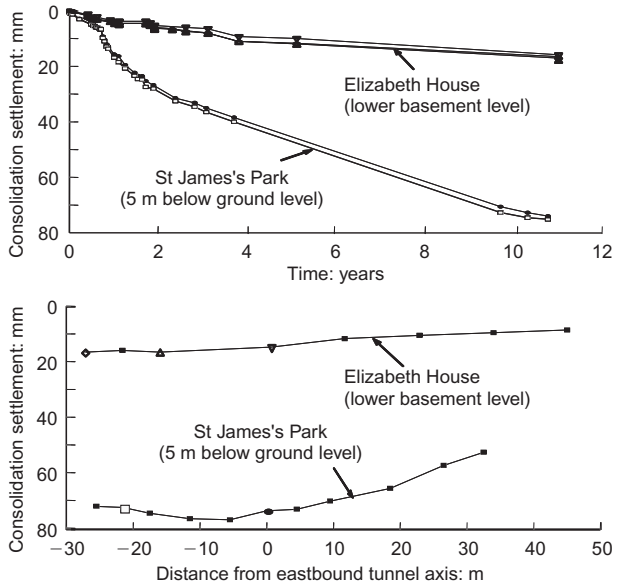

Fig. 46. Comparison of consolidation settlements at St James's Park and Elizabeth House: settlement measurements with time, and transverse distribution after 11 years (Standing, personal communication, 2006)

tunnelling) was close to hydrostatic at St James's Park but significantly less than hydrostatic at Elizabeth House: this too is a likely reason for the differences in consolidation settlements.

Finite element parametric study

The importance of the relative permeability of the tunnel lining and soil, and its effect on long-term settlements, has been explored by means of a finite element parametric study. The analyses were undertaken in connection with the Crossrail project by Geotechnical Consulting Group as part of a study with which the author has been associated, using the ICFEP program developed by Professor David Potts. Fig. 47

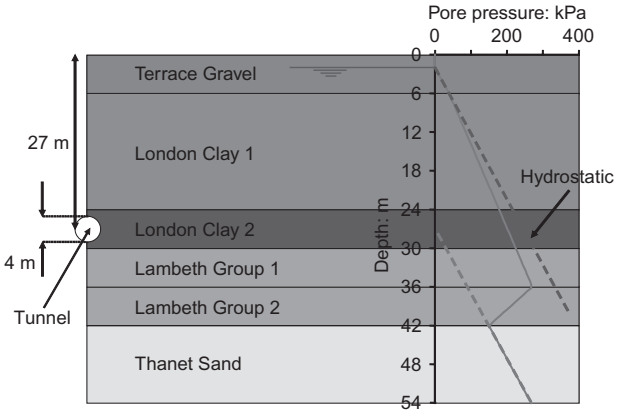

Fig. 47. Finite element analysis of long-term tunnel behaviour: a parametric study

illustrates the problem that was studied. A single 4 m diameter tunnel at a depth of 27 m in London Clay was analysed, representing a bolted cast iron tunnel constructed for the London Underground many years ago, similar to those listed in Table 3. Tunnel construction was modelled two-dimensionally by using the 'volume loss control' method as outlined by Potts & Zdravkovic (2001) to create a volume loss of 1·5%; the segmental nature of the tunnel lining was accounted for by modelling the joints between individual segments. The constitutive soil model adopted was a non-linear elastic, small-strain, Mohr–Coulomb formulation; details of the pre-yield model and the parameters assumed are given in Appendix 2.

The parametric study investigated, among other things, the influence of the tunnel lining permeability and the soil permeability. Only the effect of varying these two parameters is reported in this lecture. The permeability of the two London Clay layers was initially assumed to be 10^{-9} m/s and isotropic. Only the permeability of the 6 m thick London Clay layer ('London Clay 2') in which the tunnel is located was varied in the study. All other soil parameters were kept constant, as detailed in Appendix 2. The initial pore water

pressure profile, prior to tunnel construction, was slightly underdrained in the London Clay; the water table in the Thanet Sand was specified to be equivalent to hydrostatic from a depth of 27 m, as shown in Fig. 47. The coefficient of effective horizontal pressure at rest, K_0, was assumed to increase linearly from 0·5 at a depth of 6 m to a maximum of 1·5 at a depth of 12 m, and then decrease linearly to 1·0 at a depth of 24 m; below 24 m K_0 was assumed to be constant at 1·0.

The pore pressure profile generated immediately following tunnel construction (assumed to be a rapid, undrained process) is shown in Fig. 48. Above the tunnel crown, for a distance of about 7 m, and a similar distance to the side of the tunnel, there is a substantial reduction of pore pressure. (A slight rise in pore pressure is also seen at higher levels above the tunnel crown.) Fig. 48 also shows the long-term pore pressure for the following five cases, where only the permeability of the tunnel lining or the tunnel soil layer ('London Clay 2') is varied.

(*a*) Case 1: impermeable tunnel lining. Tunnel soil layer: $k = 10^{-9}$ m/s, isotropic.
(*b*) Case 2: fully permeable tunnel lining. Tunnel soil layer: $k = 10^{-9}$ m/s, isotropic.
(*c*) Case 3: Tunnel lining permeability: 5×10^{-11} m/s. Tunnel soil layer: $k = 10^{-9}$ m/s, isotropic.
(*d*) Case 4: fully permeable tunnel lining. Tunnel soil layer: $k_v = 10^{-9}$ m/s, anisotropic permeability $k_h/k_v = 4$.
(*e*) Case 5: fully permeable tunnel lining. Tunnel soil layer: $k_v = 5 \times 10^{-9}$ m/s, anisotropic permeability $k_h/k_v = 4$.

An impermeable lining (Case 1) was modelled by prescribing the flow rate into the tunnel as zero throughout the analysis. A fully permeable lining (Cases 2, 4 and 5) was modelled by prescribing the pore water pressure u on the tunnel boundary as zero. Immediately after tunnel excavation, however, suctions exist in the clay adjacent to the soil, and in such cases prescribing $u = 0$ will allow flow of water from the tunnel into the soil. This problem was overcome by setting a special boundary condition that maintained a no-flow boundary if the pore pressure at any point around the tunnel was less than zero (see, for example, Shin *et al.*, 2002). A lining with finite permeability was modelled by the same method as adopted by Shin *et al.* (2002), in which a combination of structural beam elements and solid elements was used.

For this parametric study constant values of permeability for the London Clay were assumed for the various cases analysed. In reality the permeability reduces with increasing effective stress level (Vaughan, 1989). In the case of permeable linings this leads to a reduction in permeability in the soil close to the tunnel in the long term. However, in an analysis of a tunnel in London Clay at a depth of 20 m assuming a log law permeability model proposed by Vaughan (1989), Shin *et al.* (2002) showed that the long-term reduction in permeability of the soil immediately adjacent to the tunnel was very small.

As can be seen from Fig. 48, for Case 1 (impermeable lining) the long-term pore pressures return to their original value, because the tunnel lining is fully impermeable. For Case 2 the fully permeable tunnel lining allows steady-state seepage to develop, with a consequent reduction in pore pressure above and to the side of the tunnel. For Case 3, as would be expected, the tunnel lining of finite permeability results in a long-term pore pressure distribution intermediate between the fully impermeable lining (Case 1) and the fully permeable lining (Case 2).

Of particular interest are Cases 4 and 5, for which the tunnel lining is assumed to be fully permeable, but the permeability of the tunnel soil layer is changed. For Case 4 the assumed anisotropy of permeability ($k_h/k_v = 4$) results in only a small change in the long-term pore pressure profile above the tunnel compared with Case 2, but there is a significant reduction to the side of the tunnel, extending to a considerable distance. The effect of changing the permeability of the tunnel soil layer is even more marked for Case 5, in which the same anisotropy is assumed ($k_h/k_v = 4$) but the permeability is increased by a factor of 5. This results in a substantial reduction in long-term pore pressure both above and to the side of the tunnel.

The corresponding long-term settlement profiles at the ground surface (following tunnel construction) for the five cases are shown in Fig. 49. For Case 1 a very small heave is predicted, corresponding to the swelling that occurs as the negative excess pore pressures generated by tunnel construction dissipate, with the pore pressures returning to their original values. For Case 2 the reduction of long-term pore pressure associated with the fully permeable lining results in a maximum long-term settlement of 40 mm, with discernible settlement extending to a distance of about 60 m from the tunnel. As would be expected, Case 3 results in a long-term settlement profile intermediate between Cases 1 and 2.

Cases 4 and 5 are of considerable significance. Simply varying the permeability of the tunnel soil layer (either in magnitude or by assuming anisotropy) has a substantial effect on both the magnitude and distribution of the long-term settlement. For Case 5 the maximum long-term settlement increases to almost 80 mm, and the settlement trough is very wide, extending to a distance of 100 m. The five

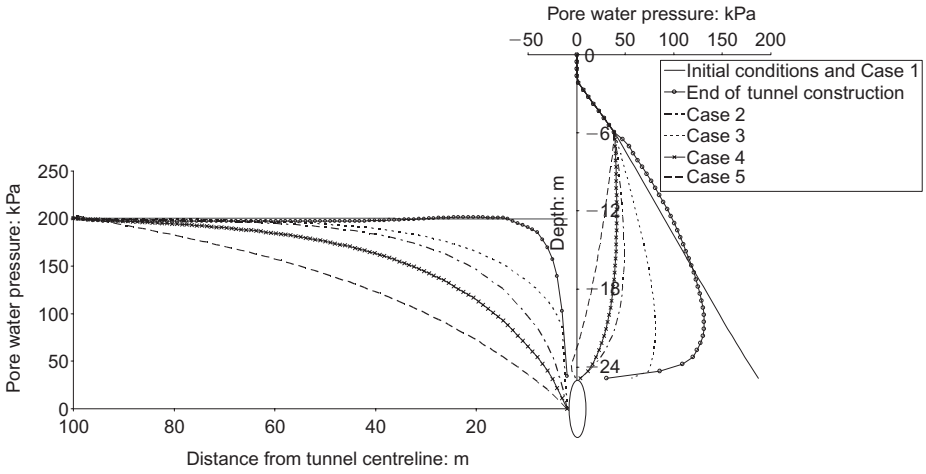

Fig. 48. Pore pressure profiles on the centreline above the tunnel and at axis level: immediately after tunnel construction, and in the long term for Cases 1–5

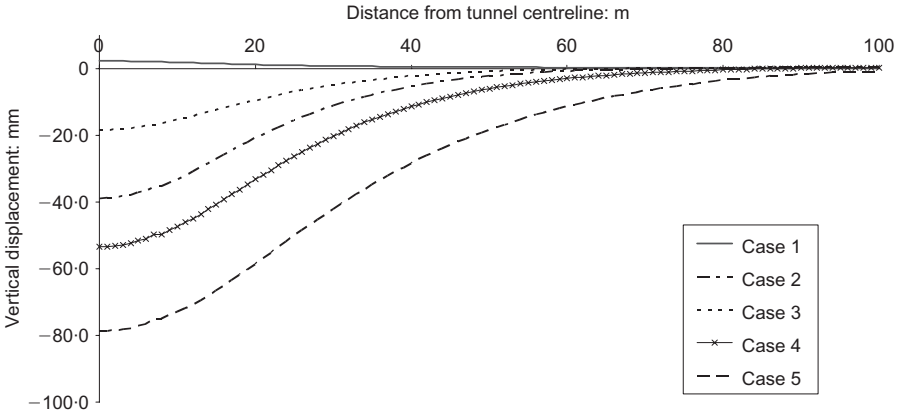

Fig. 49. Influence of soil and tunnel lining permeability on long-term settlement profiles: Cases 1–5

cases show that by simply varying the permeabilities of the tunnel lining and the tunnel soil layer within reasonable, credible bounds, with no other parameter being changed, the magnitude of the maximum long-term settlement varies from zero to 80 mm: the width of the settlement trough correspondingly increases.

The long-term distortion of the tunnel is also affected by the assumed permeabilities of the tunnel lining and the tunnel soil layer. There is a general tendency for a tunnel lining in clay soils to squat with time, as shown in Fig. 39, with a reduction in the vertical diameter (Δ_v) and a corresponding increase in the horizontal diameter (Δ_h). The changes in vertical and horizontal diameter with time for the five cases analysed for the parametric study are shown in Fig. 50. For Case 1 there is a very slight (but almost negligible) long-term increase in vertical diameter and a corresponding reduction in horizontal diameter. For Cases 2–5 the tunnel squats, with the reduction in vertical diameter approximately matching the increase in horizontal diameter.

The magnitude of the tunnel squat shown in Fig. 50 follows the same trend as the maximum long-term settlement illustrated in Fig. 49. The squat increases simply as a result of the change in permeability of the tunnel lining or of the tunnel soil layer, and varies from zero to around 20 mm depending on the assumptions made. Field measurements of differences from circularity include construction effects as well as long-term consolidation effects; 20 mm squat (corresponding to $\Delta_v/D = 0{\cdot}5\%$) is sometimes observed in old tunnels in London Clay, and in some cases can be more; the differences observed in the field are probably a consequence of different lining or tunnel soil layer permeabilities as well as differences in construction tolerances.

Wongsaroj (2005) conducted three-dimensional and two-dimensional finite element analyses of shield tunnel construction in London Clay, using ABAQUS and a critical-state model; many factors were explored, including stiffness anisotropy, influence of K_0, initial pore pressure conditions and the influence of tunnel and soil permeability (Wongsaroj, 2005; Wongsaroj *et al.*, 2006). An extensive parametric study was undertaken of the influence of tunnel lining and soil permeability on long-term ground movements; similar assumptions were made regarding the tunnel boundary flow conditions as in Shin *et al.* (2002), referred to earlier. As shown in Fig. 51, Wongsaroj (2005) defined a dimensionless settlement as

$$\mathrm{DS} = \frac{\delta - \delta_{\mathrm{imp}}}{\delta_{\mathrm{perm}} - \delta_{\mathrm{imp}}} \tag{15}$$

where δ is the maximum long-term settlement for a particular case, δ_{imp} is the maximum long-term settlement for a fully impermeable tunnel lining, and δ_{perm} is the maximum long-term settlement for a fully permeable tunnel lining.

For a fully impermeable tunnel lining, where there is no flow, DS = 0, whereas for a fully permeable tunnel lining DS = 1. Wongsaroj (2005) also expressed the permeability of the tunnel lining relative to that of the soil in terms of the relative permeability RP, a dimensionless number defined as

$$\mathrm{RP} = \frac{k_{\mathrm{lining}}}{k_{\mathrm{soil}}} \cdot \frac{C}{t_{\mathrm{L}}} \tag{16}$$

where k_{lining} is the permeability of the tunnel lining; k_{soil} is the permeability of the soil ($k_{\mathrm{soil}} = (k_v.k_h)^{0{\cdot}5}$ in cases of anisotropic permeability); C is the clay cover above the tunnel crown; and t_{L} is the thickness of the tunnel lining.

Figure 52 shows Wongsaroj's results plotted in terms of

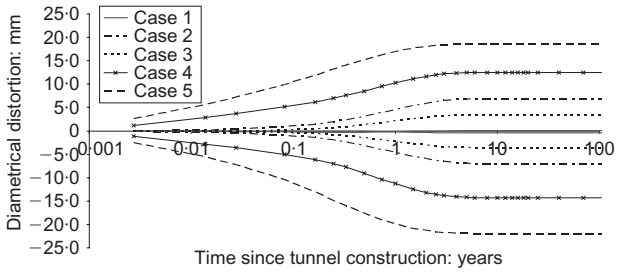

Fig. 50. Influence of soil and tunnel lining permeability on time-dependent diametral distortion of tunnel: Cases 1–5 (increase in horizontal diameter shown positive, decrease in vertical diameter shown negative)

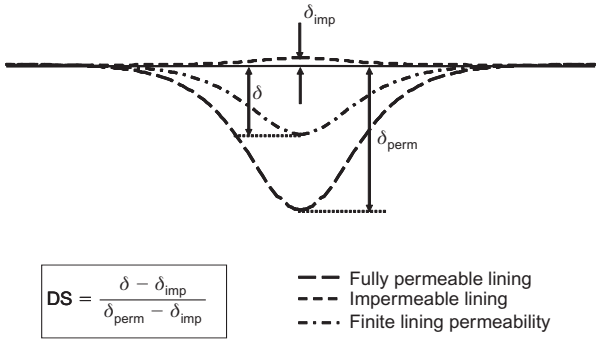

Fig. 51. Definition of dimensionless settlement DS (Wongsaroj, 2005)

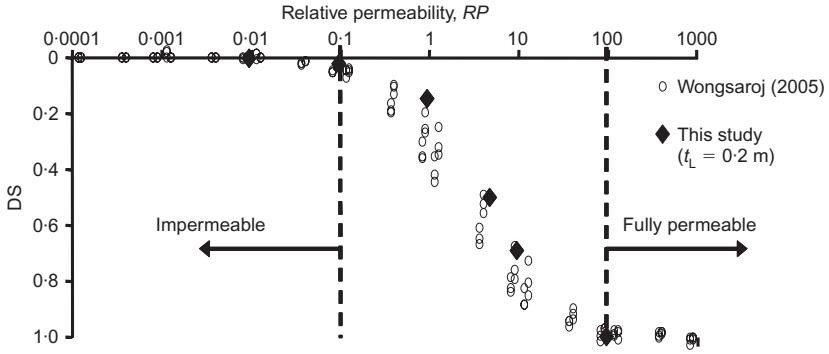

Fig. 52. Influence of tunnel lining permeability on maximum predicted surface settlements: see Fig. 51 and equation (15) for definitions of dimensionless settlement DS, and equation (16) for definition of relative permeability RP)

DS and RP defined above. They all fall within a relatively narrow band, and the results of the parametric study described in this paper also fall within the same band (the equivalent lining thickness t_L was 200 mm). From Fig. 52 it can be seen that DS = 0, indicating an impermeable system, for RP $<$ 0·1; and DS = 1, indicating a fully permeable system, for RP $>$ 100.

The results of the ICFEP finite element analyses, described above, shown in Fig. 52 (as the points 'This study'), are in reasonably good agreement with Wongsaroj's results.

It is clearly a simplification to consider the tunnel lining as uniformly permeable. In reality it is more likely that there are specific leaks, perhaps associated with segmental lining joints (although in most cases, except for expanded linings, the linings are grouted). In the case of in situ concrete linings, shrinkage cracks and construction joints can provide leakage paths. Further research is needed to investigate the influence of leaks at specific locations in a tunnel lining. Nevertheless, the results summarised in Fig. 52 are of practical value in enabling engineers to evaluate whether or not the lining–soil system is likely to be impermeable or permeable.

Summary

The pore pressure measurements around old tunnels in London Clay presented earlier indicate that in general the tunnels act as drains, but not in all cases. This is probably the case for tunnels in many types of clay. Many parameters influence the long-term behaviour, but the key factors are

(*a*) the relative permeability of the tunnel lining and soil, RP: if RP $<$ 0·1 the tunnel lining system is effectively impermeable, whereas if RP $>$ 100 the tunnel lining system is effectively fully permeable
(*b*) the degree of anisotropy of the soil permeability and its variability
(*c*) the initial pore pressure prior to tunnelling.

It is clear from the field evidence from St James's Park and Elizabeth House in London, as well as from the parametric study presented in this lecture and from the analyses by Wongsaroj (2005), that long-term settlement associated with tunnels in clays can be appreciable, and can extend to large distances from the tunnel (at least 100 m in some cases). Tunnel linings also squat more when there is larger long-term settlement. Although the magnitude of long-term settlement can be appreciable, the settlement profiles are generally very wide, with consequent curvature and differential settlements being generally small: hence the potential damage to buildings and services caused by long-term settlements is likely to be of little consequence in most cases. However, in cases of multiple tunnel construction it may well be of importance to understand how time-dependent settlements caused by construction of an earlier tunnel might affect the ground through which a later tunnel is to be constructed.

A good understanding of the permeability characteristics of the ground (including the degree of anisotropy), together with sophisticated finite element analysis, is essential for realistic prediction of long-term settlement associated with tunnels.

EFFECTS OF TUNNELLING ON BURIED PIPES

Analytical solution and proposed new design approach

In urban environments underground congestion is becoming increasingly important to tunnel designers. Fig. 53 illustrates the typical variety of underground objects to be considered when contemplating construction of a tunnel: pile foundations (both existing and under construction), other tunnels, and pipelines for services. Estimating the effects of tunnelling on pipelines can be important (see Fig. 54), especially when the infrastructure is old and vulnerable: this generally receives less attention than the assessment of

Fig. 53. Underground congestion in the urban environment (courtesy Keller)

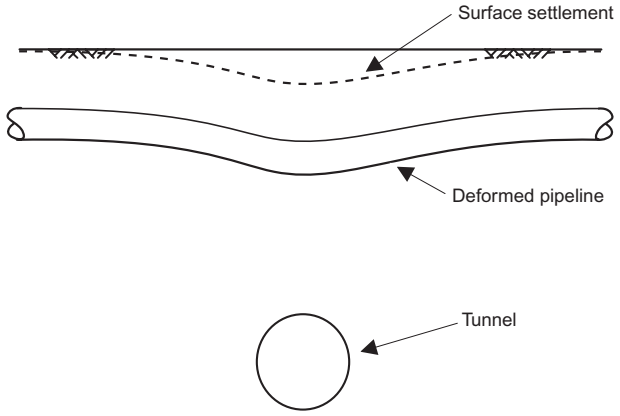

Fig. 54. Deformation of a pipeline due to tunnelling

tunnelling effects on buildings. Different approaches have been followed, most of which have been based on approximating the problem to Winkler-based elasticity models (e.g. Attewell *et al.*, 1986). Limited validation of such models has been obtained from laboratory experiments and analysis of a number of case histories (O'Rourke & Trautmann, 1982; Yeates, 1984; Takagi & Nishio, 1984; Bracegirdle *et al.*, 1996). Most of this work, however, relates to small-diameter pipes. A problem with analytical models based on Winkler springs is that designers face a difficulty with selection of appropriate values for the subgrade modulus or coefficient of subgrade reaction, especially bearing in mind the dependence of these parameters on pipe diameter.

Recent work at Cambridge University has focused on undertaking centrifuge model tests and developing new analytical solutions of pipeline response to tunnelling in terms of continuum elasticity (Vorster, 2005; Klar *et al.*, 2005a; Vorster *et al.*, 2005); monitoring field performance of large-diameter pipes affected by tunnelling has also been undertaken (Vorster, 2005; Vorster *et al.*, 2006). A closed-form solution for a pipe in a continuous elastic medium affected by tunnelling, developed by Klar *et al.* (2005a), is expressed in terms of the parameters defined in Fig. 55. For a pipe with its axis at a depth z_p affected by a tunnel with its axis at a depth z_0, it may for convenience be assumed that the 'greenfield' settlement (ignoring the presence of the pipe) at the level of the pipe is Gaussian. The relevant soil parameters are: V_L, the volume loss associated with the tunnelling; S_{max}, the maximum soil settlement at a level corresponding to the axis of the pipe, and i, the trough width parameter. In addition, elastic soil parameters are Young's modulus E_s and Poisson's ratio ν. For a continuous pipeline the relevant parameters are: the bending stiffness E_pI_p (where E_p is Young's modulus and I_p is the second moment of area), the axial stiffness E_pA (where A is the cross-sectional area), the outer pipe radius r_o, and M, bending moment induced in the pipe.

A closed-form solution for the maximum sagging and hogging bending moments induced in a continuous pipeline by tunnelling is shown in Fig. 56: this was derived by Klar *et al.* (2005a) using an elastic continuum method employing Mindlin's solution (Green's function). Normalised bending moment is plotted against relative pipe–soil bending stiffness R on a logarithmic scale. The bending moment M is normalised as M_n, defined as

$$M_n = \frac{Mi^2}{E_pI_pS_{max}} \tag{17}$$

where E_pI_p is the pipe bending stiffness, and S_{max} and i are the 'greenfield' settlement trough parameters at the level of the pipe axis (see Fig. 55). Infinitely flexible behaviour for settlement described in a Gaussian form corresponds to the maximum normalised sagging moment $M_n = 1$ (and the maximum normalised hogging moment $M_n = 0{\cdot}45$). The relative pipe–soil bending stiffness R is defined as

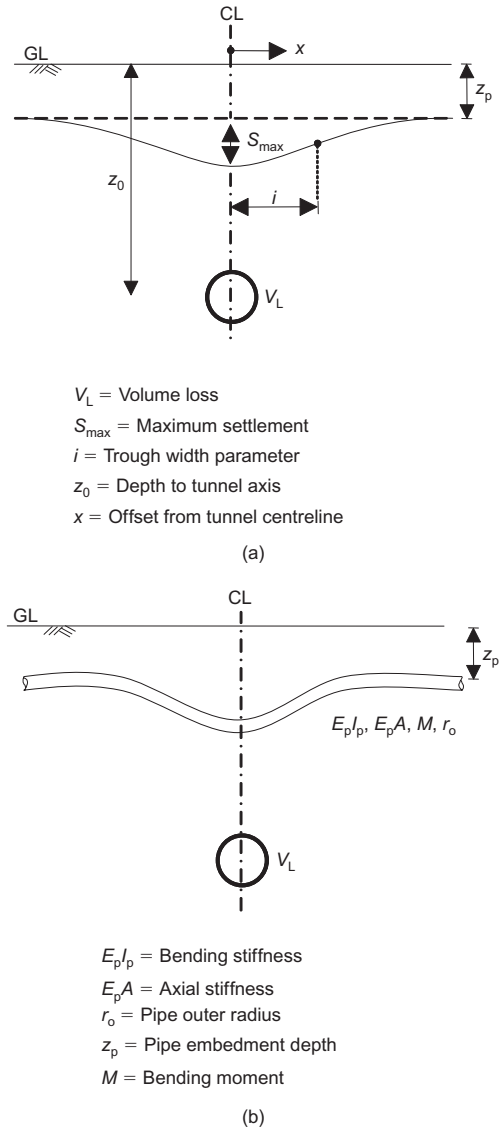

Fig. 55. Definitions of parameters for a pipeline affected by tunnelling: (a) subsurface soil settlement in the greenfield; (b) continuous pipeline

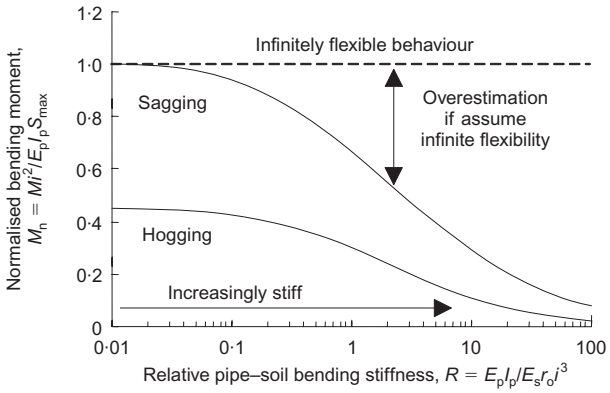

Fig. 56. Pipe–soil interaction using continuum elasticity (Vorster *et al.*, 2005)

$$R = \frac{E_p I_p}{E_s r_o i^3} \tag{18}$$

where r_o is the pipe outer radius and E_s is the Young's modulus of the soil around the pipe. Key assumptions in the derivation of this closed-form solution are as follows.

(*a*) The pipe is buried in homogeneous soil.
(*b*) The pipe is always in contact with the soil (i.e. no separation occurs).
(*c*) The presence of the pipe does not affect the tunnel.
(*d*) The soil response to loading at pipe level is not affected by the tunnel.
(*e*) The 'greenfield' soil displacement at pipe level is given by the Gaussian equation (see equation (12) and Fig. 55).

The closed-form solution shown in Fig. 56 was derived for the greenfield settlement being Gaussian, but the method can be applied to any shape function used to describe the settlement curve (Vorster *et al.*, 2005).

It can be seen from Fig. 56 that the bending moments can be significantly overestimated if the pipe is assumed to be infinitely flexible—that is, if it is assumed to follow the 'greenfield' settlement profile, when it in fact reacts in a stiffer manner. The assumption of infinitely flexible behaviour is valid only for R values less than about 0·1. A pipeline may behave 'flexibly' under a given set of circumstances, but 'stiffly' in another depending on its associated value of R. For smaller values of R ($< 0{\cdot}1$) it is reasonable to disregard pipe–soil interaction and simply assume that the pipe follows the curvature of the soil; for larger values, this will significantly overestimate the bending moment, and interaction analysis is required.

It is important to note that the scale for R in Fig. 56 is logarithmic. Therefore, if a reasonable estimate can be made for E_s, R can be determined with sufficient accuracy for practical purposes. Many pipes are embedded in granular soils, often because they are installed in trenches that have been filled with compacted sand or gravel. As with all soils, there is a degradation of stiffness of such soils with strain level; typical data for Toyoura and Ticino sands are shown in Fig. 57 (Tatsuoka *et al.*, 1997), showing the secant shear modulus G_{sec} measured in triaxial compression (TC) and plane strain compression (PSC) tests at two different levels of confining stress (comparable to the stress levels applicable to many shallow pipelines). Jovicic & Coop (1997) also provide useful data on the stiffness of coarse-grained soils at small strains.

Vorster (2005) derived an expression for the average soil shear strain γ_a along the pipe between $+2{\cdot}5i$ and $-2{\cdot}5i$; this is also given in Vorster *et al.* (2005). For pipelines near to the ground surface, it can be shown that the expression leads to a simplified approximation for γ_a, useful for preliminary design purposes, given by

$$\gamma_a = 0{\cdot}5 \frac{V_L}{(z_0/D_T)^2} \tag{19}$$

where V_L is the tunnel volume loss, and z_0 and D_T are the depth and diameter of the tunnel respectively. The average soil shear strain increases with volume loss V_L, and hence the value of the Young's modulus E_s correspondingly reduces, in the manner shown in Fig. 57. It could be expected, therefore, that the relative pipe–soil bending stiffness R would increase with increasing tunnel volume loss; from Fig. 56 it can be seen that the normalised bending moment M_n would correspondingly reduce.

A design procedure based on an approach proposed by Vorster *et al.* (2005) is as follows.

(*a*) Establish the likely 'greenfield' soil displacements at pipe level (volume loss V_L, trough width parameter i).
(*b*) Estimate the average soil shear strain at pipe level (using equation (19)) and hence an appropriate soil stiffness E_s.
(*c*) Calculate the relative pipe–soil bending stiffness R from equation (18).
(*d*) Calculate the maximum bending moments (and resulting pipe bending strain) using the interaction diagram in Fig. 56.

Vorster (2005) showed that the estimation of only bending strain for cases where $R > 0{\cdot}3$ provides a conservative estimate of the maximum tensile pipe strain. Where $R < 0{\cdot}3$ the combination of axial and bending tensile strains in the hogging location is likely to produce the critical tensile strain for which the pipe should be designed. In the latter case the method should be supplemented by estimates of axial strain (e.g. Attewell *et al.*, 1986; Bracegirdle *et al.*, 1996) to find the maximum tensile strain for which the pipe should be designed.

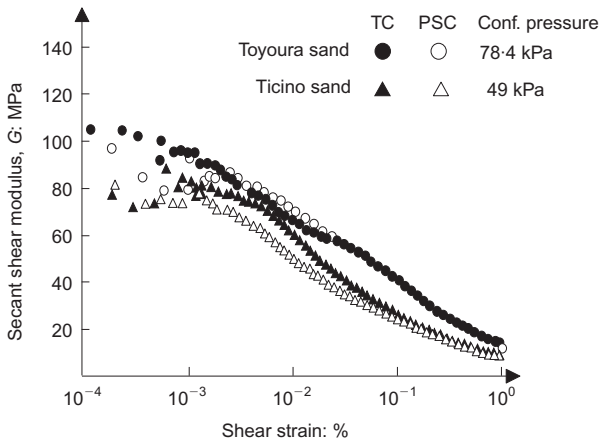

Fig. 57. Stiffness measurements for Toyoura and Ticino sand (Tatsuoka *et al.*, 1997)

Validation by centrifuge model tests

A series of centrifuge model tests was undertaken by Vorster (2005) on the Cambridge 8 m diameter centrifuge to validate this proposed design procedure, and to explore in detail the mechanisms of pipe–soil interaction associated with tunnel-induced ground movements (Vorster *et al.*, 2005b). Fig. 58 shows the layout of the test arrangement. The centrifuge tests were undertaken at 75*g* in dry sand in which a model tunnel of diameter $D_T = 60$ mm was used to represent a 4·5 m diameter tunnel at full scale. Pipes of different diameter D_p and stiffness (E_pI_p and E_pA) were tested at different geometries, varying the cover of the pipe, C_p, and the distance above the tunnel, H. The tunnel comprised a hollow central brass mandrel over which a latex membrane was fitted, such that a known volume of water in the annulus between the membrane and the mandrel could be extracted, thereby inducing volume loss. Settlements of the ground surface at distance from the pipe were measured with lasers and LVDTs; settlements of the pipe and of the ground at distance from the pipe (at pipe invert level) were measured using LVDTs with extensometers. Soil stresses and pipe/soil contact pressures were also monitored using miniature stress cells. Fig. 59 shows a centrifuge model during preparation, in which the tunnel and a strain-gauged pipe can be seen prior to placing the sand. Three different model pipes were tested at 1 : 75 scale (one of acrylic, two of

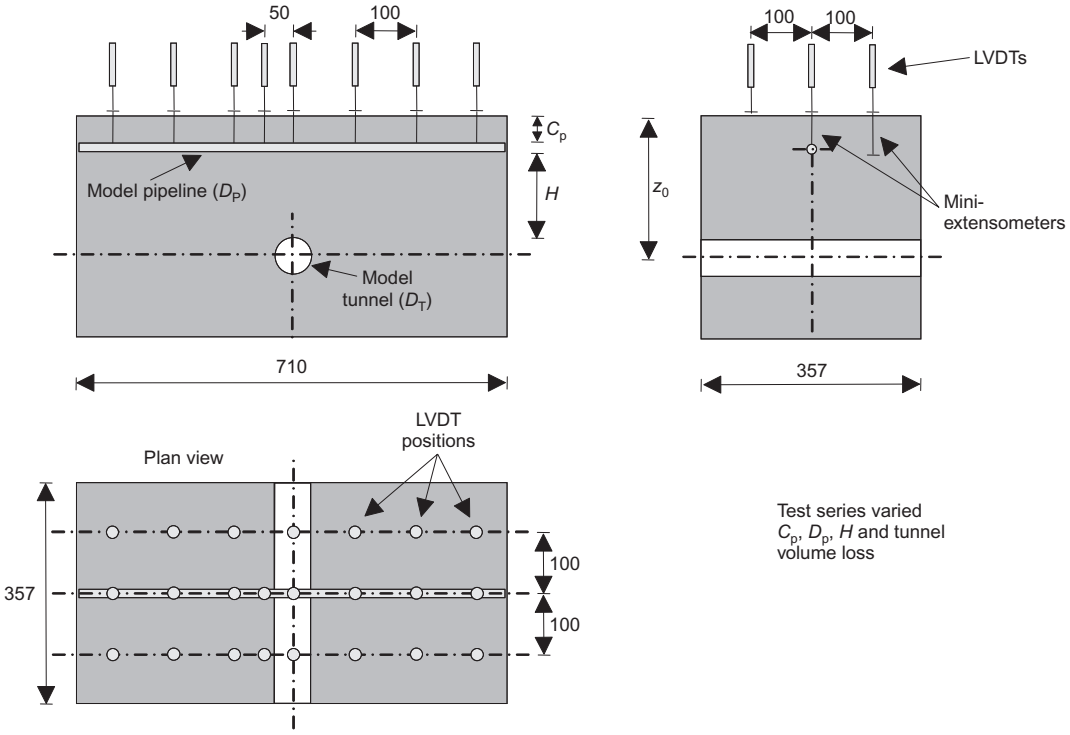

Fig. 58. Centrifuge model testing of the effect of tunnelling on pipelines (Vorster, 2005)

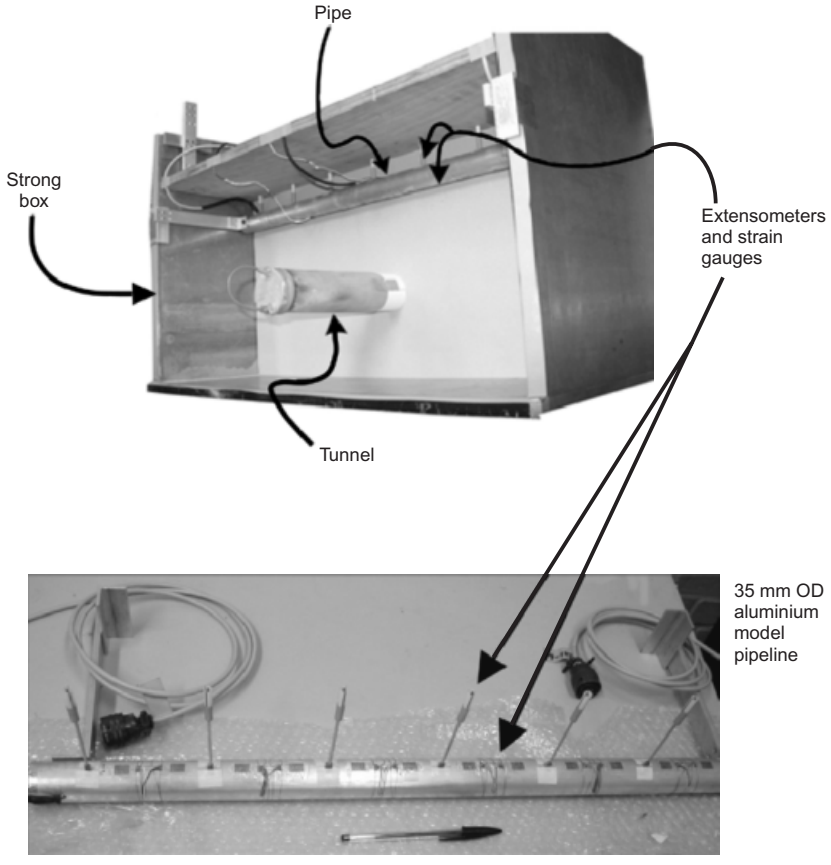

Fig. 59. Centrifuge model preparation (Vorster, 2005)

aluminium alloy), equivalent at full scale to cast iron pipes of 0·7 m and 1·2 m in diameter and a steel pipe of 2·7 m diameter, as shown in Table 4.

Figure 60 shows measurements of bending moments for tests on two pipes of different stiffness but with identical test geometries (pipe diameter $D_p = 16$ mm, $C_p/D_p = 3$, $H/D_T = 0{\cdot}93$, $z_0/D_T = 2{\cdot}5$). Pipe 1 was made of acrylic and pipe 2 of aluminium alloy; pipe 2 had a bending stiffness E_pI_p 16 times that of pipe 1. Normalised bending moment M^* is plotted against x/i, where x is the horizontal distance

Table 4. Model pipes used in centrifuge tests at 75*g* and equivalent prototype pipes in terms of stiffness (Vorster, 2005)

	Model scale	Equivalent prototype pipe
Pipe 1	16 mm OD × 2 mm Acrylic	0·73 m OD × 21·6 mm (28 in OD × 0·85 in) Cast iron
Pipe 2	16 mm OD × 1·22 mm Aluminium	1·22 m OD × 34·9 mm (48 in OD × 1·375 in) Cast iron
Pipe 3	35 mm OD × 1·6 mm Aluminium	2·7 m OD × 20 mm Steel

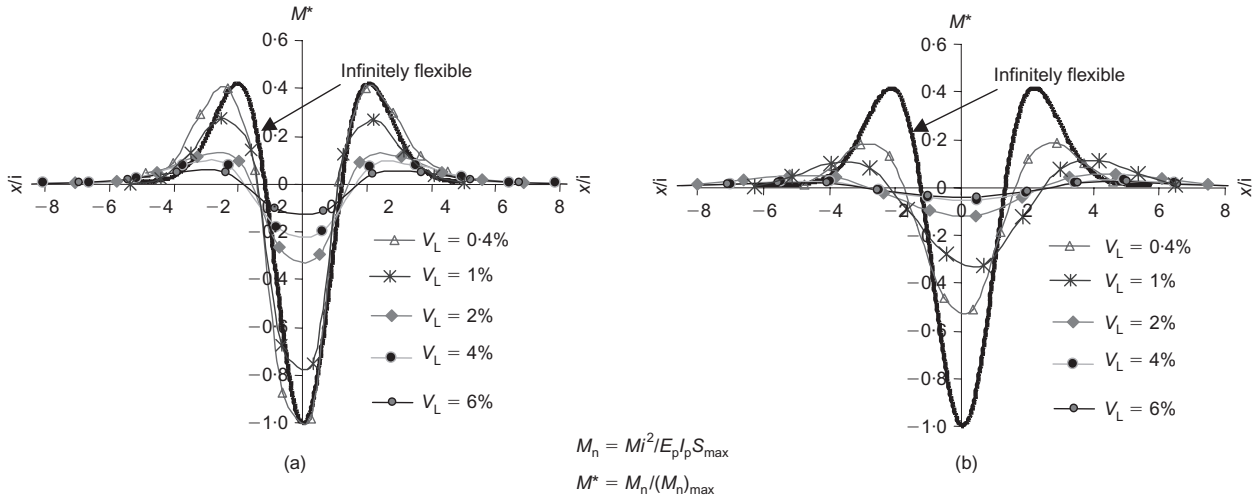

Fig. 60. Centrifuge models—influence of pipe stiffness and tunnel volume loss on bending moments: (a) pipe 1 (acrylic); (b) pipe 2 (aluminium alloy), $= 16(E_pI_p)_{pipe1}$

measured from the tunnel centreline, and i is the settlement trough width parameter for the 'greenfield' settlement; M^* is defined as M_n/M_{nmax}, with M_n as defined in equation (17) and M_{nmax} equal to the maximum value of M_n if the pipe reacts 'infinitely flexibly', following the soil curvature perfectly. The 'infinitely flexible' response is shown on both plots for comparison. At low volume loss ($V_L = 0{\cdot}4\%$) pipe 1 exhibits almost perfectly flexible behaviour whereas pipe 2 shows a significantly stiffer response (the bending moment plot differing markedly from the 'infinitely flexible' response). At $V_L = 1\%$ pipe 1 begins to show a slightly stiffer response, and at $V_L = 2\%$ and at higher volume losses a much stiffer response is seen, comparable with those for pipe 2. The reason for the response becoming stiffer with increasing volume loss is twofold: first, the shear strain is increasing, which leads to a reduction in soil stiffness and a consequent increase in the relative pipe–soil bending stiffness R; second, the settlement trough width parameter i tends to reduce with increasing volume loss, at least initially (Vorster *et al.*, 2005). This means that, while pipes of very different stiffness may behave differently at low tunnel volume loss, similar normalised behaviour is exhibited at higher volume losses.

The proposed design procedure outlined earlier was tested for pipes 1 and 2 (Vorster, 2005) and found to be reasonably accurate at low volume loss (and smaller soil strains), becoming increasingly conservative with increased volume loss (and hence larger soil strains). Fig. 61 shows a comparison of calculated normalised bending moments, using the proposed design procedure, with measured normalised bending moments in the centrifuge test on pipe 1. It can be seen that for volume losses up to around 1·1% the calculated sagging bending moments are in good agreement with the

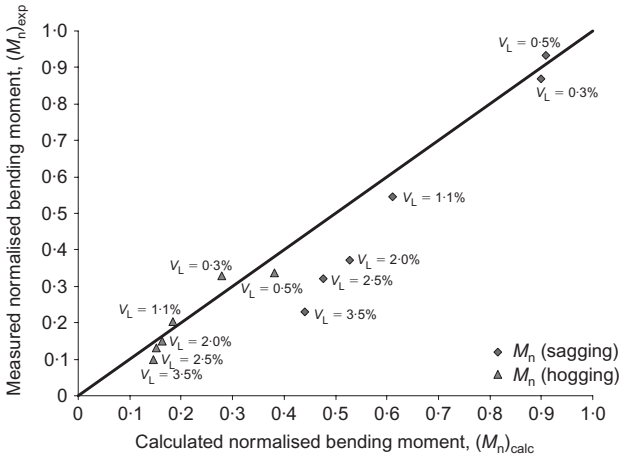

Fig. 61. Centrifuge models: comparison of measured and calculated pipe bending moments for different volume losses using proposed design approach (Vorster, 2005)

measurements, but at higher volume losses the design procedure becomes more conservative (the calculated moments exceeding the measured values by a greater margin). The agreement between calculated and measured hogging bending moments remains good for the full range of volume loss (up to 3·5%).

The increasing overestimation of the sagging bending moments at higher volume losses can be explained by the local interaction mechanisms illustrated in Fig. 62. Gap formation (mechanism A) may occur as separation of the soil from the invert of the pipe takes place; correspondingly,

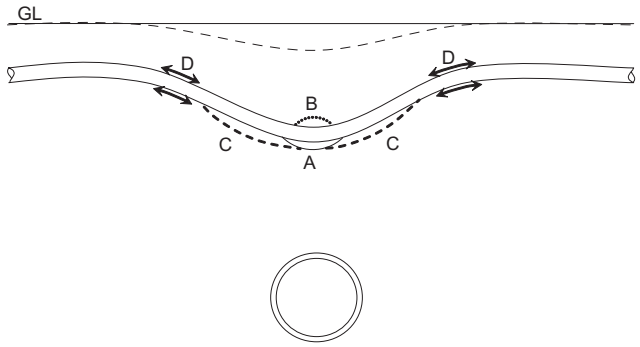

Fig. 62. Postulated local pipe–soil interaction mechanisms in centrifuge tests (Vorster, 2005): A, gap formation; B, local negative downdrag (soil settling more than pipe); C, local positive downdrag (pipe settling more than soil); D, longitudinal pipe–soil interaction

as the soil settles more than the pipeline in this region, local negative downdrag (mechanism B) may occur. At other regions the pipeline may settle more than the soil (mechanism C), and longitudinal interaction (mechanism D) may also become significant for larger ground movements. Mechanism A was observed in the centrifuge tests undertaken by Vorster (2005), particularly at higher volume losses, and the mechanisms B, C and D were postulated, based on the observations: each of these mechanisms affects the simple continuum elasticity assumptions. Gap formation (mechanism A) is illustrated in Fig. 63, in which the response of a miniature Entran stress cell (with a diaphragm of 4 mm diameter and 0·11 mm thickness) at the invert of a pipe is plotted against tunnel volume loss. It can be seen that the total stress reduces with increasing volume loss, with formation of a gap being indicated at a volume loss of about 1·5%. The influence of some of the local interaction mechanisms illustrated in Fig. 62 can be introduced into analyses, by means of local plasticity (Klar *et al.*, 2005b), but for design purposes the procedure outlined earlier is often sufficient, especially as expected tunnel volume losses in practice are usually small.

As a practical guide to estimating the need for taking account of the effect of pipe–soil interaction, Vorster (2005) showed that for $R < 0{\cdot}1$ the pipe–soil system is likely to behave infinitely flexibly, with the pipe following the curvature of the 'greenfield' soil. Good estimation of the likely 'greenfield' curvature at pipe level is required to ensure realistic analysis, but no pipe–soil interaction analysis is required. For $R > 5$ the pipe is likely to provide significant resistance to ground movement; pipe–soil interaction analysis, using the procedure outlined earlier (and in Vorster *et al.*, 2005), is then required to avoid being overly conservative, but accurate estimation of 'greenfield' curvature is of lesser importance. For cases where $0{\cdot}1 < R < 5$, good estimation of 'greenfield' soil curvature and pipe–soil interaction analysis are necessary.

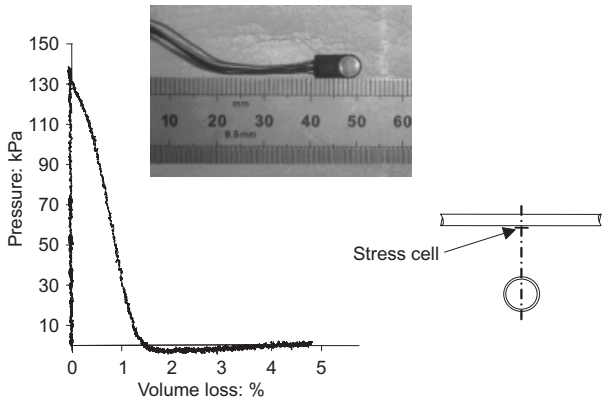

Fig. 63. Gap formation beneath pipe in centrifuge test (Vorster, 2005)

Jointed pipelines and field measurements

The foregoing relates to the response of continuous pipelines to tunnelling. In practice many pipelines are jointed, and it is known that different joints have different properties in relation to joint rotation and axial restraint (e.g. Attewell *et al.*, 1986; Maragakis *et al.*, 2003). Current design practice usually assumes that jointed pipelines respond infinitely flexibly (i.e. they follow the greenfield ground settlement profile); joint rotation and pullout are usually the only design criteria required (e.g. O'Rourke & Trautman, 1982; Bracegirdle *et al.*, 1996, Finno *et al.*, 2003). Normalised solutions to evaluate pipeline bending moments and joint rotations are given by Klar *et al.* (2008), taking account of relative pipe–soil bending stiffness and relative pipe-joint stiffness.

Vorster (2005) also undertook centrifuge model tests on jointed pipes, using the same experimental procedures as outlined earlier for continuous pipes; the model pipe joints had negligible rotational and axial stiffness compared with individual pipe sections. The influence of joint location in relation to the tunnel centreline was investigated. It was found that jointed pipelines should not necessarily be regarded as 'infinitely flexible': depending on the pipe stiffness, and on the condition and location of the joints, jointed pipelines are able to resist ground movement. There may well be cases where pipe strain should also be a design parameter (as for continuous pipes), along with joint rotation and pullout criteria: full details are given by Vorster (2005).

Jointed pipelines may in some circumstances behave as continuous pipelines, especially at low tunnel volume losses. Cambridge University undertook field measurements of the response of a 942 mm diameter high-pressure water main pipeline in Chingford to construction of a 2·47 m diameter tunnel, as shown in Fig. 64. Part of the pipeline was a jointed prestressed concrete-lined steel cylinder (PSC) and part of it was continuously welded steel. Optical fibre was used to measure the longitudinal strain induced at the crown of the PSC portion of the pipeline (the novel optical fibre sensing technique used is described later in this lecture). Fig. 65 shows how there was a transition in pipe behaviour from being continuous to fully jointed with increasing tunnel volume loss: this occurred when the tensile limit of the mortar joints was exceeded. The field monitoring confirmed observations of jointed pipeline behaviour observed in the centrifuge tests. Full details of the field measurements at Chingford are reported by Vorster (2005) and Vorster *et al.* (2006).

Summary

The new closed-form solution for continuous pipes has led to a proposed design approach taking into account the reduction of soil stiffness with increasing shear strain as a result of tunnel volume loss. Centrifuge tests have validated the design approach, and have provided new insights into mechanisms of pipe–soil interaction. 'Flexible' pipes may become 'stiffer' with increasing volume loss and associated increasing soil shear strain. Pipe strain is the key design criterion for continuous pipelines. Jointed pipelines, for which joint rotation and pullout criteria are important, may exhibit behaviour similar to continuous pipelines, depending on pipe stiffness and joint details.

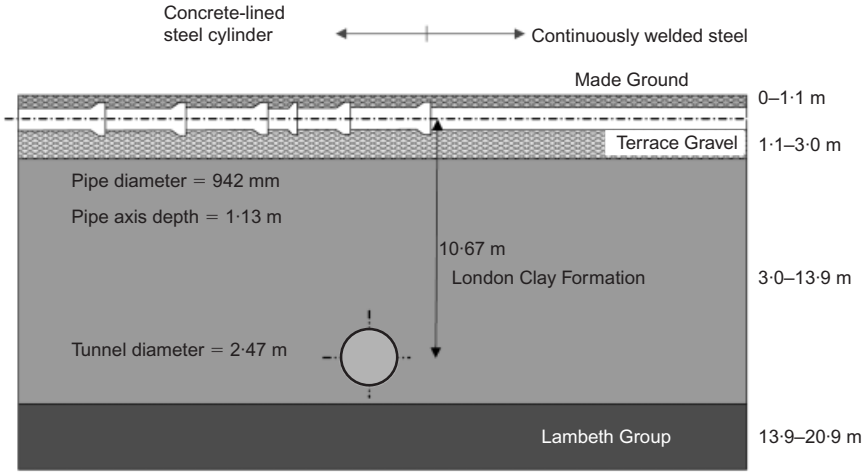

Fig. 64. Field monitoring of pipeline response to tunnelling at Chingford

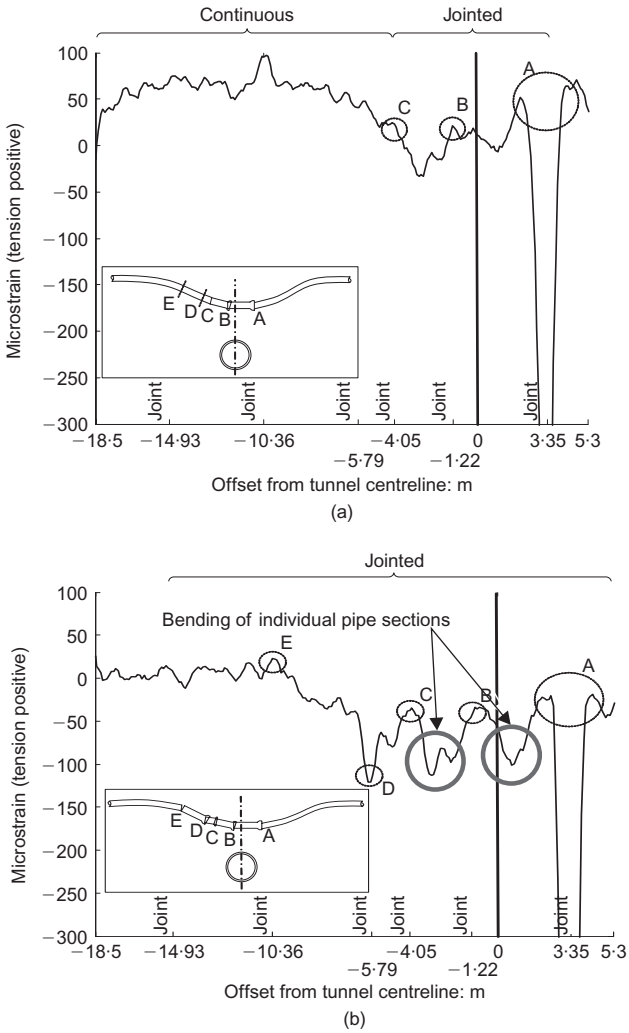

Fig. 65. Observed jointed pipeline response to tunnelling at Chingford: (a) volume loss = 1·2%; (b) volume loss = 3·8%

ADVANCES IN FIBRE OPTIC TECHNOLOGY FOR FIELD MONITORING

A recent subject of research at Cambridge University is a novel technique that uses distributed optical fibre strain sensing (Bennett *et al.*, 2006; Klar *et al.*, 2006; Vorster *et al.*, 2006; Mohamad *et al.*, 2007; Mohamad, 2008). This direct measurement of strain is of considerable potential for many geotechnical and structural applications. The distributed strain sensing technique is based on Brillouin optical time domain reflectometry (BOTDR) (e.g. Horiguchi *et al.*, 1994). Optical fibre sensing in general relies on the interaction between a laser light and the glass material in an optical fibre. A major advantage of the system is that the sensing fibre is standard single optical fibre encased with a 900 μm plastic cover, as shown in Fig. 66. This is cheap, being approximately £0·1/m at 2006 prices; a more robust cable is used to connect the sensing fibre to the monitoring base. Strains and deformations alter the refractive index and geometry of the optical fibre material. These changes perturb the intensity, phase and polarisation of the light-wave propagating along the probing fibre. The principle is illustrated in Fig. 67. If a pulse of light is launched through the fibre the majority travels through, but a small fraction is scattered back. Different components of light power, each with distinctive peaks at certain wavelengths, are identified, as shown in Fig. 67. In the case of Brillouin scattering the frequency of the backscattered light is shifted by an amount linearly proportional to the strain applied at the scattering location. By resolving the backscattered signal in time and frequency a complete strain profile along the full length of the fibre can be obtained. A particular advantage of optical fibre technology comes from the low propagation losses that can be obtained with a single-mode optical fibre. This means that strain can be measured along the full length (up to 10 km) of a suitably installed optical fibre by attaching a BOTDR analyser to one end of the fibre, as shown in Fig. 68. The system offers the following features.

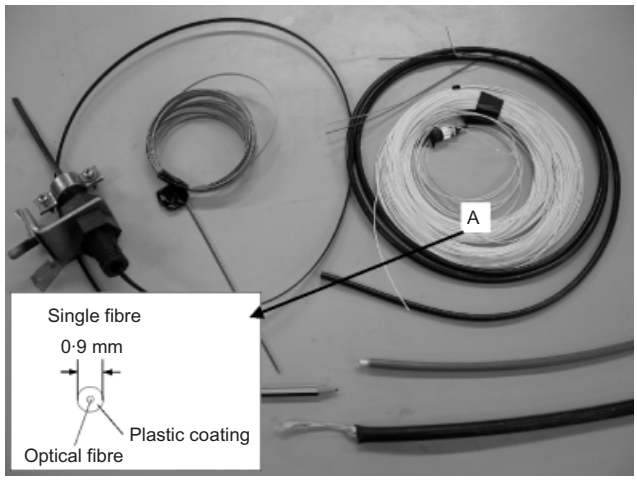

Fig. 66. Types of optical fibre cable (Type A single fibre used for sensing)

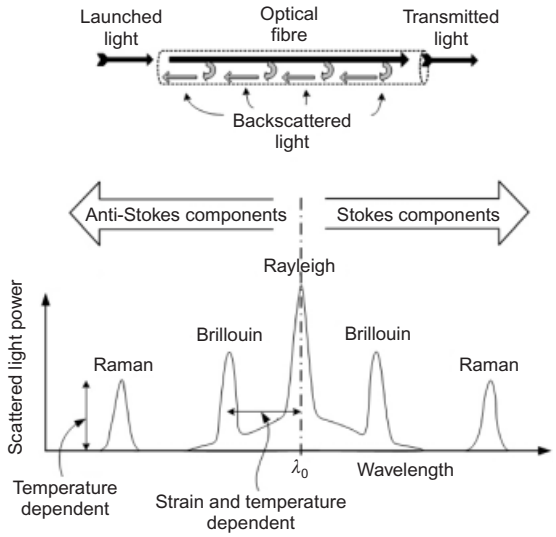

Fig. 67. Principle of distributed optical fibre sensing

(*a*) The average strain over 1 m is measured every 200 mm.
(*b*) The range over which the system can work is 5–10 km.
(*c*) The resolution is 30 με (0·003%).
(*d*) The sensors are very low cost, since the optical fibre is very cheap (although the analyser itself is expensive).
(*e*) The system is almost 'real time', typically taking 5–25 min per measurement.
(*f*) It is possible to link or switch between fibres.

Figure 69 shows a comparison of continuous strain measurement using BOTDR optical fibre in some concrete test piles with measurements from vibrating wire strain gauges (Bennett *et al.*, 2006). The optical fibre was pretensioned to 3000 με and then attached to the pile reinforcement using epoxy resin. The agreement between the two measurement systems is good. Research at Cambridge has implemented the BOTDR optical fibre system in a number of piles and has shown that very detailed information can be gained by continuous strain measurement, compared with measurement at discrete points down the pile (Klar *et al.*, 2006).

The BOTDR technique was applied to the monitoring of strains of the Thameslink Tunnel during construction of the new Thameslink 2000 tunnel beneath it, shown in Fig. 70 (Mohamad, 2008). The Thameslink Tunnel is an old masonry tunnel of external diameter 8·5 m constructed between 1865 and 1868 using the cut and cover method. In 2005 the new twin Thameslink 2000 Tunnels (TL2K) were constructed as part of the Channel Tunnel Rail Link's (CTRL) Section 2 Contract 103 (C103). The new tunnels are of 6 m internal diameter (6·5 m OD), and the northbound tunnel passes underneath the Thameslink Tunnel. with the Midland main line (MML) running at ground level. As shown in Fig. 70, the minimum clearance from the crown of the new tunnel to the invert of the brick-lined tunnel was 3·6 m. Fig. 71 shows the layout of the optical fibre, attached at three longitudinal sections (crown and west and east springlines) and five circumferential sections (CH514 to CH522) spaced over a 60 m length. As shown in Fig. 71, the fibre was attached to the brickwork by means of hooks and epoxy resin, having first been pre-tensioned to 2000–3000 με. Full details of the project are given by Mohamad (2008).

Figure 72 shows the general form of the expected strain around the inner face of the old tunnel as a consequence of constructing a new tunnel beneath it: compression around the crown and tension in the walls. A complete record of the development of strain was obtained as the new tunnel approached, was beneath the masonry tunnel, and passed beyond it. The settlement records indicated that the volume loss associated with the new tunnel construction was around 1% and the maximum settlement experienced by the masonry tunnel was 35 mm. Fig. 73 shows an extract from an animation in which the strain variation at five cross-sections is continuously shown as the new tunnel proceeded southwards beneath the masonry tunnel. The recorded strain is shown at the point when the new tunnel was directly beneath the east wall of the masonry tunnel. Fig. 74 shows the strain when the new tunnel was directly beneath the west wall. In the latter case it can be seen that the maximum tensile strain is 0·25%. However, this was highly localised, and reduced to 0·17% when the new tunnel passed beyond the masonry tunnel. Visual inspection was made at this point, and some visible hairline cracking was indeed observed at the position where the highest tensile strain was recorded. As most cracks in masonry structures tend to appear along the joints of the brickwork, and because the joints had lost some of the mortar, it was difficult to assess whether fine cracks had developed along other sections where high tensile strain was recorded, that is, $> 0{\cdot}1\%$ (Mohamad, 2008).

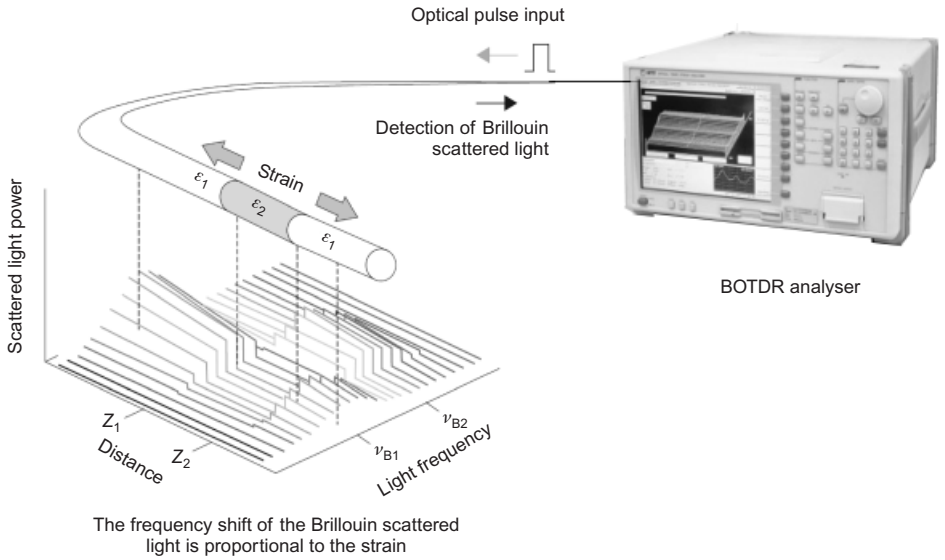

Fig. 68. Application of Brillouin optical time domain reflectometry (BOTDR) to distributed strain measurement in optical fibre

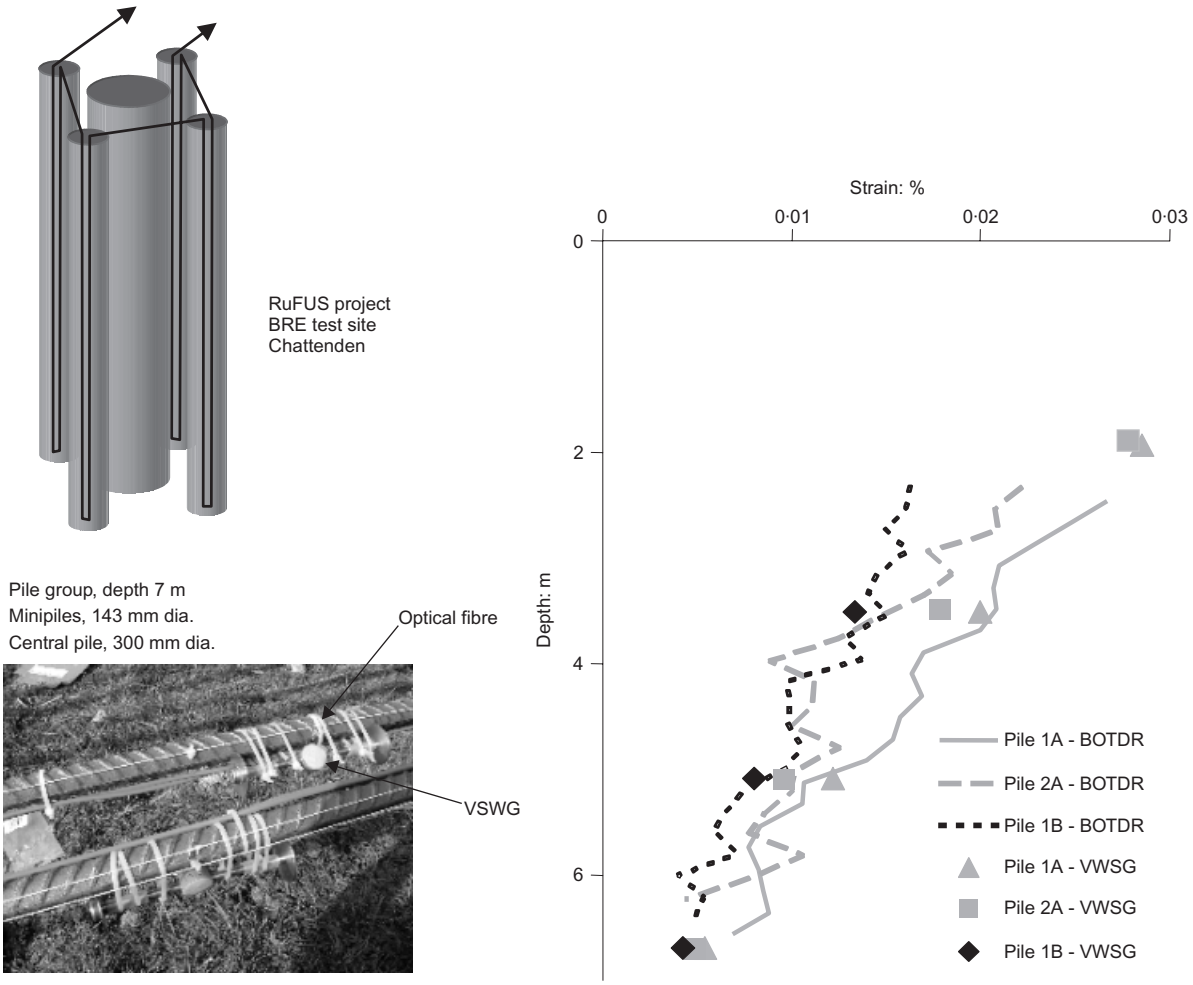

Fig. 69. Comparison of BOTDR with vibrating-wire strain gauges (VWSG) in piles (Bennett *et al.*, 2006)

In summary, the following can be concluded about BOTDR optical fibre sensing.

(*a*) It has shown good comparison with vibrating-wire strain gauge measurement in piles, and has already been used successfully for a number of piling projects.
(*b*) It has provided valuable strain data in the Thameslink masonry tunnel during construction of a new tunnel beneath.
(*c*) The measurement of a continuous strain profile is a big advantage over measurements at discrete locations.
(*d*) The low cost of installation is attractive.

The technique is a promising new development for monitoring of tunnels and many other geotechnical applications.

It allows a direct measurement of the tensile strain of masonry material, which can be extremely useful for the process of risk assessment and monitoring of masonry structures influenced by nearby construction.

CONCLUSIONS

A number of new developments in both the theory and practice of tunnelling have been covered. The following principal conclusions can be drawn.

(*a*) Simplified plasticity models are of considerable value for understanding and interpreting the behaviour of deep tunnels in clays, especially in complex ground conditions, where it may be particularly difficult for designers to characterise the ground properties, as has been demonstrated for the tunnels at Bolu. The simplified models have been validated by field measurements from a range of tunnelling projects.
(*b*) Ground movement control remains critical for tunnelling in urban environments, and earth pressure balance (EPB) tunnelling can routinely achieve low volume losses (<1%) in a wide variety of ground conditions, as has been found for the recently completed CTRL project. Good control of face pressure, through proper control of the excavation chamber pressure, depends on appropriate soil conditioning and screw conveyor operation, about which more is now known.
(*c*) Compensation grouting is an effective method of controlling building response to tunnel construction for most ground conditions. The compensation grouting at Bologna has demonstrated the innovative use of directional drilling to install curved grout tubes. It also demonstrated the successful application of compensation grouting to granular soils, for which there has been generally less experience in comparison to clay soils.
(*d*) Long-term ground movements can be significant, as demonstrated by the 11 years of measurements taken for the Jubilee Line Extension project in London. Tunnel distortions are related to the same consolidation processes associated with leaking tunnel linings that result in long-term settlements. The magnitude of long-term ground movements and tunnel distortions depends principally on the relative permeability of the tunnel lining and soil, on the degree of anisotropy of the soil permeability (and its spatial variability), and on the initial pore pressure prior to tunnelling.
(*e*) A proposed new design approach for assessing the

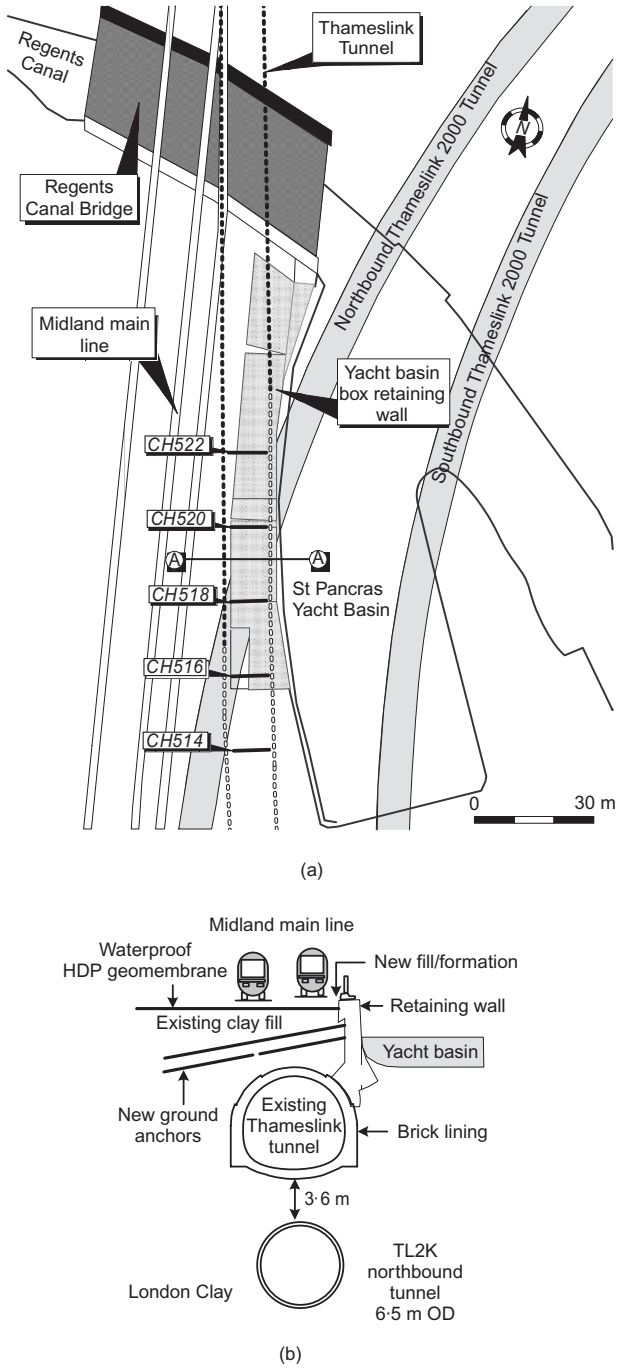

Fig. 70. New Thameslink 2000 (TL2K) tunnel crossing beneath Victorian brick-lined Thameslink tunnel (Mohamad, 2008): (a) plan; (b) section A–A

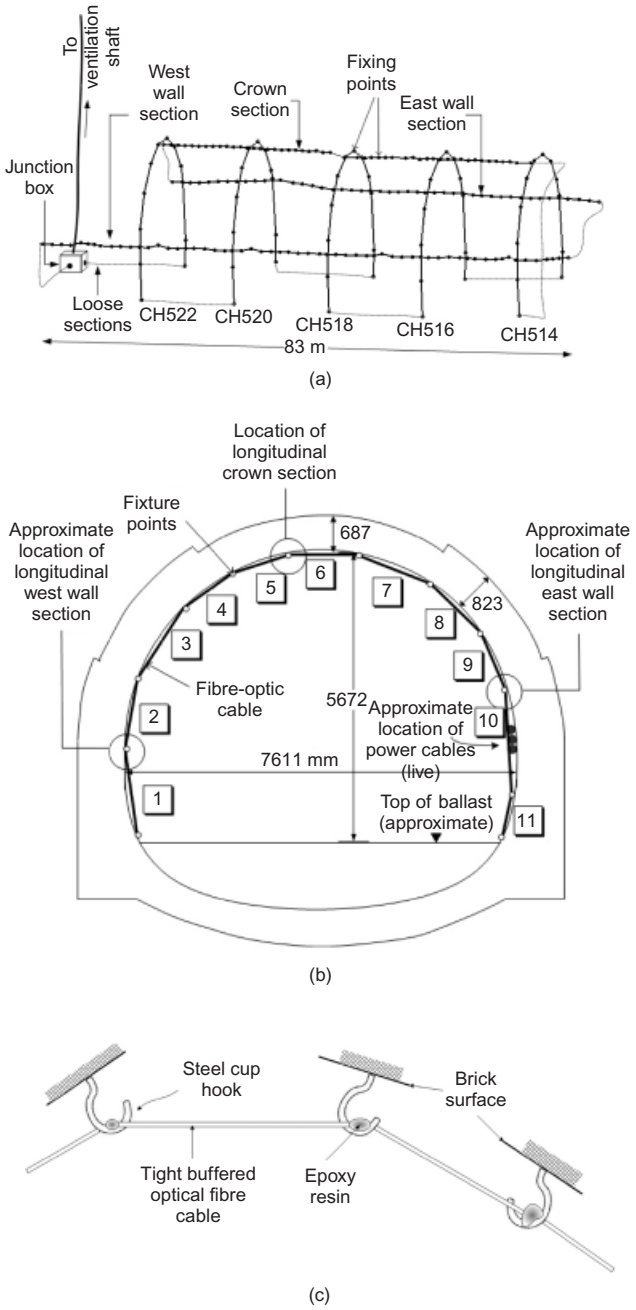

Fig. 71. Arrangement and fixing details of optical fibre for strain monitoring of Thameslink tunnel (Mohamad, 2008): (a) general layout; (b) cross-section; (c) fixing details

effects of tunnelling on pipes has been presented, taking into account the reduction of soil stiffness with increasing shear strain as a result of tunnel volume loss. Centrifuge tests have validated the design approach and have provided new insights into mechanisms of pipe–soil interaction. 'Flexible' pipes may become 'stiffer' with increasing volume loss and associated increasing soil shear strain. Jointed pipelines may exhibit behaviour similar to continuous pipelines, depending on pipe stiffness and joint details.

(*f*) BOTDR fibre optic technology has been shown to be a highly promising new strain-monitoring technique for tunnelling and many other geotechnical applications.

New horizons in tunnelling and geotechnics are ever more challenging: Fig. 75 shows the 15 m diameter Herrenknecht EPB tunnelling machine that was recently in operation for an urban motorway in Madrid (this is currently the largest EPB tunnelling machine in the world). As tunnels become bigger and more numerous, so the role of geotechnical engineering in such projects will become increasingly important. There are many exciting challenges ahead.

ACKNOWLEDGEMENTS

There are many individuals and organisations that the author wishes to thank for their help in preparing the lecture and this paper. Most of the material is drawn from research undertaken by the Cambridge Geotechnical Research Group and from consulting projects with Geotechnical Consulting Group (GCG); the author is indebted to both for their constant stimulation and challenges. He is particularly grateful to David Harris, Dr Chris Menkiti, Professor Neil Taylor, Dr

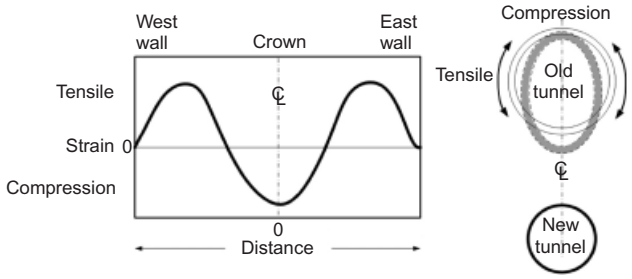

Fig. 72. Expected strain distribution around inner face of old tunnel as a result of construction of new tunnel beneath

Felix Schroeder, Dr Jamie Standing and Dr Ming Wongsaroj for their invaluable assistance. Dr Peter Bennett, Dr Xavier Borghi, Dr Keith Bowers, Alec Marshall, Dr Andrew Merritt, Hisham Mohamad, Professor Kenichi Soga, Dr Eduard Vorster and Peter Wright were also most helpful. Much of the material in this lecture has drawn on recent research undertaken at Cambridge University, some of which has been sponsored by the Engineering and Physical Sciences Research Council, the Cambridge-MIT Institute and Nishimatsu Construction. The author is grateful to Rail Link Engineering and Union Railways (North) for their permission to include material from field research undertaken by the Cambridge Geotechnical Research Group on the recently completed CTRL tunnelling project in the London area. This lecture has also drawn on case histories and consulting projects that I have been closely involved with while working with Geotechnical Consulting Group (GCG)—on the Crossrail project in London, Bologna in Italy, and Bolu in Turkey; I am grateful to my colleagues at GCG and also to Cross London Rail Links Ltd, Italferr of Italy, and KGM and Yuksel-Rendel of Turkey for enabling me to include this material. The assistance of Tube Lines Ltd is also gratefully acknowledged. Finally, the one person who most certainly merits my sincere thanks is my wife Margaret, who has lived for a long time, very patiently, with the thinking and preparation for this lecture.

APPENDIX 1: SOIL CONDITIONING FOR EPB TUNNELLING

General principles

The quantities of soil conditioning agents used in EPB tunnelling machines are expressed in terms of the ratio of the volume of conditioning agent to the volume of ground to be excavated. Polymer injection ratios (PIR) and foam injection ratios (FIR), usually expressed as a percentage, are defined as follows:

$$\mathrm{PIR} = \frac{V_\mathrm{p}}{V_\mathrm{s}} \times 100 \tag{20}$$

$$\mathrm{FIR} = \frac{V_\mathrm{f}}{V_\mathrm{s}} \times 100 \tag{21}$$

where V_p is the volume of polymer solution, V_f is the volume of foam at atmospheric pressure, and V_s is the volume of soil. The properties of the foam strongly depend on its proportion of air and surfactant solution, which is characterised by the foam expansion ratio (FER), expressed as a percentage:

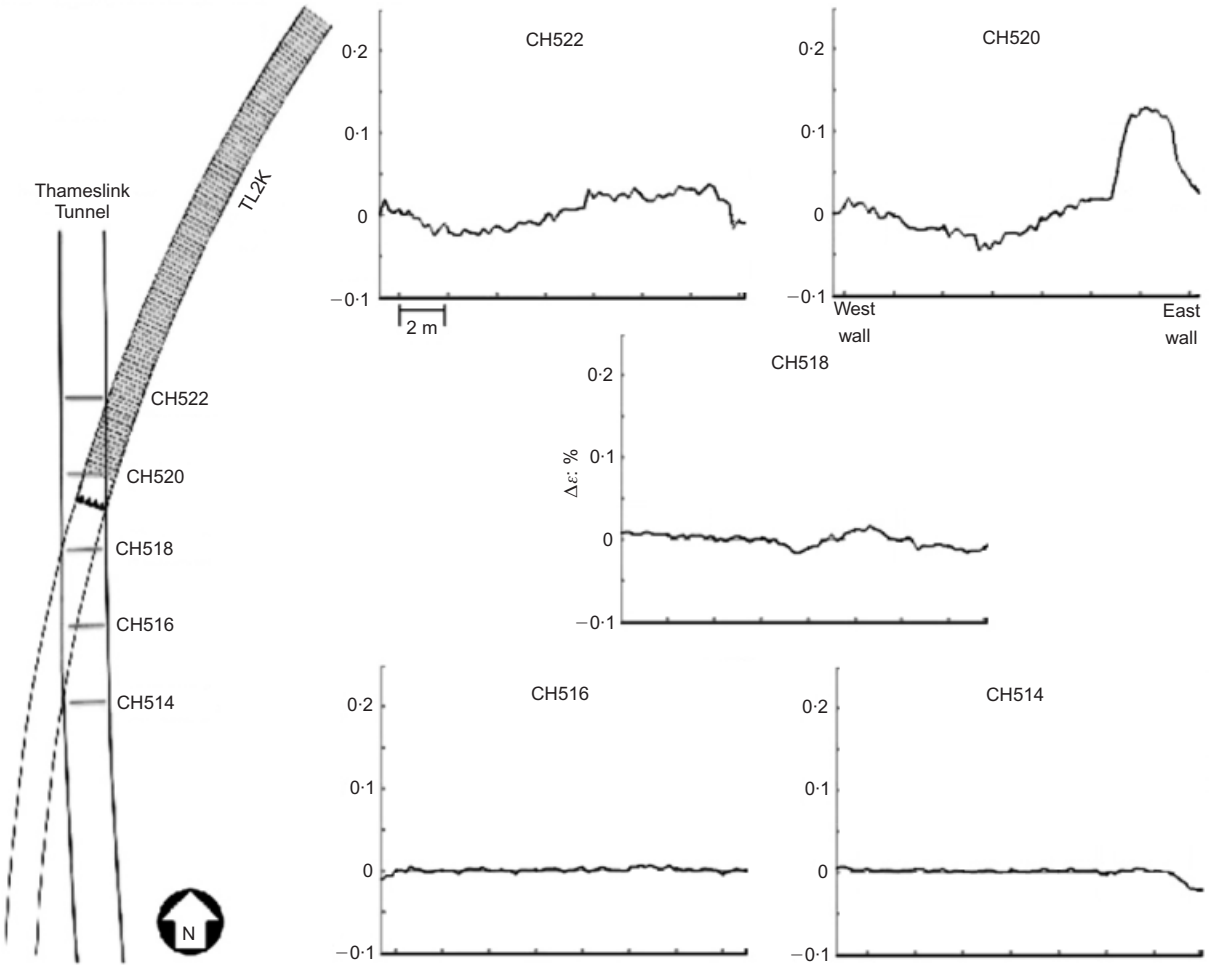

Fig. 73. Strain recorded when new tunnel is directly beneath east wall of old tunnel at CH520 (Mohamad, 2008); measurements made from west wall at track level around tunnel to east wall at track level (see Fig. 71(b))

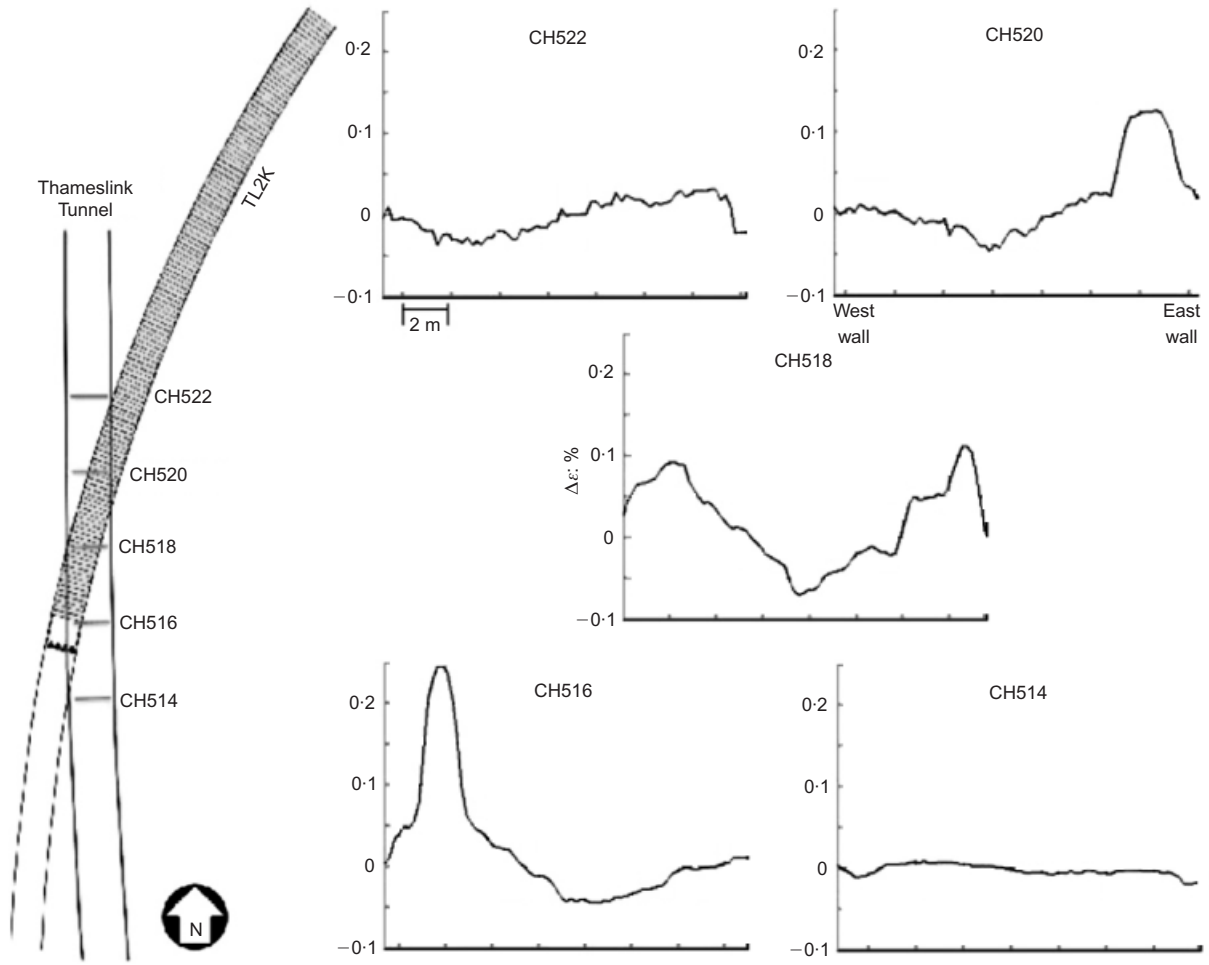

Fig. 74. Strain recorded when new tunnel is directly beneath west wall of old tunnel at CH516 (Mohamad, 2008); measurements made from west wall at track level around tunnel to east wall at track level (see Fig. 71(b))

Fig. 75. Herrenknecht EPB machine, 15 m in diameter, for urban motorway tunnel in Madrid

$$\mathrm{FER} = \frac{V_\mathrm{f}}{V_\mathrm{fl}} \times 100 \tag{22}$$

where V_fl is the volume of foaming liquid solution and V_f is the volume of foam. For a given foam agent a range of FER values can be achieved by varying a number of factors in the foam production (Mair *et al.*, 2003; Merritt, 2004). Typically, FER values are around 10 for many conditioning foams. The total liquid injection ratio (LIR) for a foam and/or polymer conditioner injection is given by

$$\mathrm{LIR} = \frac{V_\mathrm{fl} + V_\mathrm{p}}{V_\mathrm{s}} = \frac{\mathrm{FIR}}{\mathrm{FER}} + \mathrm{PIR} \tag{23}$$

In addition the concentration of surfactant and polymer (c_s and c_p respectively) used in the preparation of the foaming liquid and the polymer solution are defined as

$$c_\mathrm{s} = \frac{V_\mathrm{surf}}{V_\mathrm{fl}} \times 100 \tag{24}$$

$$c_\mathrm{p} = \frac{V_\mathrm{pol}}{V_\mathrm{p}} \times 100 \tag{25}$$

The values of c_s and c_p affect the properties of the foam and polymer solutions, thereby affecting the properties of the conditioned soil.

Limited guidelines on appropriate soil conditioning have been published by EFNARC, based on soil particle distribution only (EFNARC, 2005). Other guidelines have been published by Maidl (1995), Kusakabe *et al.* (1997), Jancsecz *et al.* (1999), Milligan (2001) and Merritt (2004).

Soil conditioning on CTRL Contract 220

Index tests were performed at Cambridge University in advance of tunnelling to assist the contractor in selecting suitable soil conditioning parameters (Mair *et al.*, 2003; Merritt *et al.*, 2003). Full details of the soil conditioning used in practice on CTRL Contract 220 are given by Borghi (2006). The foam injection ratio (FIR) and polymer injection ratio (PIR) for the soil conditioning agents used on Contract 220 are summarised in Fig. 76; further details are given by Borghi (2006) and Borghi & Mair (2006). Average FIR and PIR values are given for all rings (1·50 m excavation) of both the 7·5 km long tunnel drives in each of the

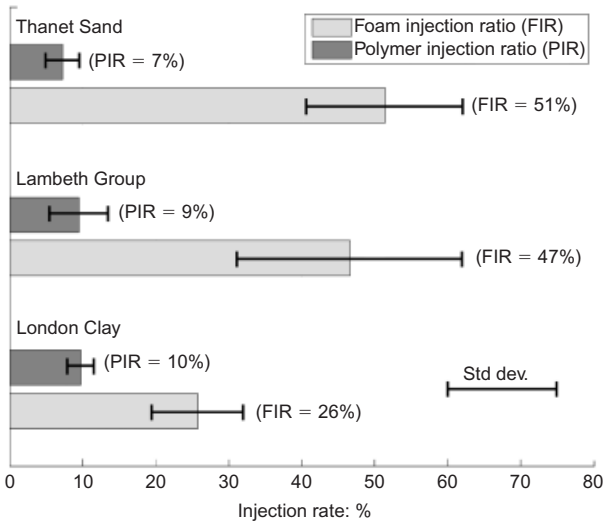

Fig. 76. Injection rates for soil-conditioning agents used in EPB tunnelling on CTRL Contract 220 (Borghi & Mair, 2006)

main types of ground conditions. In the Thanet Sand, the average FIR and PIR values were 51% and 7% respectively. The FIR falls within the range 40–60 recommended by EFNARC (2005) for sandy soils. In the Lambeth Group, an average FIR of 47% and an average PIR of 9% were measured. The FIR showed a relatively large standard deviation, illustrating the difficulty of determining appropriate conditioning treatments in this heterogeneous soil stratum. In many instances FIRs in excess of 200% were used in the Lambeth Group, but no direct benefits of such large quantities of foams could be observed (Borghi, 2006).

The average FIR used in the London Clay was 26%, that is, around 50% of the values used in the Thanet Sand and in the Lambeth Group. The average PIR was 13% for the first tunnel, but was reduced to 6% in the second, with an overall average of 10%. The FIR used in the London Clay fell below the range of 30–80% recommended by EFNARC for clays. However, analysis of machine data suggested that the principal effect of the foam in clay was mostly that of its liquid phase, and that the mechanisms that make foam a suitable additive in sand cannot be expected to be effective in clayey material (Borghi, 2006). Much lower quantities of foam were used in the London Clay than in the Thanet Sand and the Lambeth Group. PIRs of about 15% or less with little or no foam were found adequate to remould the clay mixtures and allow accurate control of the machine operation with little or no pressure decay during ring build. Observation of the conditioned London Clay at the outlet of the screw conveyor revealed poor mixing when large quantities of foam were used: intermittent discharge of large and stiff clay lumps alternated with gushing of fluid and compressed air blows. This heterogeneity is believed to be the result of foam breakdown following sorption of the foaming liquid into the clay, a process also observed in the laboratory (Mair *et al.*, 2003; Merritt *et al.*, 2003).

APPENDIX 2: ASSUMPTIONS IN FE ANALYSES FOR PARAMETRIC STUDY OF LONG-TERM SETTLEMENTS

Linear elastic parameters

See Table 5.

Non-linear elastic equations and parameters

The tangent shear modulus G and bulk modulus K are given by

$$\frac{3G}{p'} = C_1 + C_2 \cos(c_1 X^{c_2}) - C_2 c_1 c_2 \frac{X^{c_2-1}}{2{\cdot}303} \sin(c_1 X^{c_2}) \tag{26}$$

$$\frac{K}{p'} = C_4 + C_5 \cos(c_3 Y^{c_4}) - C_5 c_3 c_4 \frac{Y^{c_4-1}}{2{\cdot}303} \sin(c_3 Y^{c_4}) \tag{27}$$

where

$$X = \log_{10}\left(\frac{E_d}{1{\cdot}732 C_3}\right)$$

and

$$Y = \log_{10}\left(\frac{\varepsilon_v}{C_6}\right)$$

and the other parameters used in these equations are given in Table 6.

Mohr-Coulomb yield surface parameters

See Table 7.

NOTATION

A total face area; cross-sectional area of pipe
A_0 total openings surface area
a tunnel radius
C clay cover above tunnel crown
C_p pipe cover

Table 5. Linear elastic parameters assumed

	Young's modulus, E	Poisson's ratio, ν	Area, A: m^2	Second moment of area, I: m^4
Terrace Gravel	20·0 MPa	0·2	–	–
Thanet Sand	500·0 MPa	0·2	–	–
Tunnel lining	$100{\cdot}0 \times 10^6$ kPa	0·3	$33{\cdot}66 \times 10^{-3}$	$3{\cdot}9687 \times 10^{-5}$

Table 6. Parameters assumed in equations (26) and (27)

	C_1	C_2	C_3: %	c_1	c_2	$E_{d(min)}$: %	$E_{d(max)}$: %	G_{min}: kPa
London Clay 1	1400·0	1270·0	$1{\cdot}0 \times 10^{-4}$	1·335	0·617	$8{\cdot}66 \times 10^{-4}$	0·693	2667·0
London Clay 2	1400·0	1270·0	$1{\cdot}0 \times 10^{-4}$	1·335	0·617	$8{\cdot}66 \times 10^{-4}$	0·693	2667·0
Lambeth Group 1	1400·0	1270·0	$1{\cdot}0 \times 10^{-4}$	1·335	0·617	$8{\cdot}66 \times 10^{-4}$	0·693	2667·0
Lambeth Group 2	1400·0	1270·0	$1{\cdot}0 \times 10^{-4}$	1·335	0·617	$8{\cdot}66 \times 10^{-4}$	0·693	2667·0
	C_4	C_5	C_6: %	c_3	c_4	$\varepsilon_{v(min)}$: %	$\varepsilon_{v(max)}$: %	K_{min}: kPa
London Clay 1	686·0	633·0	$1{\cdot}0 \times 10^{-3}$	2·069	0·420	$5{\cdot}0 \times 10^{-3}$	0·15	5000·0
London Clay 2	686·0	633·0	$1{\cdot}0 \times 10^{-3}$	2·069	0·420	$5{\cdot}0 \times 10^{-3}$	0·15	5000·0
Lambeth Group 1	686·0	633·0	$1{\cdot}0 \times 10^{-3}$	2·069	0·420	$5{\cdot}0 \times 10^{-3}$	0·15	5000·0
Lambeth Group 2	686·0	633·0	$1{\cdot}0 \times 10^{-3}$	2·069	0·420	$5{\cdot}0 \times 10^{-3}$	0·15	5000·0

Table 7. Mohr–Coulomb yield surface and plastic potential parameters

	Cohesion, c': kPa	Angle of shearing resistance, ϕ': degrees	Angle of dilation, ψ': degrees
Terrace Gravel	0·0	35·0	17·5
London Clay 1	5·0	25·0	12·5*
London Clay 2	5·0	25·0	12·5*
Lambeth Group 1	5·0	25·0	12·5*
Lambeth Group 2	5·0	25·0	12·5*
Thanet Sand	0·0	40·0	0·0

* During pore water pressure dissipation in the long term an angle of dilation, $\psi' = 0{\cdot}0°$ has been assumed.

c' effective cohesion
c_p concentration of polymer
c_s concentration of surfactant
D tunnel outside diameter; diameter of tunnel lining
D_p pipe diameter
D_T tunnel diameter
DS dimensionless settlement
E_l Young's modulus of tunnel lining
E_p Young's modulus of pipe
E_s Young's modulus of soil
E_u undrained Young's modulus
f_{cu} shotcrete design cube strength
G tangent shear modulus
G_{sec} secant shear modulus
G_0 maximum shear modulus
H distance above tunnel
I_p second moment of area of pipe
i trough width parameter, settlement trough width parameter
K equivalent spring stiffness; trough width; bulk modulus
K_0 coefficient of effective horizontal pressure at rest
k permeability
k_h horizontal permeability
k_{lining} permeability of tunnel lining
k_{soil} permeability of soil
k_v vertical permeability
M bending moment induced in pipe
M_n, M^* normalised bending moment
N stability ratio $= (\sigma_0 - \sigma_L)/s_u$
N^* $= \sigma_0/s_u$
P distance of lining behind tunnel face
p average chamber pressure
p' mean normal effective stress
$p_{10\%}$ tenth percentile of distribution of chamber pressure p
R relative pipe–soil bending stiffness
RP dimensionless relative permeability
r radius
r_o pipe outer radius
S settlement
S_{max} maximum settlement
s_u undrained shear strength
t, t_L thickness of tunnel lining
u pore water pressure
V_f volume of foam at atmospheric pressure
V_{fl} volume of foaming liquid solution
V_L volume loss associated with tunnelling; tunnel volume loss
V_p volume of polymer solution
V_S volume of settlement trough per metre length of tunnel
V_s volume of soil
x, y horizontal distance measured from tunnel centreline
z_p pipe axis depth; pipe embedment depth
z_0 tunnel axis depth
Δ_h increase in horizontal diameter
Δ_v reduction in vertical diameter
δ radial ground movement/soil deformation; maximum long-term settlement
δ_{imp} maximum long-term settlement for fully impermeable tunnel lining
δ_{perm} maximum long-term settlement for fully permeable tunnel lining
δ_r radial ground movement at radius r
δ_1 radial ground movement at tunnel face
γ_a average soil shear strain
η opening ratio
ν Poisson's ratio
σ_L pressure on tunnel lining
σ_{Li} maximum pressure on tunnel lining
σ'_n normal effective stress
σ_r total radial stress acting at external radius of tunnel lining
σ_{v0} total overburden pressure at tunnel axis level
σ'_v initial vertical effective stress
σ_0 total overburden pressure at tunnel axis
τ shear stress
ϕ' effective stress friction angle; angle of shearing resistance
ψ' angle of dilation

REFERENCES

Attewell, P. B., Yeates, J. & Selby, A. R. (1986). *Soil movements induced by tunnelling and their effects on pipelines and structures*. Glasgow: Blackie.

Bennett, P. J., Klar, A., Vorster, T. E. B., Choy, C. K., Mohamed, H., Soga, K., Mair, R. J., Tester, P. & Fernie, R. (2006). Distributed optical fibre strain sensing in piles. *Proceedings of the international conference on reuse of foundations for urban sites*, Watford, pp. 71–78.

Boone, S. J., Artigiani, E., Shirlaw, J. N., Ginanneschi, R., Leinala, T. & Kochmanova, N. (2005). Use of ground conditioning agents for earth pressure balance machine tunnelling. *Proceedings of the AFTES International Congress*, Cambery, pp. 313–320.

Borghi, F. X. (2006). *Lubrication and soil conditioning in pipejacking and tunnelling*. PhD thesis, Cambridge University.

Borghi, F. X. & Mair, R. J. (2006) Soil conditioning for EPB tunnelling machines in London ground conditions. *Tunnels and Tunnelling International*, September, 18–20.

Bowers, K. H., Miller, D. M. & New, B. M. (1996) Ground movement over three years at the Heathrow Express Trial Tunnel. In *Geotechnical aspects of underground construction in soft ground* (eds R. J. Mair and R. N. Taylor), pp. 647–652. Rotterdam: Balkema.

Bracegirdle, A., Mair, R. J., Nyren, R. J., & Taylor, R. N. (1996). Criteria for the estimation of damage to services caused by ground movements arising from tunnelling. In *Geotechnical aspects of underground construction in soft ground* (eds R. J. Mair & R. N. Taylor), pp. 653–658. Rotterdam: Balkema.

British Tunnelling Society (2005). *Closed face tunnelling machines and ground stability: A guideline for best practice.* London: Thomas Telford.

Clayton, C. R. I., van der Berg, J. P., Heymann, G., Bica, A. V. D. & Hope, V. S. (2002). The performance of pressure cells for sprayed concrete tunnel linings. *Géotechnique* **52**, No. 2, 107–116.

Dimmock, P. S. (2003) *Tunnelling-induced ground and building movement on the Jubilee Line Extension*. PhD thesis, Cambridge University.

Dimmock, P. & Mair, R. J. (2006a). Volume loss experienced on two open-face London Clay tunnels. *Proc. Instn Civ. Engrs Geotech. Engng* **160**, No. 1, 3–11.

Dimmock, P. & Mair, R. J. (2006b). Estimating volume loss for

open-face tunnels in London Clay. *Proc. Instn Civ. Engrs Geotech. Engng* **160**, No. 1, 13–22.
EFNARC (2005). *Specification and guidelines for the use of specialist products for soft ground tunnelling*. Farnham: European Federation for Specialist Construction Chemicals and Concrete Systems, Surrey, UK (www.efnarc.org/pdf/TBMGuidelinesApril05.pdf).
Finno, R. J., Molnar, K. M. and Rossow, E. C. (2003). *Analysis of effects of deep braced excavations on adjacent buried utilities*. Report for the US Department of Transportation, No. A450, A464. Northwestern University, Illinois.
Gaerber, R. (2003). *Design of deep galleries in low permeable saturated porous media*. Doctoral thesis, École Polytechnique Fédérale de Lausanne.
Gourvenec, S. M., Mair, R. J., Bolton, M. D. & Soga, K. (2005). Ground conditions around an old tunnel in London Clay. *Proc. Instn Civ. Engrs Geotech. Engng* **158**, No. 1, 25–33.
Harris, D. (2001). Protective measures. In *Building response to tunnelling: Case studies from construction of the Jubilee Line Extension, London* (eds J. B. Burland, J. R. Standing and F. M. Jardine), Vol. 1, *Projects and methods*, pp. 135–176. London: Thomas Telford, CIRIA special publicaion 200.
Harris, D. (2002a). The Big Ben Clock Tower and the Palace of Westminster. In *Building response to tunnelling: Case studies from construction of the Jubilee Line Extension, London* (eds J. B. Burland, J. R. Standing and F. M. Jardine), Vol. 2, *Case studies*, pp. 453–508. London: Thomas Telford
Harris, D. I. (2002b) Long term settlement following tunnelling in overconsolidated London Clay. In *Geotechnical aspects of underground construction in soft ground* (eds Kastner, Emeriault, Dias and Guilloux), pp. 393–398. Lyon: Spécifique.
Harris, D. I., Mair, R. J., Love, J. P., Taylor, R. N. & Henderson, T. O. (1994). Observations of ground and structure movements for compensation grouting during tunnel construction at Waterloo Station. *Géotechnique* **44**, No. 4, 691–713.
Harris, D. I., Menkiti, C. O., Pooley, A. J. & Stephenson, J. A. (1996). Construction of low-level tunnels below Waterloo Station with compensation grouting for the Jubilee Line Extension. In *Technical aspects of underground construction in soft ground* (eds R. J. Mair and R. N. Taylor), pp. 361–366. Rotterdam: Balkema.
Harris, D. I., Mair, R. J., Burland, J. B. & Standing, J. (1999) Compensation grouting to control tilt of Big Ben Clock Tower. In *Geotechnical aspects of underground construction in soft ground* (eds O. Kusakabe, K. Fujita and Y. Miyazaki), pp. 225–232. Rotterdam: Balkema.
Higgins, K. G., Potts, D. M. & Mair, R. J. (1996). Numerical modelling of the influence of a deep excavation and bored tunnels on the Palace of Westminster clock tower. In *Geotechnical aspects of underground construction in soft ground* (eds R. J. Mair and R. N. Taylor), pp. 525–530. Rotterdam: Balkema.
Hight, D. W., Higgins, K. G., Jardine, R. J., Potts, D. M., Pickles, A. R., De Moor, E. K. & Niyrenda, Z. M. (1993). Predicted and measured tunnel distortions associated with construction of Waterloo International Terminal. In *Predictive soil mechanics* (eds G. T. Houlsby and A. N. Schofield), pp. 317–338. London: Thomas Telford.
Hight, D. W., Gasparre, A., Nishimura, S., Minh, N. A., Jardine, R. J. & Coop, M. R. (2007). Characteristics of the London Clay from the Terminal 5 site at Heathrow Airport. *Géotechnique* **57**, No. 1, 3–18
Hoek, E. & Brown, E. T. (1980) *Underground excavations in rock*. London: Institute of Mining and Metallurgy.
Horiguchi, T., Kurashima, T. & Koyamada, Y. (1994). 1-m Spatial resolution measurement of distributed Brillouin frequency shift in single-mode fibers. *Proceedings of the NIST/IEEE symposium on optical fiber measurements*, Boulder, CO, pp. 73–76.
Jancsecz, S., Krause, R. & Langmaack, L. (1999). Advantages of soil conditioning in shield tunnelling: experiences of LRTS Izmir. *Proceedings of the ITA Conference*, Oslo, pp. 865–875.
Jovicic, V. & Coop, M. R. (1997). Stiffness of coarse grained soils at small strains. *Géotechnique* **47**, No. 3, 545–561.
King, C. (1981). The stratigraphy of the London Basin and associated deposits. *Tertiary Research Special Paper* **6**. Rotterdam: Backhuys.
Klar, A., Vorster, T. E. B., Soga, K. & Mair, R. J. (2005a). Soil–pipe–tunnel interaction: comparison between Winkler and elastic continuum solutions. *Géotechnique* **55**, No. 6, 461–466.
Klar, A., Vorster, T. E. B., Soga, K. & Mair, R. J. (2005b). Continuum solution of soil–pipe interaction including local failure. *Proc. 11th Int. Conf. of IACMAG: Prediction, Analysis and Design in Geomechanical Applications, Turin*, **2**, 687–694.
Klar, A., Bennett, P. J., Soga, K., Mair, R. J., Tester, P., Fernie, R., St John, H. D. & Torp-Peterson, G. (2006). Distributed strain measurement for pile foundations. *Proc. Instn Civ. Engrs Geotech. Engng* **159**, No. 3, 135–144.
Klar, A., Marshall, A. M., Soga, K. & Mair, R. J. (2008) Tunnelling effects on jointed pipelines. *Can. Geotech. J.* **45**, No. 1, 131–139.
Kummerer, C., Thurner, R., Rigazio, A. & Zamagni, A. (2007). Compensation grouting for limiting settlements of two railway bridges induced by a twin-tunnel excavation. *Proc. 14th Eur. Conf. Soil Mech. Geotech. Engng, Madrid*.
Kusakabe, O., Nomoto, T. & Imamura, S. (1997). Geotechnical criteria for selecting mechanised tunnel systems and DMM for tunnelling: Panel discussion. *Proc. 14th Int.Conf. Soil Mech. Geotech. Engng, Hamburg* **4**, 2439–2440.
Lake, L. M., Rankin, W. J. & Hawley, J. (1992). *Prediction and effects of ground movements caused by tunnelling in soft ground beneath urban areas*, CIRIA Project Report 30. London: Construction Industry Research and Information Association.
Lambe, T. W. (1973). Predictions in soil engineering. *Géotechnique* **23**, No. 2, 149–202.
Leinala, T., Grabinsky, M., Delmar, R. & Collins, J. R. (2000). Effects of foam soil conditioning on EPBM performance. *Proc. North American Tunnelling '00*, 514–524.
Macklin S. R. (1999). The prediction of volume loss due to tunnelling in overconsolidated clay based on geometry and stability number. *Ground Engng* **32**, No. 4, 30–33.
Maidl, U. (1995). *Erweiterung der Einsatzbereiche der Erddruckschilde durch Bodenkonditionierung mit Schaum*. PhD thesis, Ruhr University, Bochum (in German).
Mair, R. J. (1993). Developments in geotechnical engineering research: application to tunnels and deep excavations. Unwin Memorial Lecture 1992. *Proc. Instn Civ. Engrs Civ. Engng* **93**, No. 1, 27–41.
Mair, R. J. (1996). General report on settlement effects of bored tunnels. In *Geotechnical aspects of underground construction in soft ground* (eds R. J. Mair and R. N. Taylor), pp. 43–53. Rotterdam: Balkema.
Mair, R. J. & Hight, D. W. (1994). Compensation grouting. *World Tunnelling*, November, 361–367.
Mair, R. J. & Taylor, R. N. (1993). Predictions of clay behaviour around tunnels using plasticity solutions. In *Predictive soil mechanics* (eds G. T. Houlsby and A. N. Schofield), pp. 449–463. London: Thomas Telford.
Mair, R. J. & Taylor R. N. (1997). Bored tunnelling in the urban environment: State-of-the-art report and theme lecture. *Proc. 14th Int. Conf. Soil Mech. Found. Engng, Hamburg* **4**, 2353–2385.
Mair, R. J. & Taylor, R. N. (2001). Elizabeth House: settlement predictions. Building response to tunnelling. In *Case studies from construction of the Jubilee Line Extension, London. Vol. 1: Projects and methods* (eds J. B. Burland, J. R. Standing and F. M. Jardine), pp. 195–215. London: Thomas Telford, CIRIA special publication 200.
Mair, R. J., Gunn, M. J., & O'Reilly, M. P. (1981). Ground movements around shallow tunnels in soft clay. *Proc. 10th Int. Conf. Soil Mech. Found. Engng, Stockholm* **1**, 323–328.
Mair, R. J., Taylor, R. N. & Clarke, B. G. (1992a). *Repository tunnel construction in deep clay formations*. Commission of the European Communities Report EUR 13964 EN. Luxembourg: Office for Official Publications of the European Communities.
Mair, R. J., Hight, D. W. & Potts, D. M., (1992b). *Finite element analyses of settlements above a tunnel in soft ground*, TRRL Contractor Report 265. Crowthorne: Transport and Road Research Laboratory.
Mair, R. J., Taylor, R. N. & Bracegirdle, A. (1993). Sub-surface settlement profiles above tunnels in clays. *Géotechnique* **43,** No. 2, 315–320.
Mair, R. J., Harris, D. I., Love, J. P., Blakey, D. & Kettle, C.

(1994). Compensation grouting to limit settlements during tunnelling at Waterloo Station. *Proceedings of Conference Tunnelling '94, London*, 279–300.

Mair, R. J., Taylor, R. N. & Burland, J. B. (1996). Prediction of ground movements and assessment of risk of building damage due to bored tunnelling. In *Geotechnical aspects of underground construction in soft ground* (eds R. J. Mair and R. N. Taylor), pp. 713–718. Rotterdam: Balkema.

Mair, R. J., Merritt, A. S., Borghi, F. X., Yamazaki, H. & Minami, T. (2003) Soil conditioning for clay soils. *Tunnels and Tunnelling Int.*, **35**, No. 4, 29–32.

Maragakis, E., Siddhartan, R. & Meis, R. (2003). *Static axial behaviour of pipe joints*. University of Nevada, Reno, USA (http://bric.ce.unr.edu/networking/Pipest/)

Menkiti, C. O., Mair, R. J. & Miles, R. (2001a). Tunnelling in complex ground conditions in Bolu, Turkey. *Proc. Underground Construction 2001*, London, 546–558.

Menkiti, C. O., Sanders, P., Barr, J., Mair, R. J., Cilingir, M. & James, S. (2001b). Effects of the 12th November 1999 Duzce Earthquake on Stretch 2 of the Gumusova-Gerede Motorway in Turkey. *Proc. Int. Road Federation 14th World Road Congress, Paris*, CD-ROM.

Merritt, A. S. (2004). *Soil conditioning for earth pressure balance machines*. PhD thesis, Cambridge University.

Merritt, A. S. & Mair, R. J. (2006). Mechanics of tunnelling machine screw conveyors: model tests. *Géotechnique* **56**, No. 9, 605–615.

Merritt, A. S. & Mair, R. J. (2008)**.** Mechanics of tunnelling machine screw conveyors: a theoretical model. *Géotechnique* **58**, No. 2, 79–94.

Merritt, A. S., Borghi, F. X. & Mair, R. J. (2003). Conditioning of clay soils for earth pressure balance tunnelling machines. *Proc. Underground Construction 2003, London*, 455–466.

Milligan, G. W. E. (2000). *Lubrication and soil conditioning in tunnelling, pipe jacking and microtunnelling: A state-of-the-art review.* London: Geotechnical Consulting Group (www-civil.eng.ox.ac.uk/research/pipejack/soilcond.html).

Milligan, G. W. E. (2001). Soil conditioning and lubricating agents in tunnelling and pipe jacking. *Proc. Underground Construction Symp. 2001, London*, 105–116.

Mohamad, H. (2008). *Distributed fibre optic strain sensing of geotechnical structures*. PhD thesis, University of Cambridge.

Mohamad, H., Bennett, P. J., Soga, K., Mair, R. J., Lim, C.-S., Knight-Hassell, C. K. & Ow, C. N. (2007). Monitoring tunnel deformation induced by close-proximity bored tunnelling using distributed optical fiber strain measurements. *Proc. 7th Int. Symp. on Field Measurements in Geomechanics, Boston*.

Neerdael, B. & De Bruyn, D. (1989). Geotechnical research in the test drift of the HADES underground research facility at Mol. *Proceedings of the CED Technical Session on Geomechanics of clays for radioactive waste disposal*, Commission of the European Communities Report EUR 12027 EN/FR, pp. 83–94.

Nyren, R. (1998). *Field measurements above twin tunnels in London Clay.* PhD thesis, Imperial College, University of London.

O'Carroll, J. B. (2005). *A guide to planning, constructing and supervising earth pressure balance TBM tunnelling*. New York: Parsons Brinkerhoff.

O'Reilly, M. P., Mair, R. J. & Alderman, G. H. (1991). Long-term settlements over tunnels: an eleven-year study at Grimsby. *Proc. Conf. Tunnelling '91, London*, 55–64.

O'Rourke, T. D. & Trautmann, C. H. (1982). Buried pipeline response to tunnel ground movements. *Proc. Europipe '82 Conf., Basel*, 9–15.

O'Rourke, T. D., Goh, S. H., Menkiti, C. O. & Mair, R. J. (2001). Highway tunnel performance during the 1999 Duzce earthquake. *Proc. 15th Int. Conf. Soil Mech. Geotech. Engng, Istanbul* **2**, 365–1368.

Palmer, J. H. L. & Belshaw, D. J. (1980). Deformations and pore pressure in the vicinity of a precast, segmented, concrete-lined tunnel in clay. *Can. Geotech. J.* **17**, No. 2, 174–184.

Panet, M. & Guenot, A. (1982). Analysis of convergence behind the face of a tunnel. *Proc. Tunnelling '82, London*, 197–204.

Peck, R. B. (1969). Deep excavations and tunnelling in soft ground. *Proc. 7th Int. Conf. Soil Mech. Found. Engng, Mexico City*, 225–290.

Potts, D. M. & Zdravkovic, L. (2001). *Finite element analysis in geotechnical engineering: Application*. London: Thomas Telford.

Poulos, H., Day, P., Valenzuela, L., Crawford, S., Mayne, P., Bolton, M., Tatsuoka, T. & Koseki, J. (2005). Practitioner/academic forum. *Proc. 16th Int. Conf. Soil Mech. Geotech. Engng, Osaka* **5**, 2917–2936.

Rankin, W. J. (1988). Ground movements resulting from urban tunnelling: predictions and effects. In *Engineering geology of underground movement*, Engineering Geology Special Publication No. 5, 79–92. London: Geological Society.

Ratnam, S., Soga, K. & Whittle, R. W. (2005). A field permeability measurement technique using a conventional self-boring pressuremeter. *Géotechnique* **55**, No. 7, 527–537.

Schmidt, B. (1969). *Settlements and ground movements associated with tunnelling in soil*. PhD thesis, University of Illinois.

Schubert, P., Moggiolli, M., Brandl, H. & Golser, J. (1997) Extraordinary difficulties driving the motorway tunnels through Bolu Mountains, Turkey. *Felsbau* **15**, No. 5.

Selemetas, D. (2005). *The response of full-scale piles and piled structures to tunnelling*. PhD thesis, Cambridge University.

Shin, J. H., Addenbrooke, T. I. & Potts, D. M. (2002). A numerical study of the effect of groundwater movement on long-term tunnel behaviour. *Géotechnique* **52**, No. 6, 391–403.

Shirlaw, J. N. (1995). Observed and calculated pore pressures and deformation induced by earth pressure balanced shield. *Can. Geotech. J.* **32**, 181–189.

Shirlaw, J. N., Ong, J. C. W., Rosser, H. B., Tan, C. G., Osborne, N. H. & Heslop, P. E. (2003). Local settlements and sinkholes due to EPB tunnelling. *Proc. Instn Civ. Engrs Geotech. Engng* **156**, No. 4, 193–211.

Standing, J. R. (2001). Elizabeth House, Waterloo. In *Building response to tunnelling: Case studies from the Jubilee Line Extension, London. Vol. 2, Case studies* (eds J. B. Burland, J. R. Standing and F. M. Jardine), pp. 547–612. London: Thomas Telford, CIRIA special publication 200.

Standing, J. R. & Burland, J. B. (2006). Unexpected tunnelling volume losses in the Westminster area, London. *Géotechnique* **56**, No. 1, 11–26.

Takagi, N., Shimamura, K. & Nishio, N. (1984). Buried pipe response to adjacent ground movements associated with tunnelling and excavations. *Proc. 3rd Int. Conf. on Ground Movements and Structures, Cardiff*, 97–112.

Tatsuoka, F., Jardine, R. J., Lo Presti, D., Di Benedetto, H. & Kodaka, T. (1997). Characterising the pre-failure deformation properties of geomaterials. *Proc. 14th Int. Conf. Soil. Mech. Found. Engng, Hamburg*, **4**, 2129–2164.

Vaughan, P. R. (1989). Non-linearity in seepage problems: theory and field observation. In *De Mello volume: A tribute to Prof. Dr Victor F. B. de Mello*, pp. 501–515. São Paulo, Brasil : Editura Edgard Blücher.

Viggiani, G. (2001). Grout intensities. In *Building response to tunnelling: Case studies from the Jubilee Line Extension, London Vol. 1: Projects and Methods* (eds J. B. Burland, J. R. Standing and F. M. Jardine), pp. 311–313. London: Thomas Telford, CIRIA Special Publication 200.

Vorster, T. E. B. (2005) *The effects of tunnelling on buried pipes*. PhD thesis, Cambridge University.

Vorster, T. E. B., Klar, A., Soga, K., & Mair, R. J. (2005). Estimating the effects of tunneling on existing pipelines. *ASCE J. Geotech. Geoenviron. Engng* **131**, No. 11, 1399–1410.

Vorster, T. E. B., Soga, K., Mair, R. J., Bennet, P. J., Klar, A. & Choy, C. K. (2006). The use of fibre optic sensors to monitor pipeline response to tunnelling. *Proc. Geo-Congress 2006, Atlanta*, CD-ROM.

Ward, W. H. (1969). Yielding of ground and the structural behaviour of linings of different flexibility in a tunnel in London Clay. *Proc. 7th Int. Conf. Soil Mech. Found. Engng, Mexico City* **3**, 320–325.

Ward, W. H. (1978). Ground support for tunnels in weak rocks. *Géotechnique* **28**, No. 2, 133–170.

Ward, W. H. & Pender, M. J. (1981). Tunnelling in soft ground: General report. *Proc. 10th Int. Conf. Soil Mech. Found. Engng, Stockholm* **4**, 261–275.

Ward, W. H. & Thomas, H. S. H. (1965). The development of earth loading and deformation in tunnel linings in London Clay. *Proc. 6th Int. Conf. Soil Mech. Found. Engng, Toronto* **2**, 432–436.

Wong, H., Trompille, V., Subrin, D. & Guilloux, A. (1999). Tunnel face reinforced by longitudinal bolts: analytical model and in situ data. In *Geotechnical aspects of underground construction in soft ground* (eds O. Kusakabe, K. Fujita and Y. Miyazaki), pp. 457–462. Rotterdam: Balkema.

Wongsaroj, J. (2005). *Three-dimensional finite element analysis of short- and long-term ground response to open face tunnelling in stiff clay.* PhD thesis, Cambridge University.

Wongsaroj, J., Borghi, F. X., Soga, K., Mair, R. J., Sugiyama, T., Hagiwara, T. & Bowers, K. J. (2005). Effect of TBM driving parameters on ground surface movements: Channel Tunnel Rail Link Contract 220. In *Geotechnical aspects of underground construction in soft ground* (eds Bakker *et al.*), pp. 335–341. London: Taylor & Francis Group.

Wongsaroj, J., Soga, K. & Mair, R. J. (2006). Modelling of long-term ground response to tunnelling under St James' Park London. *Géotechnique* **57**, No. 1, 75–90.

Woods, E., Battye, G., Bowers, K. & Mimnagh, F. (2007). Channel Tunnel Rail Link Section 2: London Tunnels. *Proc. Inst. Civ. Engrs Civ. Engng* **160**, special issue 2, 24–28.

Yeates, J. (1984). The response of buried pipelines to ground movements caused by tunnelling in soil. *Proc. 3rd Int. Conf. Ground Movements and Structures, Cardiff*, 129–144.

VOTE OF THANKS

ANTONIO GENS, Professor of Geotechnical Engineering, Technical University of Catalonia, Barcelona

It is an honour, and also a great personal pleasure, to propose the vote of thanks to Professor Mair, the 46th Rankine Lecturer.

When Lord Palmerston, the Prime Minister of the day, was invited to the opening of the Metropolitan Line, the first underground railway in the world, he declined with the argument that, at 79, he wanted to remain above ground as long as possible. We, as a profession, are very fortunate that Robert Mair did not make the same decision at an obviously much younger age. We would have missed an excellent, lucid and well-illustrated lecture that has spanned the whole range of tunnelling issues from stability during construction to the often forgotten long-term settlements that occur long after everybody has packed up and gone home.

Robert Mair has proved throughout his career that he is able to move with ease from academic life to professional practice and back while maintaining the same intellectual outlook when tackling both theoretical and practical problems. If there ever was an argument against the possibility of simultaneous excellence in academia and in professional practice, those arguments have been thoroughly disproved tonight, at least in the case of some exceptional individuals. I remember being impressed already by this versatility when I first met him while we were both research students toiling with our PhD work. This ability has allowed him to remain at the forefront of the tunnelling field throughout his career.

I presume that here in the audience there are a substantial number of people who are or have been involved in tunnelling, and I am sure that we would all agree that tunnelling is a rather messy business. However, I think it would be difficult to infer this from this Rankine lecture, in which the important issues have been shrewdly identified, elegantly analysed, and usefully concluded. Some time ago, I came across a collection of short essays discussing the work of eminent Cambridge scientists from William Gilbert in the sixteenth century to our times. It was interesting to detect a common thread in the tradition: an ability to reduce complex phenomena, through illuminating insights, to rational theories and frameworks. This Rankine lecture is a clear proof that this tradition is very much alive today.

We have seen, for instance, how apparently simple models can be usefully applied to the understanding and solution of stability problems when tunnelling in extremely complex geological conditions. This is refreshing at a time when three-dimensional analyses often plucked from thin air seem to be replacing judgement. The combination of theoretical insight, field observations, laboratory testing and sound engineering demonstrates without any doubt a total command of the subject. This expertise has also been apparent in the other topics of the lecture, where he has used, as needed, machine performance observations, numerical analyses, field trials and centrifuge modelling. As a consequence of this comprehensive approach, conclusions are never commonplace. A constant feature is the consideration and importance given to field measurements, always the stamp of a good geotechnical engineer. We are thankful to Robert for having drawn our attention to exciting new developments in this area.

Ladies and gentlemen, we have had this evening the good fortune to listen to a memorable lecture delivered with the clarity and authority that we have come to expect, as a matter of course, from Professor Mair's presentations. It has been said that it is only possible to transmit experience in the language of science. This lecture is a prime example of the truth of this statement. I am convinced that, well into the future, we shall look back on this occasion as an important landmark that identified the new horizons opening for the perennial and often complex relationship between tunnelling and geotechnics. On behalf of the British Geotechnical Association, I thank you, Robert, for an outstanding lecture, and I call upon all those present here to endorse my thanks by acclamation.